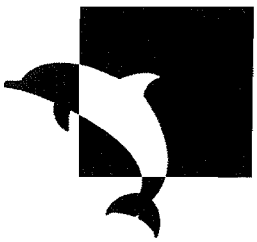

University of Southampton

DEVELOPMENT OF A MICRO HOLLOW CATHODE FOR USE AS AN ION MICROPROPULSION ELECTRON SOURCE

Keith G. Hutchison MPhys

Thesis submitted for Doctor of Philosophy

Department of Aeronautics & Astronautics

June 2006

UNIVERSITY OF SOUTHAMPTON

ABSTRACT

SCHOOL OF ENGINEERING SCIENCES

ASTRONAUTICS RESEARCH GROUP

Doctor of Philosophy

DEVELOPMENT OF A MICRO HOLLOW CATHODE FOR USE AS AN ION MICROPROPULSION ELECTRON SOURCE

Keith G. Hutchison MPhys

Recent interest in small-scale satellites has encouraged the development of novel miniaturised propulsion systems. A variety of technologies exist which could be applied to this role, generally focused around chemical and electric thruster designs. The propulsion system must be durable, low in mass and must be able to efficiently propel the spacecraft to a range of velocities, on the order of kilometres per second.

Electrostatic thrusters demonstrate high combined levels of power efficiency and specific impulse in relation to other propulsion technologies including other electric systems. Electron bombardment ion thrusters are therefore an excellent candidate for use on small-scale satellites. The reduction in size of existing technologies presents design challenges, due to difficulties faced in fabrication and the effects on operation when scaling to such small sizes. The goal of this research project has been to develop and test a miniaturised electron source to establish the effects of novel materials and design on functionality.

Electron sources are key components of electron bombardment ion thrusters, used for both ionisation and beam neutralisation. Initial research conducted during this study showed thermionic filament and field emission sources were difficult to apply to inert gas ion propulsion systems. This was due to their lack of robustness at the higher pressures required to efficiently ionise the propellant. A study into micro hollow cathodes was therefore conducted due to their demonstrated performance at larger scales.

Three types of micro hollow cathode were designed, fabricated and tested. The most complex design developed during this project had a body formed from a low-diameter metal tube with a turned orifice and an internal carbon matrix impregnated with compounds designed to promote electron emission. The other two models were a simple metal body and a surface impregnated body, and were primarily used to compare performance with the more complex model. All 3 types exhibited similar initiation voltage properties, with the impregnated insert cathode showing slightly higher initiation voltages at low flow rates. The keeper discharge could be established in each case, but transfer to the anode discharge could not be performed. The keeper current and voltage showed that the impregnated insert device operated at the lowest power for similar flow rates and keeper distances, suggesting impregnated carbon inserts deserve more study.

Acknowledgements

The author would like to thank all those who have given their support, advice and encouragement throughout this project.

Thanks are due to Prof S B Gabriel for instigating the project and providing invaluable assistance and encouragement throughout.

Deepest thanks go to the staff at the Rutherford Appleton Laboratory, for providing funds, equipment and expertise. I would particularly like to thank Doctors Barry Kent and Bob Stevens for their excellent technical advice and aid in fabricating the device.

Special thanks go to Miss L Tarantino without whom this project would have seen no end. Her unflagging encouragement and boundless patience have enabled me to finally finish here writing these acknowledgements. But it doesn't finish here. You see I'd like to ask Miss L Tarantino to marry me. With any luck when she's reading this for the first time we're in a suitably romantic location, and there's a little bit of carbon and platinum nearby that, if she accepts it, will signify a life shared.

I love you more than I thought it was possible to love.

So?

Table of Contents

CONTENTS

List of Figures

LIST OF FIGURES

LIST OF FIGURES

List of Tables

List of Equations

LIST OF EQUATIONS

Constants & Variables

a	Acceleration, ms^{-2}
A'	Fowler-Nordheim Contant
A_G	Grid area, m^2
a_g	Gate radius for FEA, m
A_{or}	Cathode orifice area, m^2
A_{int}	Cathode internal cross-sectional area, m^2
A_{pe}	Primary electron collection area, m^2
A_{pipe}	Cross-sectional area of vacuum feed orifice, m^2
a_s	Tip radius of FEA cone, m
A_R	Richardson Constant, $1.2x10^6$ Am^{-2}
B	Magnetic field, T
B'	Fowler-Nordheim Contant
C	Conductance of a short round orifice, m^3s^{-1}
C_P	Specific heat capacity at constant pressure, $Jkg^{-1}K^{-1}$
C_V	Specific heat capacity at constant volume, $Jkg^{-1}K^{-1}$
D	Pipe diameter, m
d_I	Ion acceleration distance, m
E	Electric field, Vm^{-1}
e	Electronic charge, $1.602x10^{-19}$ C
E_C	Electric field at cathode surface, Vm^{-1}
E_{Inc}	Incident particle energy, J
$E_{Threshold}$	Threshold energy for sputtering, J
E_{Trans}	Energy transferred to the target, J
F^{++}	Ratio of multiple ionisation constant
g_0	Acceleration due to gravity at sea level, $9.8ms^{-2}$
I_b	Beam current, A
I_D	Discharge current, A
I_e	Electron emission current, A
I_i	Ion current, A

I_{sp}	Specific impulse, s
J_+	Maximum current density, Am^{-2}
J_D	Current density, Am^{-2}
J(FN)	Fowler-Nordheim emission current density, Am^{-2}
J_S	Schottky emission current density
J_{Th}	Thermionic emission current density, Am^{-2}
K	Ratio of multiple ionisation constant
k	Boltzmann Constant, $1.3807x10^{-23}$ JK^{-1} or $8.617x10^{-5}$ eVK^{-1}
k_g	Geometrical factor for FEA emission calculation, $4 < k_g < 20$
Kn	Knudsen number
L_{Char}	Characteristic length, m
l_{emit}	Length of the emitting region in the cathode, m
m	Particle mass, kg
$\dot{m}$	Propellant mass flow rate, kgs^{-1}
M_0	Initial spacecraft mass, kg
M_b	Spacecraft mass at burnout, kg
m_e	Electronic mass, $9.11x10^{-31}$ kg
m_i	Ion mass, kg
m_{Inc}	Mass of incident atom or ion, kg
m_n	Neutral mass, kg
m_{Tgt}	Target atom mass, kg
n	Number of particles per unit volume, m^{-3}
n_+	Number of singly charged atoms
n_{++}	Number of doubly charged atoms
n_0	Neutral number density, m^{-3}
n_e	Electron number density, m^{-3}
n_i	Ion number density, m^{-3}
n_{pe}	Primary electron density, m^{-3}
P_A	Chamber pressure at time A, Nm^{-2}
P_B	Chamber pressure at time B, Nm^{-2}
$P_{Chamber}$	Chamber pressure, mBar

P_{Down}	Downstream pressure, Nm^{-2}
P_{or}	Gas pressure at orifice, m^2
P_{Up}	Upstream pressure, Nm^{-2}
Q	Volumetric pumping speed, m^3s^{-1}
q	Particle charge, C
Q_{PS}	Manufacturers quoted pumping speed, ls^{-1}
Q_{Pump}	System volumetric pumping rate, ls^{-1}R Universal gas constant, 8.3144 $Jmol^{-1}K^{-1}$
r_c	Insert internal radius, m
Re	Reynolds number
r_L	Larmor radius, m
r_{or}	Cathode orifice radius, m
T	Thrust, N
T_0	Gas temperature, K
T_C	Cathode temperature, K
T_e	Electron temperature, K
T_i	Ion temperature, K
$t_{Pumpdown}$	Time to pumpdown between two known pressures, s
U	Flow speed, ms^{-1}
u_{or}	Gas flow velocity at the orifice, ms^{-1}
$U_{Sublimation}$	Atomic heat of sublimation, J
V	Voltage, V
v	Particle velocity, ms^{-1}
v_{avg}	Average electron velocity, ms^{-1}
$V_{Chamber}$	Chamber volume, m^3
V_D	Discharge voltage, V
V_{Gate}	Potential on the gate electrode above field emitter, V
V_{ex}	Exhaust velocity, ms^{-1}
V_F	Fall voltage, V
V_{fp}	Floating potential, V
V_p	Applied potential between grids, V

V_{pl}	Plasma potential, V
v_S	Velocity of sound in an ideal gas, ms^{-1}
W	Molar weight, kg
Z	Ion charge
α	Degree of ionisation
β	FEA cone angle, degrees
ΔV	Spacecraft change in velocity, ms^{-1}
ϵ_o	Permittivity of free space, $8.854x10^{-12}$ Fm^{-1}
ϕ	Work function, eV
ϕ_2	Second ionisation potential of the propellant, eV
ϕ_{eff}	Effective work function, eV
ϕ_I	Grid open area to ions, m^2
γ	Ratio of specific heats
λ_D	Debye length, m
λ_{MFP}	Mean free path between molecular collisions, m
μ_V	Dynamic viscosity, Pa.s
η_u	Mass utilisation efficiency of the propellant, %
Ω	Electron flux, s^{-1}
ρ	Gas density, kgm^{-3}
ρ_{or}	Gas density at upstream side of orifice, kgm^{-3}
σ	Gas particle collisional cross-sectional area, m^2
σ_{ion}	Cross-section for ionisation, m^2
ν_c	Cyclotron frequency, Hz

Chapter 1

Introduction

1.1. Propulsion System Requirements

The wide variety of roles and configurations a spacecraft can take introduces a large range of propulsion requirements, and options to meet these requirements. Many propulsive techniques have been proposed and investigated [1] with varying success. There are a number of propulsive techniques that can be employed in a spacecraft to provide both primary propulsion and attitude and orbit control. Each has its own benefits and shortcomings and must meet the design constraints placed on the system. Examples of the major constraints that may affect the choice of a space propulsion system for a specific mission are:

- Thrust
- Spacecraft Mass
- Specific Impulse
- Mission Duration
- Environment

1. INTRODUCTION

The required thrust, or force applied by a propulsion system, is a primary factor in determining its suitability to a variety of missions. The thrust a propulsion system can develop places limits on mission duration and the manoeuvres that can be made, directly related to system mass [2]. High thrust systems can develop large spacecraft velocity changes (ΔV) in short timescales; though typically exhibit low specific impulses. In contrast, missions where the spacecraft mass is low, or velocity changes are minor, or where such changes can take place over long timescales, can employ more efficient, low thrust, propulsion systems.

The thrust equation (1.1) and ideal rocket equation (1.3) describing these relations are given by:

$$T = \frac{dm}{dt} V_{ex} = \dot{m} V_{ex} \qquad 1.1$$

T is the thrust; V_{ex} is the exhaust velocity and $\dot{m}$ is the propellant mass flow rate. The thrust equation shows that the force a system develops is determined by mass flow through the thrusters and by exhaust velocity. It is beneficial to maximise V_{ex} to minimise the requirement on mass flow rate and thus total propellant used for a manoeuvre. The exhaust velocity is the average velocity of the propellant exiting the system. In some cases portions of the propellant are exhausted at different velocities, readily apparent in electric propulsion systems where ions are exhausted at speeds far in excess of that of neutrals. In this case the exhaust velocity of ions can be several hundred times greater than the thermal velocity of neutrals and an additional term denoting the mass utilisation efficiency of the propellant, η_u, must be added to the equation:

$$T = \eta_u \frac{dm}{dt} V_{ex} = \eta_u \dot{m} V_{ex} \qquad 1.2$$

As stated, the change in velocity or ΔV, undergone by a spacecraft is also dependent on the exhaust velocity and the relative masses of propellant and spacecraft. The ΔV defines the extent to which a spacecraft can be altered in its velocity. This will impact the flight time and can be used to determine the amount of propellant required to meet mission requirements. ΔV is given by [2]:

$$\Delta V = V_{ex} \ln\left(\frac{M_0}{M_b}\right) \qquad 1.3$$

Where M_0 is the initial spacecraft mass and M_b is the spacecraft mass at burnout. It should be remembered that this equation describes an idealised case and may not be generally applicable e.g. in the case of minor manoeuvres.

As stated, the total system mass, including payload, constrains the possible propulsion solutions for a space mission. High mass systems generally require high thrust propulsion devices to develop moderate levels of ΔV. This generally limits choices to chemical propulsion techniques. The exception arises when the mission duration is long enough that manoeuvres can be made over long timescales at lower thrusts. Mission duration therefore impacts on the choice of any propulsion systems. Under conditions of a fixed electrical power budget with a variable trip time, ion thrusters perform well due to their high specific impulse, mass utilisation efficiency and good reliability in comparison to other forms of propulsion, including other forms of electric propulsion [3].

The specific impulse of a thrusters system is a measure of the efficiency of the propulsion system in that it defines the thrust output per unit mass flow rate of propellant.

$$I_{sp} = \frac{T}{\dot{m}.g_0} \qquad 1.4$$

I_{sp} is the specific impulse and g_0 is the acceleration due to gravity at sea level, equal to $9.8ms^{-2}$. A high specific impulse signifies a high performance level. Chemical systems typically show specific impulses of the order of several hundred seconds, while electric propulsion systems can have specific impulses of the order of several thousand seconds. Electric propulsion techniques therefore generally use their propellant more efficiently in terms of thrust per unit mass flow rate.

The mission environment is another major factor which can influence propulsion system choice. Many propulsion systems will not operate in the Earth's atmosphere requiring vacuum for operation. Further, at launch, the Earth's high escape velocity places a lower limit on total thrust for a system of a specific mass. Other environmental considerations include such effects as that in certain orbits high energy particles affect spacecraft operation. High particle and UV radiation levels can severely affect solar panel performance and thus available power for electric systems. Another factor is that highly precise scientific experiments on spacecraft may also require propulsive systems that do not contaminate the spacecraft [4], requiring designers to take account of the propellants properties.

1.2. Space Propulsion Systems

This section covers a brief review of varying propulsion options. As stated, a variety of methods can be used to propel a spacecraft, some have seen extensive use, others are theoretical or experimental and require further work to develop fully functional, economic and demonstrably reliable systems. Chemical and electrical propulsion options have seen wide use on spacecraft, while other options, such as nuclear and photonic propulsion systems, have been investigated and tested with varying degrees of success [2, 5].

1.2.1. Chemical Propulsion

Chemical propulsion is the method by which all payloads are put into orbit and currently the primary propulsion system for all but a few satellites. Primary chemical propulsion systems, specifically solid and liquid rockets and hybrid propulsion systems, are the only viable option to reach orbit from the surface of the earth. No other system can develop the high thrusts required to reach escape velocity, except nuclear propulsion techniques which have not seen significant development, primarily due to safety concerns. Chemical rockets can develop thrusts over one million Newtons at specific impulses of a few hundred seconds [2].

Monopropellant hydrazine is an example of a secondary chemical propulsion system for attitude and orbit control. Exothermic decomposition under thermal or catalytic action results in a hot gaseous mixture ejected through a nozzle, providing thrust. Storable bipropellant systems work on the same operating principles but have two parts to the propellant mix. These two propulsion system options can have specific impulses in the range of several hundred seconds and operate, as low as 10mN up to tens of Newtons, dependent on size and technology.

Cold gas systems are another secondary chemical propulsion option and work on the principle of ejecting a gas under high pressure into space. They have low specific impulses of less than 100s with thrusts of several to hundreds of millinewtons, but are extremely robust and simple, both to build and to operate.

1.2.2. Electric Propulsion

Electric propulsion systems are of considerable interest as thruster options, due to their high specific impulses, highly controllable thrusts and ability to be started and stopped easily. Electric propulsion techniques fall into the three broad categories of electrothermal, electromagnetic and electrostatic thrusters.

Electrothermal propulsion relies on the energisation and expulsion of a propellant, working by heating the propellant, either by heaters (resistojet), or exposure to an electric arc (arcjet) [2]. Resistojets typically have specific impulses around 200s and thrusts of 5-100mN, while arcjets have specific impulses of up to 500-1500s at thrusts of 2mN-1N. Resistojets are simple and have seen extensive use. Arcjets have generally not seen wide use due to the problems of high plasma temperature and excessive electrode wear, however hydrazine types have been used on numerous communication satellites. Figs 1.1 and 1.2 show examples of a resistojet and arcjet.

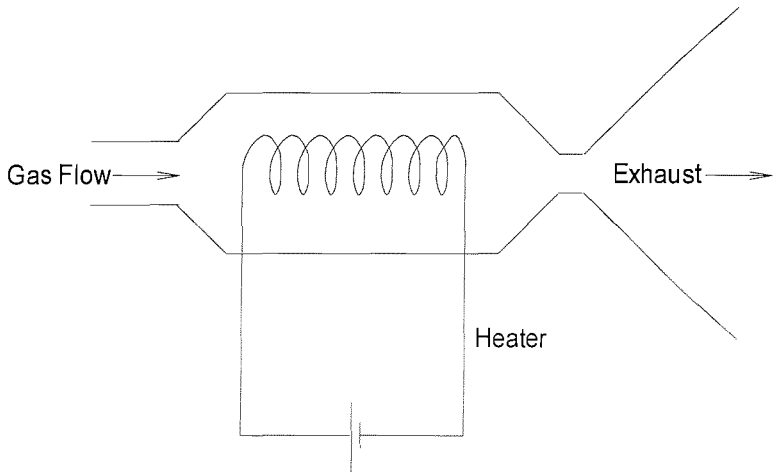

Fig 1.1 Resistojet Schematic

Arcjets are generally used to provide short bursts of thrust for such tasks as station-keeping. The non-flammable propellant (generally hydrazine as it can be used in chemical systems too) is accelerated through a nozzle under heating from an electric arc.

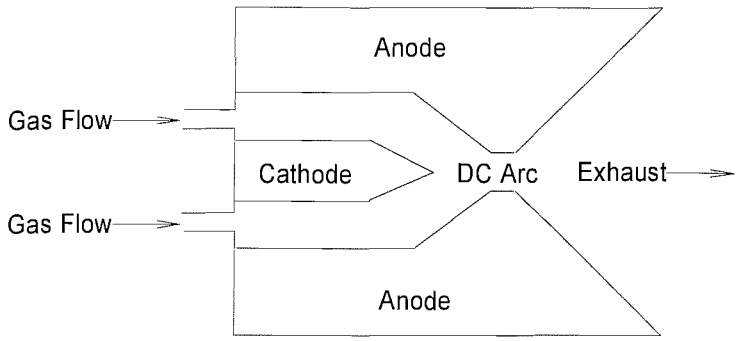

Fig 1.2 Arcjet schematic

Electromagnetic or electrodynamic thrusters work on the principle of production of a plasma, or ionised gas, which is ejected by applied or self-induced magnetic fields. Specific impulses, in excess of 2000s have been demonstrated, but at low thrusts of micronewtons to millinewtons. Again, excessive cathode erosion has been the major problem preventing more extensive use, but they have been flight-tested [5]. An example of such a device is a pulsed plasma thrusters, or PPT [6] which produces a plasma by electric decomposition and excitation of the propellant (typically Teflon) which is then accelerated by Lorenz forces (superposed electric and magnetic fields).

Magnetoplasmadynamic (MPD) devices used superposed magnetic fields to exhaust the plasma from the thruster body. They are very scalable devices generally operating between a few mN up to hundreds of Newtons. They have very high specific impulses but have problems with high power requirements and excessive cathode erosion. Self-induced magnetic fields only form at high power so most low power MPD's are based around magnetic fields produced from outside the discharge chamber. Operating the device in a pulsed mode also improves efficiency as the thruster can then operate at high powers during the pulse, when the discharge is most efficient, but maintain overall low power consumption. A diagram of an MPD can be seen in fig 1.3.

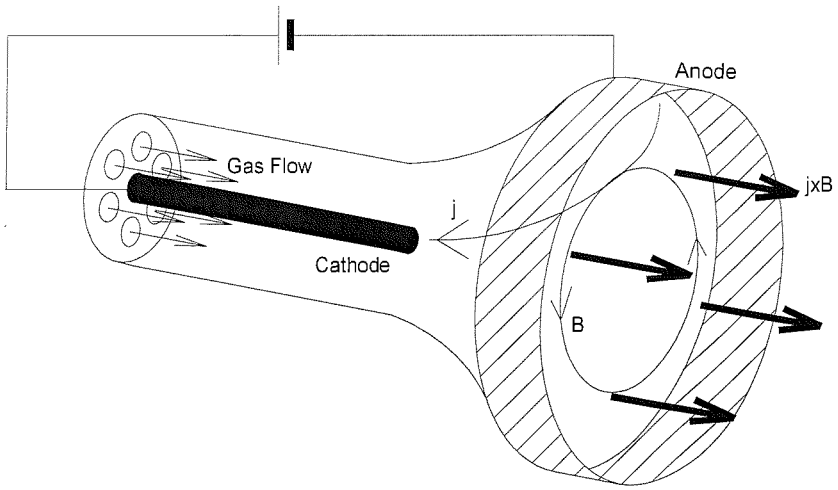

Fig 1.3 Magnetoplasmadynamic thruster

The PPT or pulsed plasma thrusters works on the same principles as the MPD, but is specifically designed to use the pulsing technique for the discharge. Teflon has been successfully used in an electrothermal PPT, where a cloud of ablated Teflon, coming from the discharge pulse (spark plug) is used as the propellant. See fig 1.4 below.

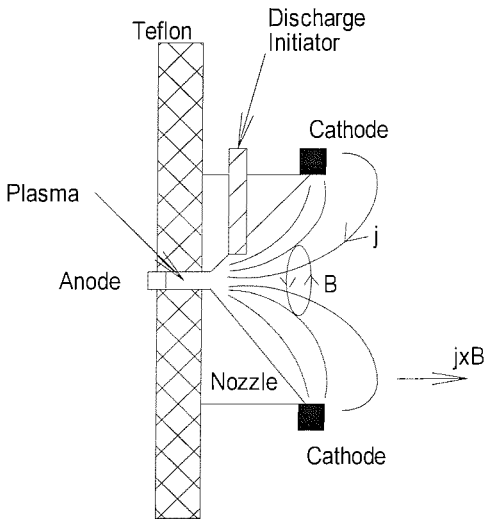

Fig 1.4 Pulsed Plasma Thruster

Electrostatic thruster systems work on the principle of accelerating an ionised propellant through an electric field. Ion thruster systems, field effect electric propulsion (FEEP thrusters), colloid thrusters, hall thrusters and hollow cathode thrusters are all examples of electrostatic thrusters:

Ion thrusters ionise a propellant through electron bombardment or through application of radiofrequency waves, then accelerate the ions through an electric field. They typically exhibit specific impulses of 1500-4000s and existing designs can develop thrusts from micronewtons up to approximately 0.5N [5]. Mid-range ion thrusters of approximately 10cm diameter are typically used for station-keeping and on-orbit repositioning [7]. Ion thrusters have been used as secondary propulsion systems for attitude and orbit control for many years, for example Boeing Satellite Systems' 702 commercial communications satellites. However, Deep Space 1, launched in 1998, was the first spacecraft to use ion thrusters as its primary propulsion system. Of all the available electric propulsion options, ion thrusters are one of the most interesting and important, a result of their demonstrated viability, relative simplicity and continued good performance over extended timescales. Fig 1.5 shows a typical ion thruster schematic. Cathodes are used to provide electrons for ionisation and neutralisation. Mass flow controllers set the flow to the cathodes and into the chamber itself. Keepers are used to initiate and maintain discharges from the cathodes and to prevent sputtering of the hollow cathode by ions traveling back to it. In the discharge chamber an anode maintains the electric field for electrons to travel down, while a series of magnets placed radially creates cusps to ensure electrons have a small Larmor radius and hence do not migrate to the walls. A baffle energises electrons and vectors them in the required direction down the thruster. This creates an internal plasma which is extracted through confinement and acceleration grids to produce a thrust.

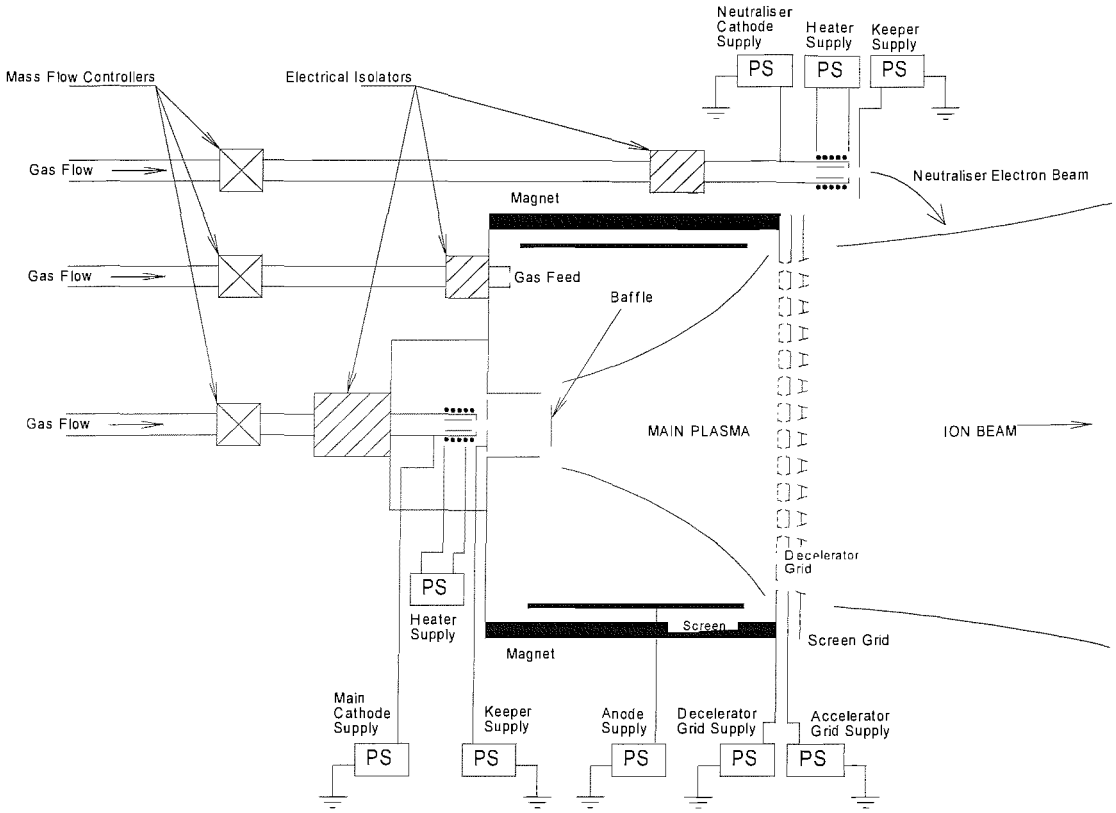

Fig 1.5 Electron Bombardment Ion Thruster Schematic

FEEP thrusters are operated by exhausting a beam of mainly singly-ionised atoms. Ions are produced by field evaporation of a propellant, usually Chromium or Indium, through an electrostatic field. Field evaporation is essentially the liberation of ions from a surface in the presence of an electric field of the order of 10^9 Vm^{-1}. They exhibit very high specific impulses (6000-10000s) at low thrust values (1μN to 2 mN). However, field emission microthrusters produced so far have shown limited mass utilisation efficiencies and relatively low output currents [8], though thrusts of 5mN have recently been achieved.

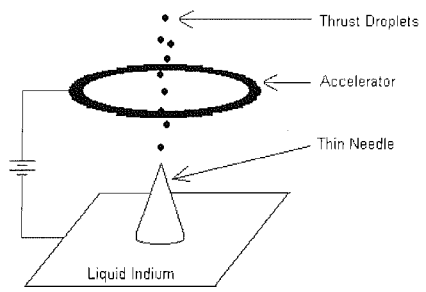

Fig 1.6 FEEP thruster schematic

Colloid thrusters, another electric propulsion option, also accelerate ionised particles but instead use a non-metallic liquid propellant. Thrusts are comparable to FEEP systems but specific impulses are significantly lower (1000-1500s), though power consumption is also much lower [9].

Hall thrusters work by the superposition of an axial electric field and a radial magnetic field. Electrons are prevented from moving easily to the anode and a strong electric field is maintained in a central channel. The ions in this device are produced by electron bombardment, and are accelerated by the strong electric field of the space-charge layer formed near the exit. This space-charge layer is where the plasma is separated from the anode and a large potential is set up [10]. Specific impulse is in the range 1000-2000s and thrusts of 20-80mN are typically observed, comparable to ion thruster systems, but the devices are complex, require significant optimisation and are subject to wear.

Hollow cathode thrusters, distinct from ion thrusters, are believed to work on the principle of production of high-energy ions, rather than the electrons normally produced within hollow cathodes. These ions are then directly accelerated through electric fields to produce thrusts of around 0.1 to 5mN at specific impulses around 500s, though very low propellant utilisation efficiencies are evident [11].

1.2.3. Experimental Propulsion Techniques

Nuclear propulsion covers systems that either initiate a nuclear reaction or use a nuclear reactor to energise a propellant. Initiation of a nuclear reaction, otherwise known as nuclear pulsed propulsion, produces thrusts of millions of Newtons or more using controlled nuclear explosions beneath the spacecraft. The ORION project, initiated in the 1950's [12], and the DAEDALUS project of the 1970's [13] both appeared to be practical solutions to interplanetary flight, however, the international moratorium on this type of propulsion has been a significant obstacle to implementation.

Nuclear thermal propulsion systems work on the principle of heating a propellant using a nuclear reactor. The ROVER and NERVA (Nuclear Engine for Rocket Vehicle Application) programs of the 1950's and 1960's [14] mimicked the dynamics of a chemical thruster by energising a propellant and ejecting it at great velocity. Systems developed as part of the ROVER program included KIWI, Phoebus, Peewee-1, and Nuclear Furnace-1. The two projects developed as part of the NERVA program were known as the Nuclear Reactor eXperiment (NRX) and the eXperimental flight Engine Prototype (XE-Prime).

Nuclear electric propulsion systems use a nuclear source to power electric propulsion systems. As the power supply for other propulsion techniques they are only a part of the entire system. Radioisotope thermoelectric generators (RITG) or nuclear reactors could be used in such a role. Radioisotope thermal generator based systems could develop hundreds of kilonewtons thrust at high specific impulses, dependent on the technology of the attached thruster, but are generally only used at hundreds of Watts to a few KW and have been neglected in favour of other systems due to safety concerns [2].

All potential photonic propulsion systems work on the principle of radiation pressure of photons incident to a surface. Photons impart momentum to an object through conservation of momentum as the energy of a photon, hv, has an equivalent

mass through $E=mc^2$. For solar sail propulsion, at 1 astronomical unit, the distance between the Earth and the Sun, solar radiation exerts a pressure of $5x10^{-6}$ Nm^{-2} which would require an extremely large solar sail for any appreciable thrust [2]. In June 2005 Cosmos-1 was launched, to be the first solar sail mission, but failure of the launch vehicle meant that it never reached orbit. Other possible novel future alternatives include using ground-based lasers or microwave lasers (masers) to provide the power. The major potential benefit of photonic propulsion techniques is the lack of propellant.

1.3. Electron Bombardment Ion Micropropulsion

Due to increasing interest in small scale, low-cost satellites [15], the relatively new field of micropropulsion has recently seen increased interest. Micropropulsion is the developing field of small scale thrusters systems designed to provide low thrusts (~mN) for low mass satellites (≤~10kg). As already stated, a number of propulsion options are generally available, though this can be limited when operating at low thrusts due to the intrinsic problems of miniaturisation. The reduction in scale of chemical thrusters has certain limiting factors. These include the ratio of heat release to heat transfer, quenching as a result of flame stretching and quenching as a result of laminar flow as turbulence is required to mix the propellants [16]. Increased heat transfer losses are due to the higher gradients in temperature as the length scale is reduced and result in lower combustion chamber temperatures. Laminar flow occurs as the Reynolds number is seen to characteristically decrease with thruster size. Increasing the flow speed to enhance turbulence results in flame stretching which can ultimately result in quenching through detachment of volumes of the flame from the orifice. Due to these shortcomings electric propulsion techniques therefore become a suitable area for study in terms of propulsion system miniaturisation.

Scaling down electric thrusters to provide micropropulsion systems is difficult. The difficulties can either be related to problems seen in any electric thruster system at any size, or problems uniquely related to the reduction in dimensions [17]. The primary

problem is that the high surface to volume ratio of small ion thrusters results in increasing plasma losses to the anode walls. Altering the magnetic field configuration can reduce these losses, creating a need for mass-efficient magnets with high fields.

The diverse techniques used in electric propulsion systems have seen wide-ranging application to the problem of thruster system miniaturisation. Low power DC Arcjets have been fabricated and tested in the power range of 2-20 watts at reasonable values of specific impulse and propellant utilisation [18]. Pulsed plasma thrusters (PPT's) have been developed for use in micropropulsion applications with specific impulses in excess of 800s and cycle lifetimes exceeding $5x10^5$ pulses [19]. A PPT is a solid state device, observed to operate at relatively high efficiencies with the benefit of solid fuel which can be stored easily and have been flight tested [20]. Field emission electric propulsion (FEEP) devices, which have the advantages of precisely controllable and continuous thrusts, have been observed to operate in the μN to mN range, measured using nulled pendulum balances [21].

Development of a viable electron bombardment ion microthruster system has been the goal of engineers from many backgrounds and countries, most notably the U.K., Germany, Brazil and the U.S. [22,23,24,25]. Models developed so far have met with limited success. A viable ion microthruster would require a minimum specific impulse of 1000s and mass utilisation efficiency of 25% and power consumptions of less than 50 watts [25]. Specific impulses and mass utilisation efficiencies levels which drop below this level reach the point where the mass savings of ion propulsion technology are no longer apparent. This applies equally when the system becomes excessively power consumptive necessitating larger power sources.

If the mass flow rate and the exhaust velocity are known and the thrust is measured, the specific impulse and mass utilisation efficiency can be defined. If the goal of 1000s and 25% are to be reached at an attainable exhaust velocity of $40kms^{-1}$, the thrust to mass flow rate ratio must be around 10000:1. Therefore a 1mN thruster should operate at a flow rate no greater than $1x10^{-7}$ kgs^{-1} or a few sccm (Standard Cubic

Centimeter per Minute, dependent on atomic mass, ~$1x10^{-7}$ kgs^{-1} for Xenon, ~$3x10^{-8}$ kgs^{-1} for Argon). It should be noted that the external neutraliser cathode emits an equal current to the extracted ions preventing the ions from migrating back to the extraction grids, which would reduce ion velocity and hence thrust.

If operation of a microthruster is to occur at these levels, operational parameters, such as mass flow rate through the system, and discharge voltage and current of the source, must be fully optimised. Further, an understanding of the underlying physics must be met.

Empirical data on larger devices can be extrapolated for use in the microthruster design if it is assumed that physics are roughly comparable at the different scales. Factors which must be considered as variables with respect to ionisation chamber design in an ion thruster are:

- The primary electron confinement length
- Total propellant mass flow rate
- Grid open area to ions
- Magnetic field strength

The primary electron confinement length is the average distance which ionising electrons cover through the chamber, and is therefore related to the probability of an ionising collision when the gas density and cross-section for ionisation are accounted for. The primary electron confinement length must therefore be maximised to ensure that the maximum number of emitted electrons interact with and ionise propellant atoms. The total propellant mass flow rate includes that through secondary feeds as well as any through the ionising source. It must be such that sufficient pressure is maintained within the chamber to give a high probability of an ionising collision between an electron and a propellant atom, and low enough to minimise propellant loss through escape of neutrals to the external environment. It must therefore be defined in relation to a number of other factors. It is linked to the grid open area to ions, which must be optimised to permit the

maximum number of ions to pass, a level which is restricted by the space-charge limit, but also maintaining the chamber pressure, minimising the passage of neutrals. The most problematic of these variables is the inverse scaling of the magnetic field, requiring successively higher fields at small chamber sizes. A chamber of 10mm diameter would require a field approaching one Tesla to confine the electrons and prevent them from migrating to the chamber walls [17]. This level of field strength is now attainable with permanent magnet technology. Smaller chambers lie outside current permanent magnet manufacturing abilities, when size and mass constrictions on the magnet assembly are considered. Fig 1.5, seen previously, illustrates the design of an ion thruster, showing magnets placed around the exterior and the extraction grid system. The first two variables discussed, primary electron confinement length and mass flow rate, scale directly with thruster length. The grid open area scales with the square of the length as it is a 2-D area, and is therefore related to length squared. The magnetic field scales with the inverse of the length as successively smaller chambers demand stronger fields to maintain the electrons in the chamber, decreasing the Larmor radius. All other parameters, e.g. gas temperature and limiting ion current density through the grids, are assumed to be invariant under scaling the size of the thruster [17].

The electron source is the key element to ionisation in an electron bombardment ion thruster. Emitters are of various designs and structures. Development of a cathode specifically adapted for use in microthrusters was deemed a suitable and profitable direction for research. Cathodes operating in electron bombardment ion thrusters must have sufficient current outputs at relatively low powers for an extended period. For existing large scale thrusters this current will typically be in the range of amps at tens of volts and must operate for thousands of hours. However, for a microthruster currents in the tens or hundreds of mA are sufficient, though operating voltages, and hence power input per electron output must be similar to that seen in existing thrusters. Several candidate electron sources for this mission were investigated: thermionic devices, field emission arrays and hollow cathodes.

Thermionic devices have seen extensive use in contact ion thrusters, since the 1960's [26]. Thermionic emission of electrons occurs from metallic materials at high temperatures, generally in excess of 1300K. Emission is a function of temperature and material work function, which can be considered as the potential barrier over which emission takes place. Properties of tungsten hairpin thermionic emitters underwent initial studies as part of this project for use as primary electron emitters in a micro hollow cathode. Milliamps of ions can be produced by electron bombardment without emitter failure but lifetime is generally low, measured in hours at pressures of $4x10^{-4}$ mBar and these devices are extremely power consumptive, operating at a minimum of several Watts. This type of device was therefore ruled out as a suitable primary electron emitter. Further, initial studies of Field Emission Arrays showed that their low output current and intolerance to pressures in excess of $\sim 5x10^{-5}$ mBar made them unsuitable to the environment of an ion thruster discharge chamber. Sputtering of the surface at high pressures caused the emitters to rapidly erode, greatly affecting electrical properties and lifetime. This type of device was therefore also ruled out as a suitable primary electron emitter.

Hollow cathodes have seen extensive use in thruster systems. Hollow cathodes are already used for spacecraft charge neutralisation, Hall-effect thrusters & Arcjets [27], space plasma simulation, material processing techniques on the ground [28] and, of interest here, electron sources for ion propulsion. The design of the cathode and the desired operating characteristics are highly dependent on the use to which it is being put. In the case of the two cathodes seen in a conventional ion thruster, used for production of either ionising or neutralising electrons, there are substantial differences, particularly in flow rate. The main discharge cathode is directly within the ionising chamber and will thus operate at much larger flow rates, as propellant flow into the chamber must be maintained. For the neutraliser, minimisation of the flow rate is desirable to prevent needless loss of valuable propellant. Further, the current demand on the neutraliser will be less than that on the main discharge cathode. This is because the neutraliser must only produce as much electrons as the extracted ion beam current, whereas a significant

number of electrons produced by the main discharge cathode are lost without ionising a propellant atom.

Current hollow cathode design is based around a noble gas flowing through a metallic tube, typically Tantalum, with an orifice, insert and keeper. The orifice can either be connected or integral to the body and is often made of a relatively low work function metal such as thoriated tungsten. The insert is a tungsten matrix impregnated with a low work function mix to promote electron emission. Hollow cathodes without inserts show poorer emission characteristics in comparison as this area is the major contributor to electron emission under optimal operating conditions. Fig 1.7 shows a cross section of a typical cathode.

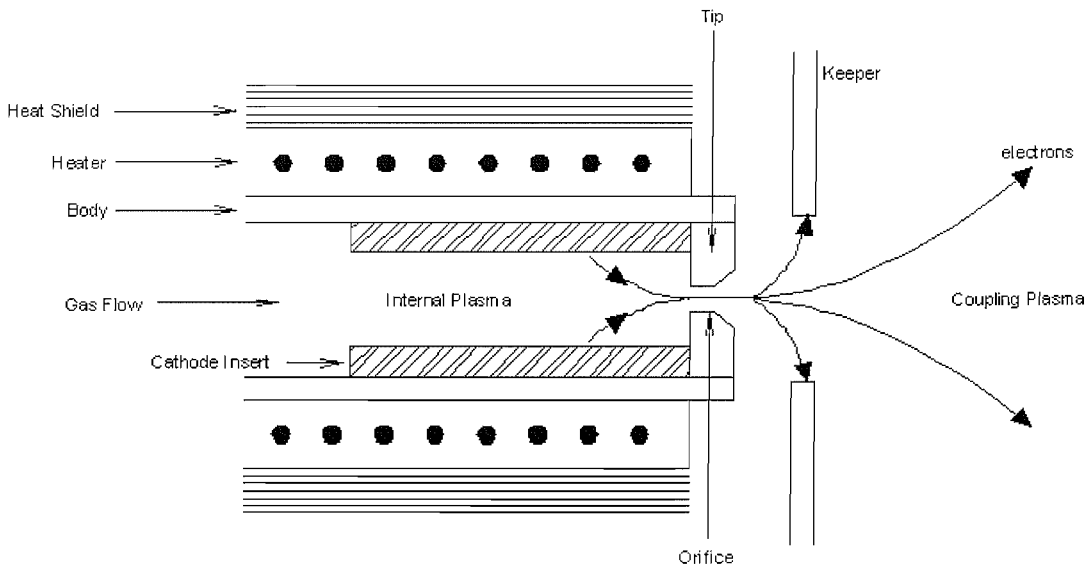

Fig 1.7 Hollow Cathode Schematic [29]

A heater is often used to initiate the discharge. This creates thermionically emitted electrons which are accelerated by the positive potential on the keeper to ionise the propellant atoms. Alternatively the discharge can be initiated purely by applying a large enough potential to the keeper to create electrical breakdown of the gas between the tip and keeper, though this will necessarily be at high flow rates.

In the main discharge chamber, an anode accelerates the electrons down the length of the chamber towards the extraction grids and prevents ions from recombining with chamber walls. The difference between the anode and cathode potentials is known as the discharge voltage. This will typically be tens of volts in an ion thruster. The plasma inside the discharge chamber is observed to be close to the anode potential [30]. When an anode is present, the keeper voltage will typically be several volts below the anode voltage. When configured without the anode, the discharge voltage will be the keeper voltage. In the case of the cathode as an external neutraliser, the ion beam acts as a virtual anode to which the electrons from the cathode are drawn. Without the ion beam, the plasma electrons will be attracted to the keeper. In this case the keeper will collect a significant proportion of the electrons and the keeper current will be the discharge current.

Hollow cathodes show a rise in current density from the confinement of electrons by cathode fields, resulting in a highly ionised discharge with large currents at low potentials [31]. Field-enhanced thermionic or Schottky emission is believed to be the main operating mechanism with potentially significant contributions from impact of excited metastable propellant atoms. The Richardson-Schottky law closely agrees with experiments [32] in predicting surface temperatures for a specific work function material, at a set level of current emission density.

Ionising discharges for space propulsion typically use electrons in the 30eV range. Some thrusters have discharge voltages of less than 21V at flow rates in excess of 2sccm (N.B. units are in SCCM to account for different gases used, primarily Xenon instead of Argon) and less than 25V at flow rates less than 1sccm for Xenon [29]. This is the discharge voltage, seen on the anode. Keeper voltages are lower, typically between 5 and 10 Volts.

The hollow cathode can operate in one of two distinct modes relating to the flow rate, current and power of the discharge. The main discharge hollow cathode will generally operate in what is known as the spot mode. This mode is characterised by its

low voltage operation and takes place at higher currents and flow rates than the plume mode. The plume mode is a high voltage mode seen at lower flow rates and currents. In the spot mode the cathode is less power consumptive for a given current and cathode erosion is reduced in comparison to the plume mode which is why the mode is preferred for cathodes used in electron bombardment ion thrusters. The voltage-current curve is a key measure of the operational characteristics of a hollow cathode. In fig 1.7 no discharge can form below the lower line. On the right side of the chart, spot mode operation is characterised by a low discharge voltage when the cathode operates at higher currents. On the left side the plume mode is characterised by high discharge voltages at low currents. Plume mode operation is highly variable and the discharge can exhibit a wide range of discharge voltage at similar currents.

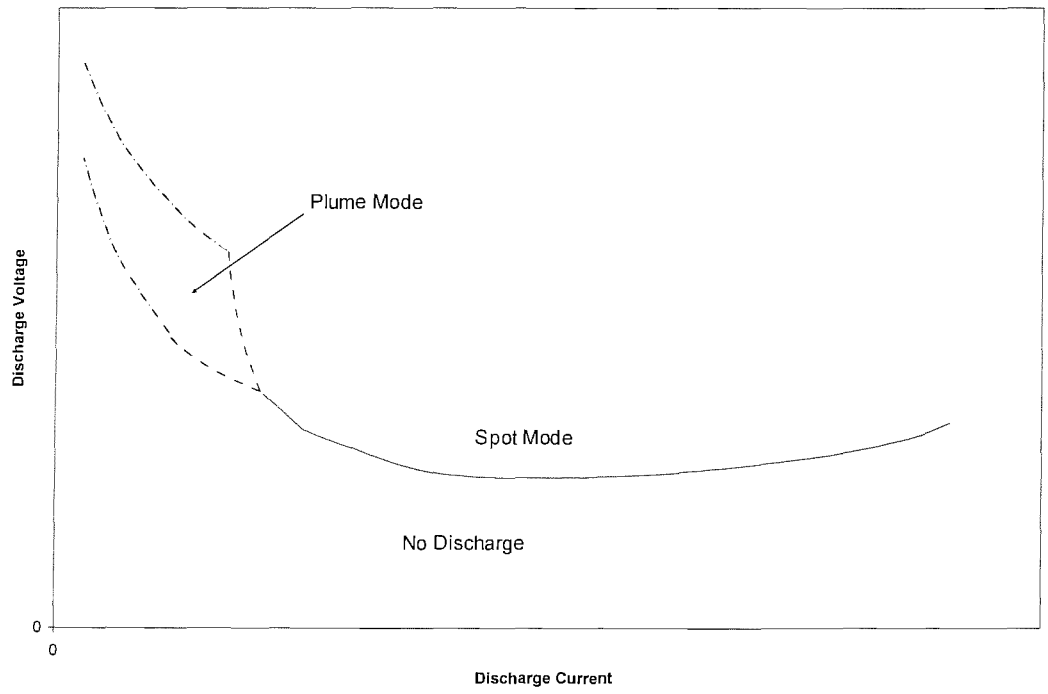

Fig 1.8 Hollow Cathode Modes

Investigations have been performed at NASA into the operating characteristics of 3.2mm external diameter orificed hollow cathodes with Xenon at low flow rates and

currents. The lowest power consumption in diode mode was 10 Watts, and the minimum mass flow rate required for spot- mode emission was approximately $8x10^{-8}$ kgs^{-1} [33].

A low-current self-heated hollow cathode has also been developed in the Ukraine, to cover the discharge current range of 0.3 to 0.5A for use in an electron bombardment ion thruster [34]. With discharge voltages of typically 16 to 35V, the main cathode has a mass flow rate of 1 to $3x10^{-7}$ kgs^{-1} Xenon. Large, at 18 mm in diameter, the lifetime should exceed 7000 hours and 10000 startups. The best initiation voltage was around 310 V.

The miniaturisation of hollow cathodes below this level, for potential application to microthruster systems requires a consideration of their operational requirements. A key factor in hollow cathode design is that initiation of a stable discharge must be a primary concern. Formation of a stable plasma sheath requires that the internal diameter of a hollow cathode must be several times greater than the Debye length, λ_D [10] as the plasma will only form beyond several times the Debye length. The plasma sheath, equal to several Debye lengths in thickness, can be considered as a potential well which confines the plasma. Debye lengths less than 10 microns are seen in discharges in the NSTAR cathode assembly inside the cathode [5].

The hollow cathode's internal geometry also effects electron emission. It has been theorised that the length of the emission region is related to the insert internal diameter [35]. The following relation illustrates this dependence:

$$I_D = J_D 2\pi r_c l_{emit} \qquad 1.5$$

Where I_D is the discharge current, J_D is the constant current density, r_c is the insert internal radius and l_{emit} is the length of the emitting region. If the orifice area multiplied by the maximum current density is below the current drawn from the cathode, erosion of the orifice will occur until these two factors balance. Other than this phenomenon there is little evidence that there is any physical difference in operational modes of the hollow

cathode dependent on scale [36]. However, geometries of the keeper electrode and orifice will have large effects on the level of applied electric field penetration into the cathode body [37,38,39]. An example of an operating micro hollow cathode is the Non-Magnetic Ion Micro-Thruster Concept (NMIMT), consisting of a hemispheric, rather than cylindrical, metallic cathode mounted on an insulator [40]. The NMIMT cathode had an exit orifice 1mm in diameter with a throughput of $3x10^{-8}$ to $1x10^{-3}$ kgs^{-1} of Argon, though typical operation took place in the 10^{-7} to 10^{-6} kgs^{-1} range. The discharge current was in the 10-15 mA range, however, discharge voltages are of the order of several hundred volts, very poor in comparison to existing large-scale cathodes.

1.4. Research Objectives

The key objective of this research project has been the investigation of innovative materials and design for potential application in micro hollow cathodes for use in ion microthrusters. The primary electron source in an electron-bombardment ion thruster makes up one of the core operational elements of such a system. Without this, ionisation cannot take place and plasma will not be generated to develop thrust. Ion microthruster systems are in development in several laboratories and universities and are extremely varied in configuration and design, using a variety of electron sources and chamber geometries [40,41]. The smallest electron bombardment ion thrusters under development today are in the 3cm diameter range [42]. However, hollow cathodes with internal inserts impregnated with low work function material, are not known to have been built at scales below 1mm external diameter. The goal of the project was to develop and investigate an electron emission device for potential use at a scale which could find application in ion microthrusters

The requirements on the primary electron emitter are the same as in any conventional Kaufman-type ion thrusters (the traditional electrostatic thruster design), except for factors introduced by the scale of the device alone. The initial requirement for a primary electron source is production of sufficient current at a reasonable power over

its lifetime. This current will be dictated by the mission itself, but a large ion thruster will typically have currents in the amp range at powers of several tens of watts, with a lifetime of thousands of hours. As this project is focused on the development of microthrusters required output currents are lower with currents of tens to hundreds of milliamps desirable, but cathode lifetime should be comparable to existing devices and further limits are placed on the mass of the device which must be small enough to be suitable for a very small spacecraft.

A micro hollow cathode was deemed the best candidate for development for application as a primary electron source in an ion microthruster. Tackled by scaling down the body and the impregnated insert beyond current limits, the miniaturisation of a hollow cathode requires novel manufacturing techniques and materials. The work making up this project should therefore be judged in the context of whether the device is novel, whether the techniques and materials used were innovative and if the final product fits the requirements of the brief. While the cathode actually fell short of the levels desired for operation in a viable thrusters system, it did operate successfully and demonstrated the potential usefulness of certain new technologies and showed that the reduction in scale of cathodes makes it increasingly difficult to obtain the desired operating characteristics.

1.5. Thesis Layout

Following this introduction, chapter 2 goes into the background of the operation of electron-bombardment ion thrusters. Initially an overview of electric propulsion systems is presented, followed by an analysis of hollow cathode technology and a final summary.

In chapter 3 a description of the design and construction of the micro hollow cathodes used in testing and some of the theory that influenced this design is presented. Some information on ancillary parts of the keeper, anode, power supply and propellant feed systems follows.

The experimental apparatus and procedures are discussed in chapter 4. This section explains the equipment used in characterisation of the cathodes, the range of experiments performed and precisely how these experiments were executed.

Chapter 5 presents the results and the analysis of the series of investigations carried out on the micro hollow cathodes. Investigations deal with initiation voltage, discharge voltage and current. The variability of these characteristics in comparison to key physical parameters of propellant flow rate, cathode design, keeper-cathode separation and device temperature are discussed.

Chapter 6 presents a summary of the major conclusions of the research, followed by a statement on the significance of the work as a whole and recommendations for future study.

Appendices are also included looking at the operational procedures followed when using the device, measurements made on the plasma potential and other plasma parameters and images of the plasma during device operation.

Chapter 2

Ion Thruster Background

Over the past two decades, space propulsion has seen many new developments and systems have been employed in a variety of roles. During this period the continuing improvements in electric propulsion devices have been seen as extremely significant. Ongoing propulsion development programs are concerned with new modes of energy production; reducing propulsion system masses; and increasing transit speed [43]. Some of these goals may be reached using ion propulsion as electric propulsion has high mass efficiency and can have extremely controllable thrust levels.

The ongoing development of small scale satellites places a requirement for viable micropropulsion systems. Little work has been carried out on hollow cathodes of very small sizes, nominally less than 3mm external diameter, for use in electron bombardment ion microthrusters and little is known about their operation. For example, problems that must be considered when developing small scale cathodes, with respect to this project, are:

- Do hollow cathodes work efficiently at such small scales?
- Can hollow cathodes with inserts be manufactured at such small dimensions?
- What materials are suitable for use as a hollow cathode inserts?

This chapter will initially cover the history and theory of electric propulsion and ion propulsion in specific. It will then go on to discuss more recent work on ion thrusters.

2.1. Plasmas and Ion Thrusters

In 1675 Robert Boyle stated that electric attraction and repulsion could act across a vacuum. The electric field itself is defined as the electric force applied per unit charge and the acceleration of a particle in an electric field is described by:

$$a = \frac{qE}{m} \qquad 2.1$$

a is the acceleration, q is the charge of the particle, E is the electric field and m is the mass of the particle.

Charged particle systems which could be accelerated by these electric fields, known as plasmas, were first identified by Sir William Crookes in 1879. A plasma is a gas in where the atomic nuclei have dissociated from one or more of their electrons, or been ionised. As such, plasmas behave in a different manner to neutral gases, notably in the presence of electric and magnetic fields. Since 1879 the field of plasma physics has seen considerable growth especially after the development of radio broadcasting resulted in the discovery of Earth's ionospheric plasma.

In 1906 Robert H Goddard proposed that plasmas could form a type of electric propulsion system for spacecraft. In this case ionised particles are accelerated by electric fields and hence imparted with momentum. The ions are then expelled from the body of the device, producing thrust. The Thrust, T, is expressed as:

$$T = \eta_u . \dot{m} . V_{ex} \qquad 2.2$$

η_u is the mass utilisation efficiency of the propellant, $\dot{m}$ is the mass flow rate and V_{ex} is the exhaust velocity.

It was not until the early 1960s that ion propulsion was actually investigated, by a team at NASA Lewis Research Centre, headed by Harold Kaufman [26]. In these tests, the first broad-beam electron bombardment ion thruster was operated [26]. The first successful ion thruster flight was in 1964, a sub-orbital mission called SERT I. When SERT II flew an extended mission in 1970 it paved the way for development from existing Caesium and Mercury propellant thrusters to modern Xenon, Argon & Krypton designs [44].

Current designs of ion thrusters use one of two configurations, dependent upon the ionisation technique. The first utilises electron-bombardment ionisation of the propellant. In this case a source bombards the propellant gas with electrons, stripping the propellant atoms of one or more of their constituent electrons. Cathodes developed for this method of ionisation can also be used as beam neutralisers. A beam neutraliser is a cathode exterior to the thruster body which emits a number of electrons with total charge equal to the extracted ion current. This neutralises the space-charge of the plasma, maintaining thrust by preventing it from returning to the extraction grids and also stops sparking between surfaces of the spacecraft, caused by potentials between different components in the spacecraft.

Electron bombardment ion thrusters generally have a long lifetime and designs have been extensively flight-tested. Lifetime tests of the ETS-6 ion thruster have exceeded 20,000 hours [45] and a redesign of the chamber decreased the discharge voltage to less than 35V, producing 23.9mN at a specific impulse of 2740s [45]. ESA's SIMONE (Smallsat Intercept Missions to Objects Near Earth) project [46] may use a carbon-gridded T5 ion engine which has a specific impulse of 4500s. In tests for ESA's GOCE mission (Gravity Field and Steady-State Ocean Circulation Explorer), the thruster is expected to exceed 30,000 hours operation at a constant thrust of 18mN, and has an operational range of 5 to 25mN. The T5 thruster hollow cathode has been operated on

timescales in excess of 15000 hours, requiring a tip temperature less than 1500K to prevent early failure of the device. [29]. Above 1400K other cathode types have demonstrated dramatic drops in lifetime due to changes in emitter chemistry [47]. Discharge currents for the T6 cathode ranged from 1 to 30 A at Xenon flow rates from $1x10^{-8}$ to well in excess of $1x10^{-7}$ kgs^{-1}. Developed to produce a thrust of over 150mN it is a hot-start device with a 7mm external diameter with a keeper voltage less than 10V and a final discharge voltage in the 20 volt range [29,48].

The second type of ion thruster ionises the propellant by application of a radiofrequency discharge in the absence of any electrodes. A radiofrequency generator provides the power to an induction coil surrounding a discharge chamber made from an insulator (e.g. quartz). This induces an electrical eddy field, sustaining the discharge. Eddy fields are produced by a varying magnetic field which creates a toroidal electric field inside the discharge chamber, creating electrical 'eddy current' flow, with the strength of these eddy currents dependent on the conductivity of the material. Optimisation of chamber pressure, plasma generator radiofrequency output, coil geometry and chamber geometry is necessary to attain viable operating conditions [22]. In their favour, RF ion thrusters require less power supplies and flow control units in comparison to electron bombardment types. They also have relatively few doubly charged ions and the problems that these can introduce. These two methods of ion production are therefore subject to their own unique advantages and disadvantages. Radiofrequency based ion thruster systems have been under development for over thirty years and have been flight tested on the EURECA and ARTEMIS missions and are under consideration for further use in other ESA missions [49]. Microwave plasma cathode electron guns have also been developed for charge neutralisation of ion beams as well as generating the ion beams themselves [50]. Small amounts of feed gas and a microwave coupling system can be used to operate the two in conjunction [50].

Another type of microwave discharge thruster has recently come into use, where the plasma is generated using Electron Cyclotron Resonance (ECR). In conventional microwave discharge thrusters ion energy costs were high due to poor coupling between

plasma and microwaves. ECR was seen as a way of improving efficiency. In a uniform magnetic field electrons orbit this field at the cyclotron frequency, ν_c:

$$\nu_c = \frac{qB}{2m} \qquad 2.3$$

q is the charge of the particle, m is its mass and B is the magnetic field. The small number of free electrons in the neutral gas in the thruster chamber will orbit the field lines at this frequency. By tuning the frequency of a microwave discharge to coincide with the cyclotron frequency energy can be efficiently supplied to the electrons. These electrons can then ionise atoms to produce more electrons. In 2003, the Hayabusa mission (formerly MUSES-C) to collect a surface sample from an asteroid, using an ECR thruster system, was launched. This type of thruster should demonstrate long lifetimes due to elimination of cathode erosion. The major disadvantage seen in ECR systems is the relatively low thrust densities. The quoted thrust density for thrusters used on MUSES-C is 1.02 Nm^{-2} [51] while 1.27 Nm^{-2} is seen on the conventional ion thruster on DS-1. Also, ECR technology is only known to have been used in larger devices (MUSES-C uses 10cm diameter thrusters), which are unlikely to prove suitable for micropropulsion in the immediate future.

2.2. Electron Bombardment Ion Thruster

Electron bombardment ion thrusters are comprised of several systems necessary for their operation (see fig 1.5):

- Ionising source
- Magnetic containment
- Ion extraction and acceleration Grids
- Beam neutraliser
- Propellant feed system

The ionising source provides electrons which produce ions through collisions which strip electrons from the propellant atoms. Diverse techniques can be used to create the electrons and maximise their path length through the discharge chamber, covered in the following sections.

Magnetic fields in ion thrusters greatly increase the overall performance of the device. By forcing the electrons to orbit the magnetic field lines, the path length through the thruster can be increased, improving the likelihood of an ionising collision. The Larmor radius, r_L, also known as gyroradius or cyclotron radius, defines the radius a charged particle circumscribes in an orbit in an applied magnetic field:

$$r_L = \frac{mv}{Bq} \qquad 2.4$$

Where m is the particle mass, v is the particle velocity, B is the magnetic field in Tesla and q is the particle charge. The electrons Larmor radius must be significantly smaller than the diameter of the ionisation chamber to contain ions and electrons, preventing them from impacting the walls. A ring-cusp magnet configuration, where a series of small magnetic cusps are established radially and linearly down the chamber, is the most efficient magnetic cusp design for a Xenon electron-bombardment ion source. This configuration generally operates at low mass flow rates and low discharge currents. Benefits are operation at lower potentials, giving a longer lifetime and higher propellant utilisation efficiencies than other designs [37].

At the downstream end of the thruster, highly charged grids are used to accelerate the ions to velocities between 30 and 100 kms^{-1}. Child & Langmuir [52] presented the mathematical model describing the maximum current density, J_+, of charged particles in an electric field, which can be applied to the extraction grids:

$$J_+ = \frac{4\varepsilon_0}{9}\left(\frac{2e}{m_i}\right)^{1/2}\frac{V_p^{3/2}}{d_1^2} \qquad 2.5$$

ε_o is the permittivity of free space, e is electron charge, V_p is the applied potential and d_1 the ion acceleration distance, approximately equal to the grid separation. The ion velocity will obviously increase in the area of the acceleration grids in the pre-sheath region and between the grids. This will increase the ion Larmor radius, however, applied grid voltages can be used to contain the ions and the separation in common two or three grid systems is small enough that deviation from the ion beamlets between grids is minimal.

A screen grid, on the interior of the discharge chamber is kept near the cathode potential, This attracts ions from the discharge plasma, reducing the number of neutrals near the grids which would be lost. After extraction, ions are accelerated over a large voltage drop, typically around 1000V, by the second acceleration grid. A final decelerator grid at ground potential focuses the beamlets and prevents ions from streaming back to the accelerator grid. Multiplying the maximum current density through the grids with the grid area, A_G, and the grid open area to ions, ϕ_I, gives the beam current, I_b:

$$I_b = J_+ . A_G . \phi_I \qquad 2.6$$

This can in turn be related to equation 2.2 describing the thrust of an ion thruster systems used to calculate the potential thrust of an ion thruster accelerator system:

$$T = \eta_u . \dot{m} . V_{ex} = I_b . \left(\frac{m_i}{e}\right) . V_{ex} \qquad 2.7$$

It can be seen that the mass utilisation efficiency multiplied by the mass flow rate is equal to the beam current multiplied by the ion mass over the electronic charge. Both cases are equal to the extracted mass of ions. If a potential microthruster were to operate at low range values of mass utilisation efficiency and exhaust velocity of 25% and 40kms^{-1}, the beam current to thrust ratio becomes apparent. This differs for propellant types due to the differing ionic masses. For Xenon, 1mN of thrust will be generated for every 18.4mA of ions extracted, for Argon, the same thrust will require 60.4mA of ions.

The value of the applied voltage between electrodes of the accelerator system must be below the Paschen minimum at specific values of the pressure-distance product. Above this threshold arcing will occur between the extraction grids, causing significant damage to these components and preventing the steady ion beam output seen under other conditions.

The beam neutraliser is an electron source external to the spacecraft. Designed to prevent charging of spacecraft surfaces, it produces a plasma from which an electron flux equal to the beam current. This ensures the ions in the beam are not attracted back to the grid and balances the buildup of negative charge resulting from the expulsion of positively charged particles by the thruster. Beam neutralisers conventionally take the form of a hollow cathode on the outside of the ion thruster.

A propellant feed system is necessary to control flow rates of the gas into the discharge chamber of the ion thruster and in any hollow cathodes used as electron sources. The gas flow into the discharge chamber may be entirely through a hollow cathode, or supplied through separate feeds. As hollow cathodes generally operate more efficiently at higher pressures, it is advantageous to supply the discharge chamber propellant through the cathode in small thrusters. Flow rate can be controlled either through varying upstream pressure, where the geometry and temperature of gas feeds will determine the flow rate, or through dedicated mass flow controllers.

Each of these systems is important in its own right and each must be balanced to attain optimum operating conditions. The ionising electron source, which can also double up as the beam neutraliser, is a particularly interesting component due its active role and the large scope for variation in its design.

2.2.1. Electron Source

The electron source is used to produce the plasma through ionisation and is therefore an essential component of the thruster. There are three main electron source types which may be used to generate the plasma, each with its distinct benefits and shortcomings:

- Hot filaments
- Field emission arrays
- Hollow cathode sources

Each of these devices shall be introduced here then discussed separately. Hot filaments emit thermionically and are simple and relatively robust. Their disadvantages lie in their high input energy per electron and their relatively short lifetime when operated at high pressures. A high input energy per electron reduces electrical efficiency. Relatively high pressures in ion thrusters are desirable as high thrust densities can be developed and electrons are more likely to undergo an ionising collision.

Field emission arrays (FEAs) work on the principle of electrons tunnelling through a potential barrier when emitted from a substance. This effect takes place under the action of intense electric fields. FEAs are relatively energy efficient devices and are being used in a variety of fields including, for example, mass spectrometry and imaging technology. However, it is evident that these too do not work well at the higher pressures necessary in ion thruster systems without extensive degradation due to destruction of the array elements through sputtering.

Hollow cathodes work by initiating an electrical discharge from a low work function tube, heated and filled with a 'seed' gas, which can also be used as the propellant. The keeper, acting as the anode to the hollow cathode, has an orifice causing the electrons produced in the cathode body to be transported out of the system with some velocity. Hollow cathodes can exhibit a negative-resistance relationship where at increasing currents a reduction in discharge voltage is observed, making them efficient plasma generators. The hollow cathode has seen extensive use in a number of applications including spectral lamps, lasers, radiation standards and space propulsion [53]. Fig 1.7, previous, shows a schematic of a hollow cathode.

2.2.1.1. Thermionic Emission Devices

Thermionic emission was first discovered in 1873 by Professor Frederick Guthrie when he found that in a vacuum, a negatively charged red-hot iron sphere would lose its charge. The loss of charge is caused by the emission of electrons with enough thermal energy to overcome the electrostatic forces which otherwise confine the electrons to the body. Applications of thermionic emission include cathode ray tubes, x-ray sources, amplifiers and plasma sources. Metal filaments have seen widespread use as thermionic emitters. Many materials have been used, with Tungsten the most widespread, though a viable alternative is Lanthanum Hexaboride.

The Richardson-Dushman equation describes thermionic emission current density in terms of cathode temperature and work function [54,55]:

$$J_{Th} = A_R T_C^2 \exp\left(-\frac{e\phi}{kT_C}\right) \qquad 2.8$$

J_{Th} is the thermionic emission current density, A_R is the Richardson Constant ($1.2\text{x}10^6$ Am^{-2}), T_C is the cathode temperature, e is the electronic charge, and k is the Boltzmann

Constant. The work function,ϕ, is the energy required to liberate an electron from the surface of the emitter.

2.2.1.2. Field Emission

The processes involved in field emission, where electrons are emitted under the action of intense electric fields, were first described by Fowler and Nordheim [56] in the 1920s. Field emission, or Fowler-Nordheim tunneling, is the emission of electrons which quantum tunnel through a potential barrier in the presence of a high electric field.

Fowler and Nordheim modelled the current density around a field emitting tip as a function of the emitting material's properties and the electric fields present around the tip. The resulting Fowler-Nordheim equation for current density is the field emission equivalent of the Richardson-Dushman equation [54]:

$$J(FN) = A'\left(\frac{E_C^2}{\phi}\right)\exp\left(-B'\frac{\phi^{3/2}}{E_C}\right) \qquad 2.9$$

A' and B' are constants, E_C is, as in the case of thermionic emission, the electric field at the cathode and ϕ is the work function of the material.

Many field emitters are in the form of sharp tipped cathodes with an anode, with a central orifice, above. These have been developed as single devices and more recently in arrays where reasonable output currents over long periods can be expected. The electric field associated with an emitting cone, with an open gate at a positive potential above it, is described by [57]:

$$E_C = \frac{V_{Gate}\left[\left(\frac{\pi}{\ln(k_g a_g / a_s)}\right) - \tan^2 \beta\right]}{a_s} \qquad 2.10$$

V_{Gate} is the potential on the gate electrode above the field emitter, a_g is the radius of the gate, or hole, around the emitter, a_s is the radius of the tip of the emitting cone, k_g is a geometrical factor, estimated at between 4 and 20 and β is the angle of the cone.

In the same case as thermionic emission, the energy required to liberate an electron from the cathode surface is known as the work function. The barrier is lowered only under a strong electrostatic field [17] and the Fowler-Nordheim equation describes the current density. The quantum nature of the emission mechanism means that the tunnel probability can be derived using the time independent Schrödinger equation. The density of the electric field is dependent on both the applied voltage and the geometry of the array. The emitter material, applied voltage and array geometry therefore determine the total electron flux.

2.2.1.3. The Schottky Effect

The "Schottky Effect" is the combination of field and thermionic emission mechanisms and lies directly between the two. In this case the material must be at a temperature to emit electrons thermionically and also emit under application of an electric field. In the case of microtip arrays Schottky emission is evident in that the tip apices are subject to field emission, while the sides of the tips discharge electrons thermionically [54]. Rewriting the Richardson-Dushman current density equation for thermionic emission in terms of field-enhanced Schottky emission gives:

$$J_S = J_{Th} e^{0.4389\frac{\sqrt{E_C}}{T_C}} \qquad 2.11$$

E_C is the electric field at the cathode surface and T_C is the temperature of the emitting surface. This equation is derived by replacing the work function term in the original Richardson-Dushman equation with the effective work function. The effective work function, ϕ_{eff}, accounts for the effect of local electric fields on the normal work function of the surface, ϕ.

$$\phi_{eff} = \phi \pm \sqrt{\frac{eE_C}{4\pi\varepsilon_0}} \qquad 2.12$$

ϕ is the work function in eV, e is the electronic charge, E_C is the electric field at the cathode and ε_0 is the permittivity of free space. The sign of the square root term is dependent on the direction of the potential. Electron emission is therefore increased when the surface is at a negative potential and suppressed when positive. The work function of Tungsten is 4.4eV, for Tantalum it is 4.25. Minimising ϕ_{eff} by using low work function materials and intense electric fields will therefore promote emission increasing the current density for a given cathode temperature.

An example of a thermionic emitter that makes use of the effect of compressed electric fields on work function is the Tungsten hairpin gun. The Tungsten filament acts as a cathode, heated through application of a voltage. An anode, positive with respect to the filament, accelerates electrons toward itself under electrostatic forces. The hairpin also emits electrons anisotropically with a bias towards the direction that the hairpin is pointing.

The hairpin design exhibits increased brightness in comparison to tungsten cathodes where electrons are emitted from the entire surface equally, rather than preferentially from the sharp tip of the hairpin. This is a result of increased emission currents due to higher electric fields seen at the cathode surface. At high electric fields the combination of thermionic and field emission is known as the Schottky effect [58].

2.3. Hollow Cathode Electron Sources

The hollow cathode was first developed by Paschen in 1916 [52]. At its most basic, a hollow cathode is a tube of metal with a seed gas passing through it, at a negative potential to an upstream anode, known as a keeper. Electrons emitted from the tube interior and tip ionise and excite atoms in the discharge, resulting in intense radiation and high current densities – the Hollow Cathode Effect.

More complex designs use internal high-emission inserts impregnated with low work function materials and even heater systems to lower discharge initiation voltage. To improve hollow cathode operation in terms of increased output currents at a specific discharge voltage, and lower initiation voltages, a range of variations to the design can be made, covering:

- Cathode Body
  - Materials
  - Geometry
- Insert
  - Materials
  - Chemical impregnant type
  - Ratios of impregnants
  - Geometry
- Keeper
  - Geometry
  - Configuration: 'open' or 'closed'[1]
- Propellant
  - Type
  - Flow rate
- Heater
  - Materials
  - Geometry
  - Output Power
  - Thermal Insulation

[1] In a closed configuration higher gas densities are maintained around the cathode tip by creating a small cavity between the cathode and keeper

The discharge in a hollow cathode results from confinement of a negative glow discharge to a cavity. The electrical field distribution builds a positive potential well resulting in highly accelerated electrons emitted from the surface. At low currents a hollow cathode generally operates in the Townsend mode, where increasing discharge current requires a consequent increase in discharge voltage, with an axially dominant electric field. At higher currents the transfer to the hollow cathode discharge, where increasing discharge current lowers discharge voltage, is accompanied by a radially dominant electric field in the cylindrical cathode fall. The sheath, or cathode fall, is the region separating the plasma from the cathode and has a high variation in the electrical potential. Fig 2.1 shows the interior of a hollow cathode near the exit orifice, with the arrows representing electron movement

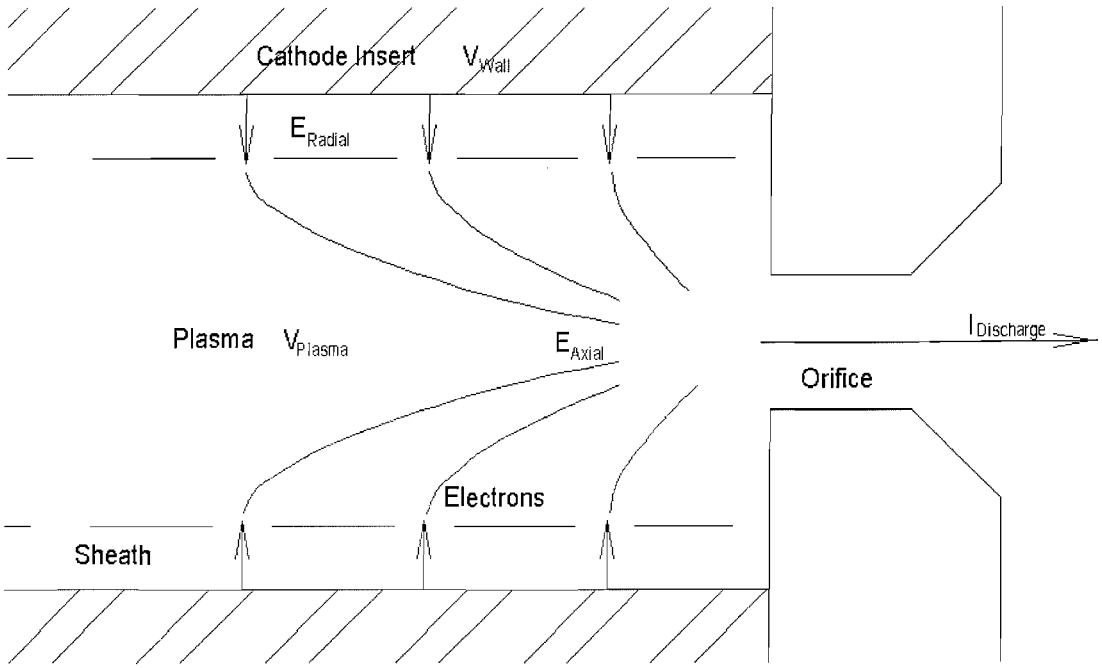

Fig 2.1 Hollow Cathode Internal Geometry

The dense internal plasma allows the thin sheath between the plasma and wall to sustain high electric fields. The high field at the emitter surface enhances the electron emission current. Further increases to the current may also result from ion bombardment of the surface. The axial field in the hollow cathode discharge is small [59] and acts as a virtual anode. Studies of this relationship have shown that Hollow Cathode discharges

are more efficient than plane cathode discharges [60] because of enhanced secondary emission processes and contribution from ionisation processes to the discharge [60].

Currently there are many types of hollow cathode under development. These include a replacement for the system tested on Deep Space 1 and a 40cm NSTAR derivative [61]. NASA has also developed a variety of cathodes covering the range 100mA to 100A [62] in a range of tube diameters (e.g. 1/2", 1/4", 1/8"). The purpose of varying hollow cathode design is to increase lifetime and efficiency and to further understanding of the underlying physics limiting operational lifetimes of the devices [63].

2.3.1. Discharge Initiation

In 1889, Freidrich Paschen set out a principle of electrical breakdown of gases which has become known as Paschen's law. Paschen's law states that electrical breakdown for a given gas type in a gap is dependent on the product of the gas pressure and gap length, though pressure should be replaced by gas density for a more accurate measure.

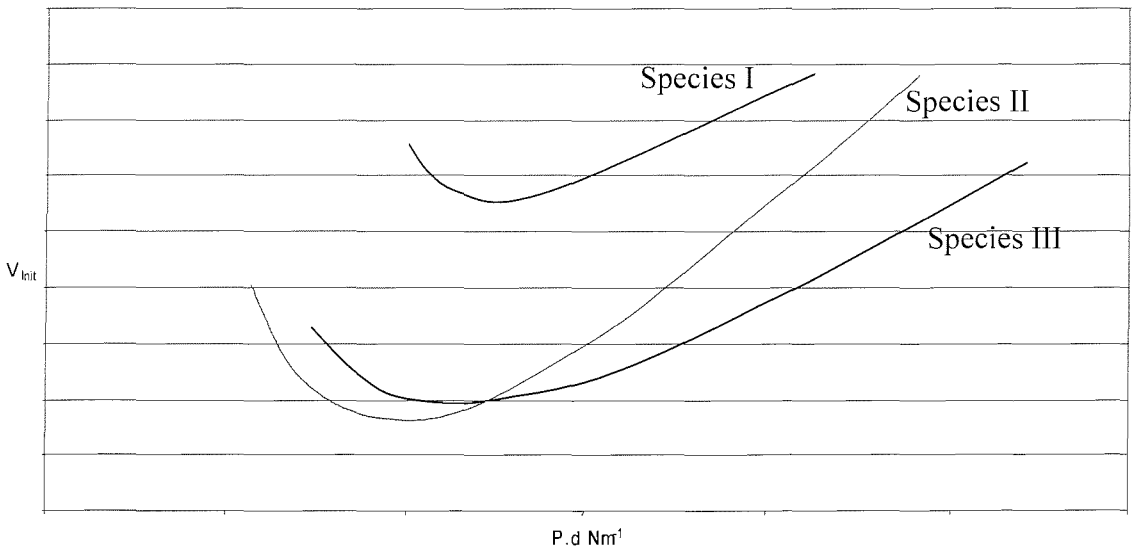

Fig 2.2 Example Paschen Curves [52]

Fig 2.2 shows the relationship between breakdown, or initiation voltage and the pressure-distance product, axes are logarithmic. Examples of the type of different Paschen curves for different gases are shown. However, Paschen's law has limits, in that it cannot be applied to non-planar geometries due to variations in the electric field and varying cathode-anode distance. Factors such as surface irregularities, gas flow and radiation further alter the breakdown voltage (UV radiation can be used to initiate a hollow cathode discharge). Theoretical analysis to determine breakdown voltage is therefore extremely difficult; sophisticated computer models are continually being developed and improved in this area. Note that for successful cathode discharge initiation, the device must first be allowed to outgas sufficiently. Exposure to air, causing oxidation of free Barium in the insert, will raise the initiation voltage, though only temporarily [29].

2.3.2. Discharge Voltage & Current

Hollow cathodes are generally operated in a constant current mode with variable discharge voltages. Electron flux is therefore maintained while electron energy is seen to vary. The voltage-current relationship is the primary measure of cathode performance at a given mass flow rate and can exhibit negative resistance, where an increase in current corresponds to a lowering of the discharge voltage. Non-linear in nature, it is influenced by a number of factors, including:

- Electric fields
- Cathode geometry and materials
- Gas pressure & flow conditions
- Cathode & gas temperature
- Gas species
- Sputtering & multiple ionisation

Hollow cathodes operate in one of two modes, each with different voltage-current characteristics. It is believed that in the spot mode the electron flux purely from the cathode surface sustains the internal plasma [35]. The spot mode takes place at low discharge voltages and exhibits low fall voltages. At low flow rates and low currents the cathode will operate in the plume mode. In this mode, it is believed that the electron flux from the cathode surface is insufficient and secondary emission of electrons through ionisation is necessary to maintain the discharge. The plume mode produces more multiply charged ions and is therefore undesirable due to the erosion this causes. Fig 1.7, previous, shows an example of the voltage-current characteristic for a hollow cathode at a constant mass flow rate. At lower currents the cathode operates in the plume mode and can show a high variability in the discharge voltage different measurements made under the same conditions. Spot mode operation shows more regular operation from test to test. However, it is still extremely difficult to theoretically predict the discharge voltage of a hollow cathode due to its dependence on the full range of operating characteristics of the device at a given current and flow rate. Measurements of the discharge current of a hollow cathode, I_D, can be used to gain a greater insight into the operating conditions of the device. The discharge current is the electron current minus the ion current and is described by the following expression:

$$I_D = I_e - I_i \qquad 2.13$$

The output electron current is related to the overall electron flux, Ω, through:

$$\Omega = \frac{I_e}{e} \quad es^{-1} \qquad 2.14$$

where I_e is the electron current and e is the electronic charge. This allows a calculation of electron number density, n_e, in the cathode interior, using:

$$n_e = \frac{\Omega}{A_{int} v_{Avg}} \quad em^{-3} \qquad 2.15$$

combining 2.14 and 2.15 gives the electron current in the cathode orifice:

$$I_e = en_e A_{\text{int}} v_{Avg} \qquad 2.16$$

A_{int} is the cathode internal cross-section, upstream of the orifice. In the cathode interior the Maxwellian velocity is applicable. The Boltzmann equation states kinetic and thermal energies of particles are comparable, giving:

$$v_{Avg} = \sqrt{\frac{8kT_e}{\pi m_e}} \qquad 2.17$$

Multiplying electron number density, the interior cross-sectional area and average electron velocity with the electronic charge e gives the electron output in Amps. The average electron temperature can thus be defined through the Boltzmann equation from equation 2.17 which becomes:

$$T_e = \frac{\pi m_e v_{Avg}^2}{8k} \qquad 2.18$$

m_e is the mass of an electron, k is Boltzmanns' constant and v_{Avg} is the linearly averaged electron velocity. Therefore, knowledge of the cathode geometry, electron number density and temperature can allow a determination of the expected electron current. T_e can be derived using measurements on the plasma by a Langmuir probe. A Langmuir probe is an electrode inserted into a plasma, also used to make measurements on electron and ion number density, electron energy distribution, plasma potential and floating potential. In a T5 thruster cathode with an internal diameter of 1mm, an electron temperature of 4000 to 6000K (~0.5eV) was observed [64]. The electron number density was believed to be around 10^{19} m^{-3}. Dividing the current by the emitting area gives the current density, in this case just above $5x10^5$ Am^{-2}. Investigation of the markings on

cathode interiors made by ion bombardment over long periods at constant current are believed to show the extent of the internal plasma and emission area, and agree well with the current densities in this range [64].

2.3.2.1. Electric Fields

Hollow cathodes are subject to a combination of intense electric fields. The major contributor to high field strength in the cathode is the plasma potential. The plasma potential, V_{Pl}, is the equilibrium point where the loss of ions and electrons from the plume are balanced [55,65]. In essence the plasma plume builds up a positive charge as electrons are lost faster than ions, to a point where ion and electron loss is balanced by the potential of the plume. It is believed that the plasma potential is equal throughout the plume in the spot mode, and varies dependent on position in the plume when in the plume mode; plasma potentials seen in hollow cathode discharges can vary from several to several hundred volts [55,65].

Contributions from processes such as secondary electron production due to ion impact and the photoelectric effect are not easily accounted for, and could alter sensor measurements on the plasma. The plasma potential is known to fall rapidly downstream of the keeper in the plume mode [35]. In the spot mode, the plasma potential, and thus electron temperature, is invariant within the plasma. As a result, measurements of plasma potential are independent of sensor position. The sensor, a Langmuir probe, is positively charged due to the electron's mobility, making them leave the plasma at a greater rate than ions. This can be used to determine ion and electron behaviour and other plasma properties [55,65]:

$$V_{pl} = V_{fp} - \frac{kT_e}{2e} \ln\left(\frac{\pi}{2}\frac{m_e}{m_i}\right) \qquad 2.19$$

V_{fp} is the floating potential, the negative potential which builds up on an electrically floating surface in contact with a plasma. It can be measured and relates to the electron temperature through [66]:

$$V_{fp} = -\frac{kT_e}{2e}\ln\left(\frac{m_i T_e}{m_e T_i}\right) \qquad 2.20$$

m_e and m_i are the electron and ion masses, T_e and T_i are the electron and ion temperatures.

The dependence of discharge current and hence the voltage-current relationship, on electric fields can be seen in the equations for thermionic (in the effective work function term), field and Schottky emission. The electric field at the cathode surface in contact with the plasma is given by [65]:

$$E_C = \frac{-dV}{dx} = -\frac{4}{3}\frac{V_F}{\lambda_D} = -\frac{4V_F}{3}\left[\frac{n_e e^2}{\varepsilon_0 kT_e}\right]^{1/2} \qquad 2.21$$

It can be seen that the electric fields in a cathode are dependent on the Debye length, λ_D, and the fall voltage, V_F. The $^4/_3$ factor comes from the Child-Langmuir law which gives the maximum current density in a region also in terms of voltage over a given distance between electrodes. However, the actual field at the cathode surface will be modified to some extent due to variations in electron emission and ion retention in the sheath.

The fall Voltage, V_F, is the difference between the cathode and plasma potentials. Only electrons with energies in excess of the fall voltage can reach the cathode surface, travelling across the cathode sheath. The fall voltage reaches a minimum when the electron flux from the cathode surface is high [10], seen in the spot mode. An empirical formula for operation of a hollow cathode in the spot mode was developed by Kaufman and Rehn [35]:

$$\frac{\dot{m}e\sigma_{ion}\sqrt{W}}{r_{or}m_i} \geq 2.78x10^{-17} \qquad 2.22$$

This equation demonstrates the spot mode's dependence on mass flow rate, $\dot{m}$, the species' cross-section for ionisation, σ_{ion}, the molar weight, W, the ion mass, m_i, and the radius of the orifice r_{or}. Hence, under the same conditions, smaller orifices can improve device performance as the minimum condition for spot mode operation is reached at lower flow rates. However, smaller orifices are often subject to erosion problems [35]. Equation 2.22 illustrates the effect of geometry, flow and gas species on hollow cathode characteristics.

The Debye length is central to understanding plasma interactions as it represents the distance over which a charged particle exerts electrostatic effects. Electron mobility in a plasma causes a state of quasi-neutrality as the electrons move to balance charge. Above the Debye length, this shielding effect prevents any electrostatic interaction between particles. Formation of a plasma requires that its dimensions are large in comparison to the Debye length. As stated, the Debye length is the dimension over which charged particles screen out electric fields in plasmas and other conductors. The Debye length is therefore the minimum distance over which significant charge separation can occur. The potential drop across the plasma sheath is known as the fall voltage. Only electrons exceeding this can reach the cathode wall, causing the partition of the plasma from the surface. Alfven stated that "In a low density plasma, localised space charge regions may build up large potential drops over distances of the order of some tens of the Debye lengths. Such regions have been called *electric double layers*. An electric double layer is the simplest space charge distribution that gives a potential drop in the layer and a vanishing electric field on each side of the layer" [67]. The length over which the potential drop from the plasma potential to the potential of the cathode insert occurs is therefore somewhere in the region of 5 to 10 times that of the Debye length. The Debye length must therefore be less than 10% of the internal diameter of the cathode and orifice to form a stable plasma column. The full expression for the Debye length is:

$$\lambda_D = \sqrt{\frac{\varepsilon_0 k T_e T_i}{e^2 n_e (T_i + Z T_e)}} \qquad 2.23$$

T_e is the electron temperature, T_i is the ion temperature, n_e is the electron number density and ε_0 is the permittivity of free space, k is the Boltzmann constant and Z is the ion charge. In a hollow cathode discharge, the electron temperature, T_e, is far in excess of the ion temperature, T_i, which can be neglected. This expression then reduces to:

$$\lambda_D = \sqrt{\frac{\varepsilon_0 k T_e}{e^2 n_e}} \qquad 2.24$$

High electron temperatures and/or low electron number densities therefore result in larger Debye lengths. The Debye length must be kept relatively low, a necessity for plasma formation within any low diameter cathode. The internal pressure (or mass flow rate) must therefore be kept high, to give a small electron mean free path and low electron temperature, below 1eV.

2.3.2.2. Cathode Geometry and Materials

Electric fields are influenced by the cathode-keeper geometry and electron emission is dependent on the emitting materials. Electric field penetration into the cathode will be highly dependent on the geometry of the cathode and keeper. Further, surface irregularities and reactions taking place here will cause local variation in the electric field and orifice and insert geometries also play a significant role as smaller orifices result in lower discharge currents due to limits on the effective maximum current density within the orifice [68]. The cathode geometry will also affect initiation voltages due to the effects of enhanced electric fields between non-uniform areas of the cathode and keeper.

The materials used to fabricate a cathode also alter electron emission through their work function. Examples of work functions of some materials that may be used in hollow cathode construction are given in table 2.1.

Material	Work Function, ϕ, eV
Tungsten	4.4
Molybdenum	4.5
Tantalum	4.25
Carbon	5
Impregnant Mix	1.6-3.77

Table 2.1 Work Functions of typical cathode materials

As stated previously an impregnant is used in the cathode interior to promote electron emission by reducing the work function. The variation of the work function of the impregnant mix is due to the different work function of its constituent compounds, and their variation under different electrochemical processes. Impregnants typically use a mix of $BaCO_3$, $CaCO_3$ and Al_2O_3, typically with around a 4:1:1 ratio. During impregnation and operation the impregnant undergoes a series of reactions to form a variety of oxides and free elements from the initial mix which will alter work function significantly. This will be further affected by the relative amounts of the initial compounds.

2.3.2.3. Gas Pressure and Flow Conditions

The density and flow rate of the gas in a hollow cathode will significantly affect the operating conditions of the device. Lower pressures result in higher discharge voltages, especially apparent at low currents [69]. The complexity of motion of neutral and charged particles in hollow cathode devices is the fundamental obstacle to understanding the underlying physics [70]. This is compounded by the problems of analysis of motion

at such small scales. However, as a first approximation charged particles can be considered to be uniformly spherically diffuse within the ionisation chamber of the thruster [71]. This lack of understanding is especially apparent at smaller scales.

There is a localised high drift velocity within the hollow cathode orifice followed by a sharp drop in pressure downstream [70]. This means that modeling the pressure and flow in the region between the cathode and keeper is very difficult. The orifice is a choke point [72] which reduces flow rate; the mass flow rate can be defined as:

$$\dot{m} = \rho_{or} u_{or} A_{or} \qquad 2.25$$

Where ρ_{or} is the density at the upstream side of orifice, A_{or} is the orifice area and u_{or} is the flow velocity at the orifice. The density at the orifice is given by:

$$\rho_{or} = \frac{P_{or}.W}{R.T_0} \qquad 2.26$$

Where P_{or} is the pressure inside the cathode, W is the molar weight, R is the universal gas constant and T_0 is the temperature of the gas. The velocity at the cathode orifice is defined by the Maxwellian energy distribution, seen in equation 2.18. Increased gas temperatures in the plasma, near to the orifice will decrease the density and raise the velocity [73]. However, the ideal gas law can be used as a first approximation as it can be assumed to be valid for neutral gas particles and has been used as the basis for monte-carlo simulations on gas flow [74,75]. Under conditions where the amount of ionisation is low, this approximation is even more likely to be acceptable.

2.3.2.4. Cathode and Gas Temperature

Emission current is affected by the temperature of the cathode and, at very high or low values, the feed gas. Variations are a result of the temperature dependence of the

thermionic emission mechanism, the pressure in the emission region, affecting reactions which contribute to emission and, to a small extent, the contribution to ionisation by through heating the feed gas.

The level of thermionic emission is determined directly by the cathode temperature. Cathode wall temperature also determines the atomic movement in the discharge and hence pressure in the emission region. Predicted and empirical models have shown that atoms move at a mean thermal velocity dependent on the wall temperature, not appreciably altered by other atomic interactions [76]. However, the pressure dependence of reactions at the emitting surface is difficult to quantify. Heating the feed gas can also increase the energy of the propellant atoms to result in increased ionisation, though this is very small unless temperatures of thousands of degrees are reached.

2.3.2.5. Gas Species

The gas used in a hollow cathode discharge will have a considerable impact on the operational characteristics of the device and of the thruster as a whole. Xenon designs are widely used due to its suitability for use in the hollow cathode and as a propellant gas for use in the discharge chamber. This is due to its relatively low ionisation potential, large cross-section for ionisation, relatively high mass and ease of use. Equation 2.22 shows that spot mode operation in hollow cathodes is dependent on both mass and ionisation cross-section. Alternatives with somewhat similar attributes are Argon and Krypton. However, due to their lower atomic masses and higher ionisation potentials they are less efficient in terms of energy cost per ion and number of ions required to maintain a specific thrust in comparison to Xenon. Further, Argon and Krypton are more difficult to store on a spacecraft but are significantly less expensive and are therefore suitable for initial ground-based tests [77].

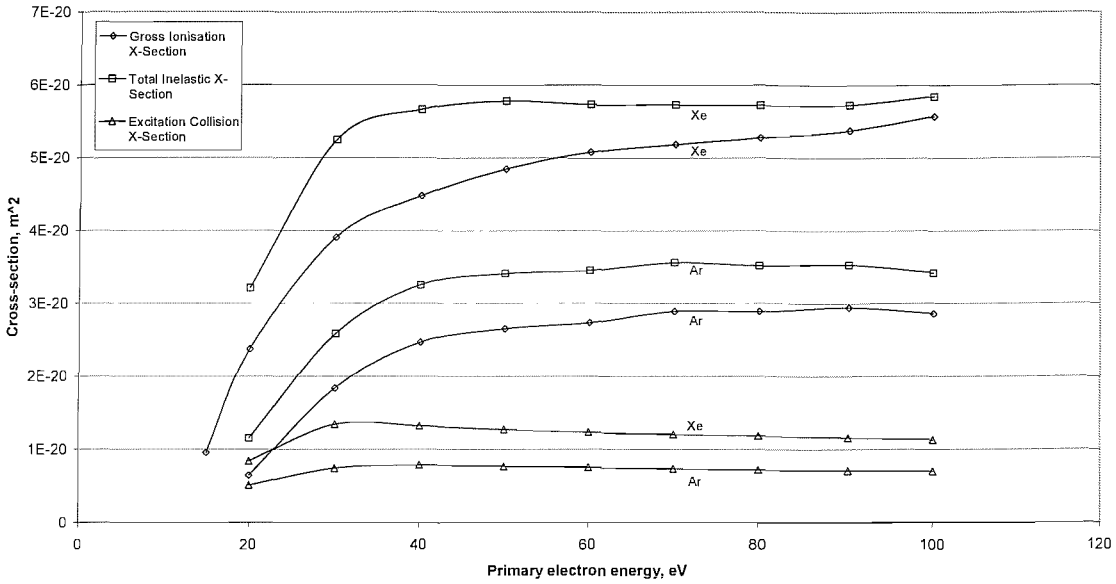

Fig 2.3 Xenon and Argon Cross-Sections Vs Primary Electron Energy [78]

Fig 2.3 shows the cross-sections of atoms for collisional processes in an ion thruster. The gross ionisation cross-section is the most important to hollow cathode operation. A high ionisation cross-section is desirable to maximise the ionisation efficiency, minimising the electron mean free path. However, the detrimental effects of multiply charged species (erosion and loss of momentum per electron-ion pair in the ion beam) are evident at the higher energies where the ionisation cross-section is high itself.

The gross ionisation cross section for Argon and Xenon varies by a factor of between two and four between 20 and 50eV and the optimum range lies between 40 and 100eV [78]. This means that a balance between the discharge voltage and the ionisation cross-section must be attained which minimises energy input per ion and multiple ionisation. Discharge voltages are therefore typically set to operate at lower levels to avoid excessive multiple ionisation. Applied discharge voltages 2 to 4 times the first ionisation potential of the propellant are typical [79].

Fig 2.4 shows the ratio of total ionisation cross-section to the total inelastic cross-section as a function of electron energy. This ratio should be maximised to reduce the

energy loss per ion to other collisional processes. However, it must also take account of the total ionisation cross-section such that mass utilisation efficiency is maximised.

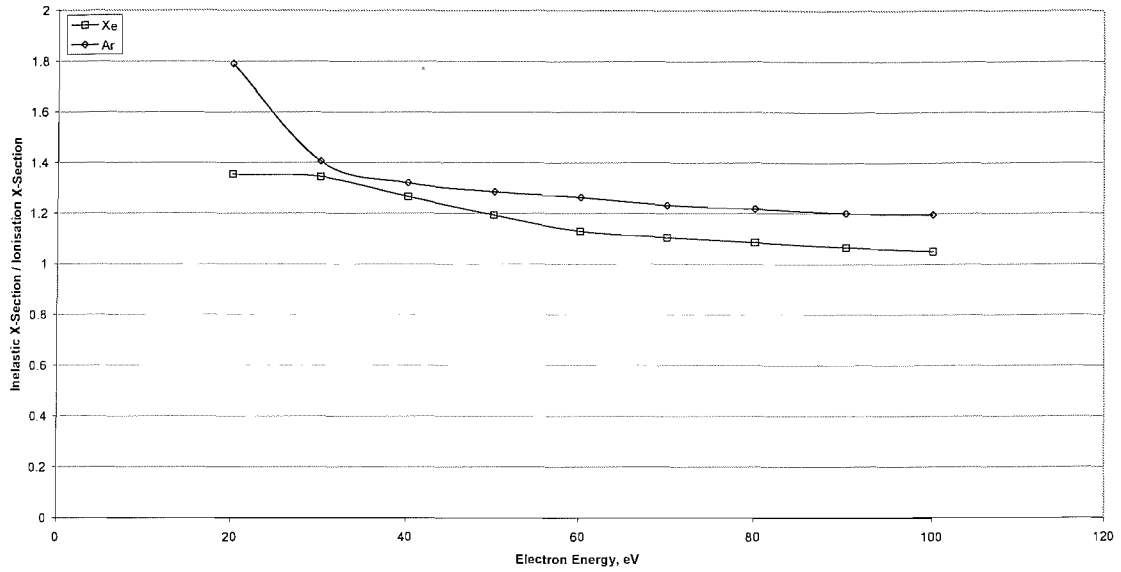

Fig 2.4 Ratio of Total Inelastic Cross-Section to Ionisation Cross-Section as a function of primary electron energy [78]

2.3.2.6. Sputtering & Ionisation

Sputtering is the displacement of atoms from a substance through the transfer of momentum from ion impact [80]. This interaction between an incident particle and the target creates a series of reactions, primarily dependent on the incident particles energy. These reactions are [81]:

- Backscattering
- Thermal equilibriation and evaporation
- Excitation followed by emission or alteration of chemical properties
- Atomic displacement (sputtering)
- Radiation damage at high particle energies

Sputtering causes erosion induced failure of the cathode and extraction grids. Damage from sputtering is the primary factor in decreasing ion thruster lifetime. The rate of sputtering is determined by a number of factors, the most important of which are:

- Atomic mass of incident species
- Atomic mass of target species
- Current density
- Target voltage (i.e. energy of incident particles)
- Chamber pressure
- Multiple ionisation of incident particles
- Angle of incident particles to surface

As a function of the atomic mass of both incident and target species, the ratio of energy transfer to initial incident particle energy is described by [81]:

$$Ratio(E_{Trans} : E_{Inc}) = \frac{4 m_{Tgt} m_{Inc}}{(m_{Tgt} + m_{Inc})^2} \qquad 2.27$$

E_{Trans} is the energy transferred to the target, E_{Inc} is the incident particle energy, m_{Tgt} is the mass of the target atoms and m_{Inc} is the mass of the incident atom or ion.

The minimum energy threshold for sputtering was initially thought to be equal to the atomic heat of sublimation, $U_{sublimation}$, divided by the above ratio, but was later shown to have two different expressions dependent on the ratio of target atom to incident atom masses. A definitive expression was later proposed by Yamamura et al [81]:

$$E_{Threshold} = U_{Sublimation}\left[1.9 + 3.8\left(\frac{m_{Tgt}}{m_{Inc}}\right)^{-1} + 0.134\left(\frac{m_{Tgt}}{m_{Inc}}\right)^{1.24}\right] \qquad 2.28$$

High current densities, corresponding to high power levels and hence high cathode currents and discharge voltages result in increased rates sputtering. A decrease in the discharge current or voltage shows a corresponding reduction in sputtering due to the reduction in ion density or energy [81]. High target voltages also increase the energy of the impacting ion, again resulting in increased rates of sputtering.

High chamber pressures result in increased ion densities, increasing the sputter rate. However, increased scattering due to denser gas reduces the energies of the ions decreasing the overall increase to sputter rate due to increased ion densities.

The degree of ionisation defines the number of ions produced as a function of the total throughput of neutrals. When $n>>n_i$ α, the degree of ionisation, approximates the ratio of ions to neutrals. The degree of ionisation is high at large ion currents if multiply charged ions and the neutral flux are small in comparison. Essentially, if the ion current is large at low flow rates, and ions are generally singly charged, then the degree of ionisation must be high.

The degree of ionisation can be determined using information on the ion saturation current and flow conditions. The normal definition of degree of ionisation, or fractional ionisation, is the ratio of the electro or ion density to total neutral density i.e. 100% means full ionisation where all the neutrals have been ionised. The ion current is given by:

$$I_i = \frac{Ze\dot{m}n_i}{m_i(n_i + n_0)} \qquad 2.29$$

Where Z is the charge on the ion, $\dot{m}$ is the mass flow rate of the feed gas, m_i is the ion mass and n_i is the ion number density. The ion number density divided by itself plus the neutral number density, n_0, is a measure of the degree of ionisation, α:

$$\alpha = \frac{n_i}{n_i + n_0} \tag{2.30}$$

Where n_i is the ion number density and n_0 is the neutral number density. This can be rearranged to give the ion number density:

$$n_i = \frac{\alpha}{(1-\alpha)} n_0 \tag{2.31}$$

The ion current can therefore be written as:

$$I_i = \frac{Ze\dot{m}}{m_i}\alpha \tag{2.32}$$

Multiple ionisation, when Z >1, is a major contributor to sputtering and is an undesirable process as it results in increased erosion of thruster surfaces. Double ionisation is generally a result of a two-step process (neutral to singly charged, then singly to doubly charged). Single step processes, from neutrals directly to doubly charged ions, become more substantial in plasmas with high electron temperatures (T_e) and primary electron energies (E_e), greater than 5 and 30 eV respectively [82]. For Xenon, the first ionisation potential is approximately 12eV, Argon is higher at 15.7eV. The second and third ionisation potentials of Argon lie at 27.63 and 40.74 eV. The ratio of doubly charged to singly charged atoms for both gases is modelled by the following equation [37]:

$$\frac{n_{++}}{n_{+}} = \frac{F^{++}V_{Pl}}{\sqrt{2}A_{pe}} n_{pe} K \frac{(eV_D - \phi_2)}{[T_0(e/m_i)]^{1/2}} \tag{2.33}$$

n_{++} is the number of doubly charged atoms, n_+ is the number of singly charged atoms, V_{Pl} is the plasma potential, n_{pe} is the primary electron density, A_{pe} is the primary electron collection area, and is dependent on the chamber geometry, T_0 is the neutral

temperature, V_D is discharge voltage, ϕ_2 is the 2nd ionisation potential of the propellant, e is the electronic charge, m_i is the ion mass and F^{++} and K are constants.

The value of this equation should be as low as possible to prevent erosion. Measurements have observed an increase in the ratio of doubly to singly charged ions in a thruster plume at increased discharge currents at a constant discharge voltage, and at increased discharge voltages at a constant discharge current [83]. Discharge current and voltage must therefore be optimised to reduce the production of multiply charged species.

Other factors, such as the presence of background gases in the vacuum chamber increase the lifetime of sputter-affected components. This is due to absorption of these gases which buffer affected surfaces. At sufficiently high pressures these surface compounds themselves are sputtered, it is therefore desirable to ensure minimal amounts of contaminants (e.g. N_2, H_2O, O_2 & C_2N_2) are present as they will affect lifetime calculations [81, 84]. These problems make a lifetime analysis by calculation extremely difficult. Empirical methods must therefore remain the main method of determining flight suitability [81, 85].

The sputter yield is the number of atoms ejected from a surface per incident ion. This can be altered by modulation of the magnetic field, resulting in an increased likelihood of ions striking the cathode surface, or altering the power level, which changes the ion incidence angle due to electrostatic repulsion between the ions [84]. The angle of incidence is important as atoms that impact directly onto the surface sputter less than those at high angles of incidence, which interact with a large area of the cathode surface as they impact across it. Sputtering will therefore increase erosion of the cathode and may also cause the deposition of a thin film of the sputtered atoms onto cathode surfaces which may be detrimental to operating parameters in the longer term.

2.3.3. Hollow Cathode Design

Hollow cathodes have been tested in a variety of configurations, using an array of materials, geometries, potentials and flow rates. Hollow cathode bodies are conventionally made from tantalum with tungsten tips, however, other substances such as Molybdenum and lately Niobium have been tested with success [86]. Thorium impregnated orifice plates are often used on the downstream end of the cathode to reduce work function in the emission region and hence increase electron flux, but in this case sputter erosion can increase by as much as a factor of three [87].

Impregnated inserts form an important part of hollow cathode emission devices. Developed by R Levi in 1955 [88], impregnation of hollow cathode inserts lowers the work function of the surface during cathode operation. In conventional designs, the mix of Barium Carbonate, Calcium Carbonate and Aluminium Oxide is imparted into a sintered tungsten matrix. This is due to tungsten's high operating temperatures. Other high temperature materials can be easily substituted e.g. Molybdenum and Tantalum. Electron production is enhanced by this impregnation as the work function of the surface is lowered. It is believed that microfilaments of metal form in the matrix from the impregnant constituents, and emit large amounts of electrons, up to the space-charge limit [64]. These microfilaments could form under the action of heating, oxide impurities and photon interaction. Closer to the exit orifice, higher temperatures allow more extensive production of barium and barium oxide from the matrix, promoting electron production. However, the production of these substances limits overall cathode lifetime, as some are lost in the gaseous phase [40, 89]. This implies that operating power is significant in determining cathode life. In an inert gas hollow cathode, the propellant flowing over the surface generally has a pressure of a few mBar. This small, but significant pressure hinders the loss of gaseous material actively produced at the insert surface during operation. This promotes further chemical reactions at the emitter surface which could alter output. Further, ion bombardment and the large thermal gradients can be seen in this type of cathode, not apparent in other designs [89], making

the analysis and development of a comprehensive model describing these factors extremely difficult. Table 2.2 lists the melting temperatures of the materials that make up a conventional impregnated insert hollow cathode.

Material	T_{melt}, K
Al_2O_3	2326
BaO	2196
CaO	2853
Mo	2896
W	3695

Table 2.2 Melting points of impregnants and other cathode materials [64]

Initially the impregnant is implanted into the insert as a barium carbonate, calcium carbonate and aluminium oxide mixture, in a 4:1:1 ratio. Ratios of 5:3:2 and 3:1:1 have also been used successfully. Heating this mixture initiates a decarboxylation reaction converting the carbonates to oxides - $BaO:CaO:Al_2O_3$. These are reduced in turn, under strong electric and thermal gradients reducing the work function at the insert surface. Hollow cathodes not impregnated with oxides require greater initiation and discharge voltages overall.

A keeper acts as the anode for the hollow cathode discharge. It takes the form of a positively charged disc downstream of the cathode with a central hole in line with the cathode orifice. The keeper can be configured to be entirely free of the cathode body or can be connected to it by an insulator maintaining the seed gas at a higher pressure between the keeper and cathode (closed keeper). For experimental purposes an open keeper configuration is easier to use as the keeper cathode separation can more easily be measured and altered as required. However, enclosed keeper configurations exhibit lower discharge voltages and decreased temperatures at a constant current [90] implying an improvement in discharge efficiency. A disadvantage is that minimum flow rates are observed to increase [91]. Note that below a threshold value for flow rate it has been observed that hollow cathodes erode rapidly [92] presumably due increased production

of multiply charged ions in the plume mode. Enclosed keeper configurations have increased the output current of an Argon operated hollow cathode by up to 70% [28].

The initiation voltage of hollow cathode discharges can be lowered from several hundred volts to several tens of volts by using a heater to increase the temperature of the cathode body and insert. The temperature must be high enough that thermionic emission of electrons from the cathode occurs. Cold start cathodes require higher initiation voltages than heated cathodes. Designs in use include devices with discharge currents in the range of 0.3 to 25A at mass flows of 0.1 to 0.8 mgs^{-1}, and ignition timescales of 1 second [40, 93].

2.3.4. Micro Hollow Cathodes

Ion thruster development programs in the proposal stage at NASA call for hollow cathodes with output currents of 100mA to 100A [28] manufactured from refractory metal alloy bodies. The development of micro hollow cathodes at and below the low end of this scale is an ongoing process with several obstacles. The main obstacles are:

- Erosion; seen in all hollow cathode discharges, but magnified at smaller scales due to lower flow rates
- Discharge initiation; heaterless ignition is generally desirable due to mass and space saving and ease of construction at small scales
- Debye length; If the plasma sheath, several Debye lengths thick, is too large the plasma cannot penetrate the cathode interior
- The mechanical problems associated with any micromachining project, exaggerated when dealing with very hard materials such as tungsten

Larger diameter hollow cathode bodies allow lower emission current densities [94] and hence lower wall temperatures, reducing erosion and increasing cathode

lifetime. However, if the discharge current is limited this effect can be moderated in smaller devices.

Initiation voltages for the T6 cathode when heated to between 900 and 1300°C at a flow rate in the region of $1x10^{-6}$ kgs^{-1} are in the region of 50V when using Argon as the propellant gas [95]. Initiation voltages at lower flow rates and temperatures will therefore be significantly higher.

NASA's efforts in the development of micro hollow cathodes is focused on continued work on a 3.2mm diameter orificed hollow cathode in both keeper-less and open keeper geometries [28]. This model, when used for neutralisation, uses Xenon at a flow rate of 0.6sccm as a seed gas and operates at 80mA and 200mA, at keeper powers of 8.4W and 4.8W respectively. An example of a micro hollow cathode in laboratory use is a non-impregnated steel cylinder with an internal, side fitted anode and an orifice diameter of 1mm. This design has been employed in the analysis of metastable spectral states of Xenon as a vacuum ultra-violet (VUV) source. Operated with Xenon as a seed gas at 5-80 mBar, it has been specifically designed for a large visible plasma column length, but is inappropriate for use as an electron source for ion propulsion applications [98]. Other micro hollow cathodes, for use as excimer lamps have been developed from mica separated electrodes with low diameter orifices ~100μm. However, this design lacks both inserts and heaters influencing performance and exhibits discharge voltages in excess of 200V, with initiation voltages of around 800V at extremely high pressures (~400 mBar) and efficiencies of less that ten percent for discharge currents of 20mA [99]. In comparison to existing cathodes used in space-based applications this device's performance is therefore poor and it could not be applied to any viable propulsion system.

To manufacture small scale devices, such as micro hollow cathodes, microfabrication techniques must be employed. Conventional cathode materials, such as tungsten, are notoriously difficult to machine. Novel micromachining techniques and materials must therefore be employed to produce such devices.

2.4. Summary

The employment of ion thruster systems in space is becoming more and more diverse. Use of electric propulsion as the primary propulsion system for space missions was first performed with Deep Space-1 [44]. An extremely successful platform for testing new technologies, DS-1 has shown the viability of ion thruster technology. Roles currently at the proposal stage include: comet nucleus sample return; Titan explorer; Venus & Mars sample return missions; Neptune orbiter; Europa lander; and the Saturn observer [100]. All of these will employ large ion thruster systems. However, research is also being conducted into the role of micro-ion thrusters for Earth-orbital and planetary missions [100].

Electron bombardment ion thrusters are made up of a variety of components necessary for their operation. These systems are all based around producing, containing and accelerating a plasma at the highest possible efficiency. Ion thrusters and particularly hollow cathodes have been investigated in many configurations. Work has been extensive in terms of the effects of propellant, keeper configuration, dimensions and insert properties. Little has been done on evaluation of micro hollow cathodes, research mainly being restricted to those of millimeters in diameter [28].

After fifty years of proposed theories no definitive hypothesis has emerged and the physics of these devices are still poorly understood, though a number of emission mechanisms are known to take place. The Hollow Cathode effect's rise in current density is ascribed to the confinement of electrons by cathode fields. This creates a highly ionised discharge capable of large currents at low potentials [31]. The dominant mechanism in electron emission from hollow cathodes is field-enhanced thermionic, or Schottky emission. This is borne out by the fact that the Richardson-Schottky law agrees closely with empirical data [32] in predicting cathode surface temperatures for a specific work function material at a specific current emission density. Studies currently in progress significant to hollow cathode design include [100]:

- Modeling plasmas within thruster system
- Sputter erosion damage to components
- Failure analysis
- Cathode development
- Adapting current systems to micro and macro roles

Aside from ionising sources for electron bombardment ion thrusters, hollow cathode assemblies are used in a number of applications. These include spacecraft charge neutralisation, Hall-effect thrusters, arcjets [101], low temperature space plasma simulation and materials processing techniques [28].

Other possible applications of this technology are the cleaning and etching of microcircuits and sputter deposition of thin films. Also the fact that hollow cathodes have been seen to produce significant amounts of high-energy ions has fuelled recent interest in using hollow cathodes as stand-alone thrusters.

During the progress of this project several questions will have to be answered about ion thrusters and hollow cathodes. Scaling and the current state of design of micro hollow cathodes shall be considered as well as the problems of manufacturing small scale inserts and what materials can be used in manufacturing hollow cathodes. It is hoped that the project will allow development of a micro hollow cathode suitable for use in an ion microthruster.

Chapter 3

Micro Hollow Cathode

This research project has been focused on the design, fabrication and test of a miniature hollow cathode. The design was based around adaptation of existing technology with several key developments, in size, geometry and materials. Fabrication required employment of novel techniques to produce components at small scales. The design and fabrication of the entire hallow cathode system is described in the following sections.

Testing took place in a vacuum system with suitable controls and diagnostics commissioned with the micro hollow cathodes specifically in mind. Analysis of the performance of the developed devices was carried out using current, voltage, temperature, flow rate and plasma potential measurements on the cathode and discharge.

3.1. Micro Hollow Cathode Development

The development of an impregnated insert micro hollow cathode was the primary research goal of this project. The development of this form of device has substantial benefits, especially apparent after a significant amount of testing on other low mass and volume electron emission devices showed poor performance in several key areas. The

largest obstacle in other electron devices was the production of a plasma at low voltages in a high pressure environment, such as the ionisation chamber of an ion thruster.

Hollow cathodes currently in use, while not extraordinarily heavy (of the order of 10 to 100 grams), could be lightened to make miniature thrusters more mass efficient. Also, as quite sizable devices, they would profit from volume reduction in some applications. In many cases hollow cathodes are extremely expensive and can be many thousands of pounds. Application of off-the-shelf parts (body and ferrule), batch processing of inserts and cold-start capability, making a heater system unnecessary, could make cathode production relatively inexpensive.

The device developed in the course of this project is novel in several aspects. The size of the device is many times smaller than current models of impregnated insert cathodes available for ion thruster systems (e.g. 3.2mm external diameter NASA devices). Other cathodes developed at such a scale are the NMIMT and the mica-separated type [40,102]; these are simple cathodes and have exhibited relatively poor performance. The materials used in the construction of the device are also original; Molybdenum is used for the body in place of the more common tantalum as it is available in prefabricated tubes of the desired size. The insert is made of a powderblasted carbon-carbon matrix, not known to have ever been used in such an application and impregnated with a barium carbonate, calcium carbonate, and aluminate mixture. Benefits of the carbon inserts include its high open volume fraction for impregnant uptake, its resistance to wear and easy fabrication. Layers in a graphite matrix (graphenes) are good conductors, the randomly oriented graphite matrix will therefore also meet the requirement that the insert is a conductor. Also the use of an orifice turned from pinching the external body, rather than a plate with a central hole, is not known to have been tested before allowing much greater ease of construction.

The most significant difference is likely to arise from the altered internal chemistry of the device. The use of carbon instead of tungsten as the insert material will alter the reactions taking place at the surface of the insert. In a tungsten matrix dispenser cathode (a low work function impregnated porous plug) the barium oxide forms a dipole with the tungsten, where the oxygen in the oxide forms a layer over the tungsten, leaving a positively charged barium layer on the exposed surface [103]. This effect makes extraction of electrons from the surface easier, significantly lowering work function from 4.5 to around 2eV. The same effect is thought to occur at the surface of impregnated insert hollow cathodes [104]. In the case of a hollow cathode, metallic barium is believed to form microfilaments which emit copiously to the space-charge limit [64] and formation of tungsten oxides eventually prevent transport of barium oxide to the surface limiting lifetime.

Another type of cathode known as the oxide cathode is made of similar materials but has a significantly different emission mechanism. Oxide cathodes exhibit low work functions, at around 1.3-1.5 eV, and therefore start emitting at low temperatures, around 800°C. In an oxide cathode a barium-strontium carbonate layer is painted or sprayed onto a nickel surface [105]. Electrons are emitted from donor sites created by oxygen vacancies from reduction of the barium oxide matrix. The oxygen vacancy acts as an electron trapping site, at which point the electrons can be more easily emitted due to changes in the energy band structure, with electrons inhabiting the conduction band at these sites [106]. Oxidisation of these vacancies on the surface decreases emission. Oxygen, carbon dioxide water and sulphur all annihilate the vacancy and are thus undesirable. Carbon monoxide is not seen to have an effect on emission.

In a conventional hollow cathode the oxygen in the barium oxide reacts to produce solid oxides of tungsten from the matrix. These accumulate and are thought to eventually block the flow of Barium Oxide to the insert surface [89]. In the case of the carbon matrix hollow cathode it is not known how the impregnant would react with the carbon. The graphite could be oxidised to produce metallic barium and carbon monoxide (under oxygen starved conditions atomic oxygen will typically produce

carbon monoxide rather than carbon dioxide). The potential loss of carbon in a gaseous phase may also cause increased erosion in the device leading to early failure, but could also improve barium transport to the surface as byproducts will not block pores. Alternatively the device could act as an oxide cathode, with oxygen vacancies being produced in the matrix promoting emission. Another event potentially altering the level of electron output could arise from arcing between matrix grains at differing potentials, which is known to occur in graphite matrices. Experiments should therefore show whether carbon is a suitable substitute for tungsten in the impregnated matrix, and what performance can be expected from a carbon insert.

The majority of ion thrusters use xenon as a propellant, but other inert gases, such as krypton and argon can also be used. Xenon performs the best in almost every category; it has a lower breakdown voltage and first ionisation potential, a higher cross-section for ionisation and a higher atomic mass, which is generally desirable to increase momentum transfer per ion. The major disadvantage is the high cost of Xenon, which is produced as a byproduct of the oxygen separation industry. It is therefore advisable to conduct ground and life testing using cheaper alternatives such as Argon, Krypton and Kr/Xe mixes at the naturally occurring ratio [107]. These other gases, while not as good performers as Xenon, do demonstrate the relative performance of the device. They can be used to benchmark the device and may even be suitable for use in certain applications where cost is a major factor or where exhaust velocity has to be maximised (which is proportional to the inverse of the square root of the propellant mass) [107].

The final design was divided into four prototypes of three available formats, the last and most complex of which had two models built for comparison, and redundancy in case of failure. The overall schematic for the final impregnated insert device is shown below, while each variation is described in the following subsections. Dimensions are the same throughout the various models.

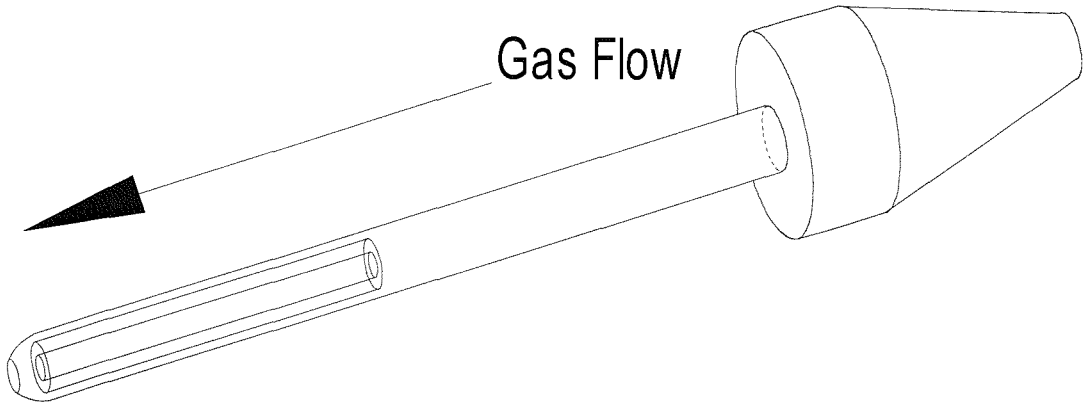

Fig 3.1 Outline Schematic of developed micro hollow cathode – Not to Scale

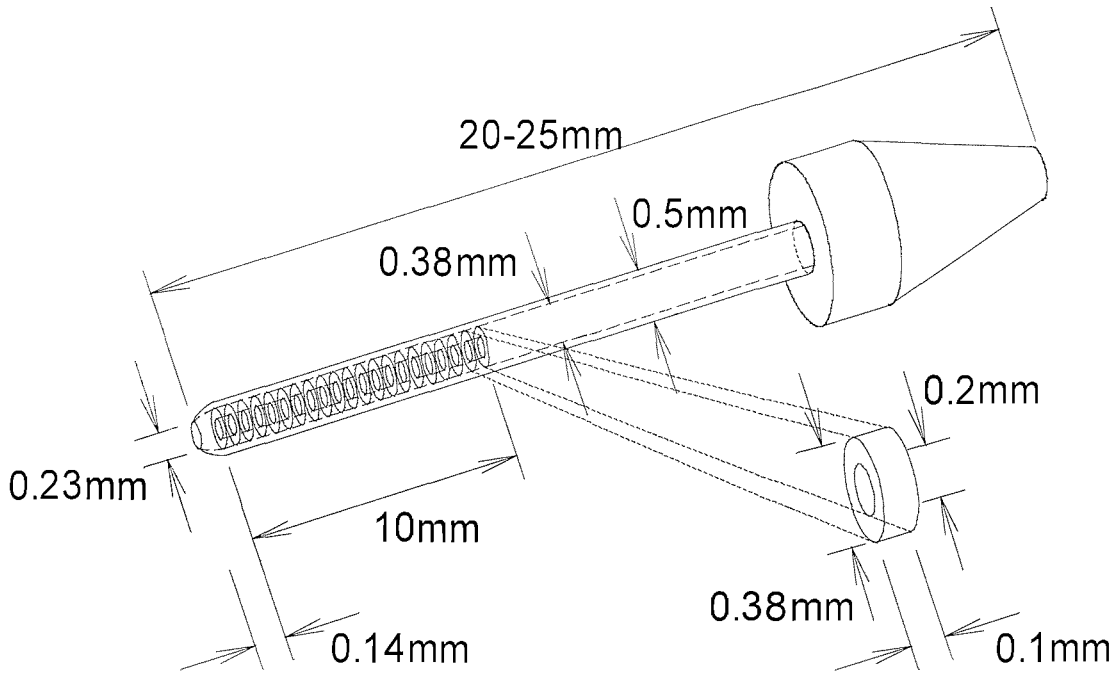

Fig 3.2 Schematic of developed micro hollow cathode including dimensions and insert array – Not to Scale

It was believed that the impregnated carbon matrix would enhance electron emission, though the mechanism of emission could not be easily predicted or

subsequently measured. The dimensions of the device should also allow formation of a plasma within the cathode body. Assuming an electron number density of $3x10^{18}$ m^{-3} and an electron temperature of around 10^4 K (typical in existing cathodes) [91], the Debye length is 3.9μm, well below the internal radius of the micro hollow cathode designed, necessary for plasma formation. Even if the number density and electron temperature diverge from these values, formation of a stable plasma column is still likely as differences would have to be considerable for the Debye length to approach a significant fraction of the internal radius of the cathode.

3.1.1. Simple Molybdenum Body

The first micro hollow cathode developed as part of this project was a molybdenum tube turned at one end to create an orifice. It was developed as a precursor to the surface impregnated and impregnated insert cathodes, primarily to be used to test the operation of the electrical and mass flow systems, as well as to provide an initial benchmark against which the performance of later models could be compared.

The upstream end was placed in a ferrule and connected to a swagelock mount. Initial flow tests suggested an amount of leakage around the ferrule. All subsequent models were therefore sealed using Rocksett high temperature sealant between the body and ferrule, suitable for use in vacuum systems and usable up to around 1300K. This device was then compressed in the swagelock mount whilst still wet to further reduce leakage and ensure that seal between body and ferrule did not fracture during fitting.

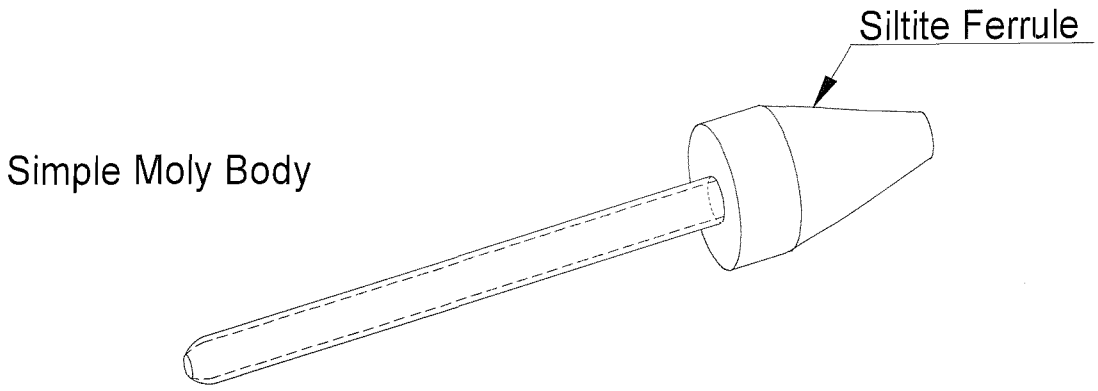

Fig 3.3 Molybdenum body with ferrule

The 0.5mm external diameter, 0.38mm internal diameter Molybdenum tube was cut into four pieces of 25mm length. Each was turned at one end to provide an orifice of 0.23mm diameter, with a 0.14mm radius of curvature (see fig 3.2). These dimensions were set by the manufacturing process, which was successful at reproducing the same orifice dimensions. Further development could have allowed more stringent limits to be placed on the orifice dimensions, but these values were deemed a suitable if somewhat arbitrary starting point. Two of the turned bodies were used to produce the impregnated insert cathodes, one had its surfaces impregnated and one was left untreated and simply fitted into the ferrule.

This first design of an untreated body with no inserts allowed a series of tests to be made. Leak tests were performed giving an indication of flow through the orifice. Testing of the electrical setup of the system was followed by a characterisation of initiation voltages and voltage-current dependence. Final tests on the establishment of higher current discharges (at 50mA) using alternative power supplies caused high rates of erosion of the orifice from spark discharges. It was therefore decided not to use these supplies to operate at high currents on more complex models due to the danger to the pumping system presented by insert detachment in the presence of no restraining orifice.

3.1.2. Surface Impregnated Body

A second model with its surfaces coated with the $BaCO_3$:$CaCO_3$:Al_2O_3 mixture was developed. This was seen as an intermediary development between the simple tube and the final inserted model. Surface coated hollow cathodes have been seen in prior developments [52], though never at this scale. The impregnant was mixed in a 4:1:1 ratio, known for its good performance in lowering work function. Other ratios are known to perform well, but this is the most commonly used ratio.

Figures 3.4 and 3.5 illustrate the system schematic and a close up of the orifice. The latter exhibits small amounts of the low work function compound adhering to the exterior surface of the body, similar to what was observed on the interior of the tube when a visual inspection was carried out at the end of life. The impregnant was placed in the tube with a 20μm tungsten wire in the orifice and down the length of the tube. This wire, when subsequently removed, ensured that the impregnant in the body did not cause any blockages and would allow gas to flow.

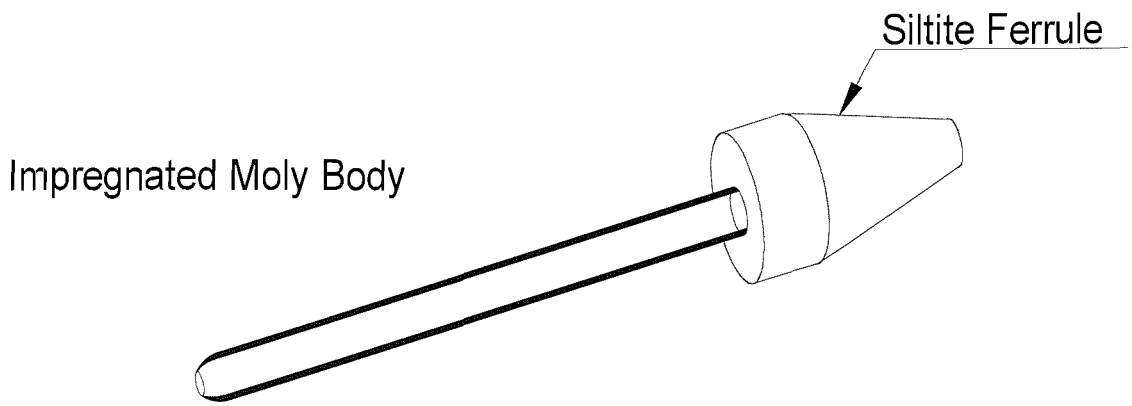

Fig 3.4 Surface impregnated body with ferrule

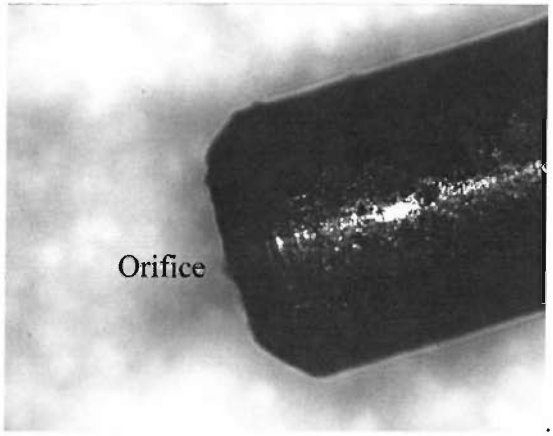

Fig 3.5 Surface impregnated tip x50

3.1.3. Impregnated Insert Molybdenum Body

The final micro hollow cathode design had an insert placed near the orifice, designed to improve emission. It was made from an uncoated molybdenum body with a turned orifice with internal impregnated inserts manufactured from a carbon-carbon matrix. Inserts were stacked to a length of 10mm with a 0.2mm diameter internal orifice channel. Two devices were built for testing and both underwent a rigorous series of examinations. Carbon was chosen as it fits the requirements for the insert well: it has a high open volume fraction allowing uptake of large amounts of propellant; it has a high melting temperature, necessary during the impregnation process; it is relatively easy to work at small scales if innovative manufacturing techniques are applied; and as it is a conductor it can emit under electric fields.

The carbon-carbon matrix was made of pulverized graphite ground to a specific grain size then pressed into wafers for processing. The large open volume of the carbon-carbon matrix allowed extensive uptake of the impregnant which is instrumental in forming high plasma densities.

Graphite crystals are randomly oriented within the insert matrix, ensuring uniform bulk properties i.e. density, resistivity and thermal properties; however, non-uniformities are apparent at microscopic levels. This can cause discontinuities which can affect the plasma. It is hypothesised that the plasma formed within such a body would be dynamic in nature and subject to some instability and variation over time. This is because the orientation of the graphite planes would affect sputtering and the granular nature of the substrate will affect its electric properties. In the case of plane orientation, ion bombardment could take place either in the large intra-plane gaps or at an angle to the planes themselves, which would exhibit a sputter yields dependent on angle of incidence. At a normal incidence, particle impact causes the least sputtering as at higher angles the incident particle effectively ploughs a furrow through the top layer of the target material. The granular nature of the matrix will also affect operation due to the potential electrostatic interactions between the graphite grains. Such instabilities could, however, allow formation of increased localised electric fields, aiding emission.

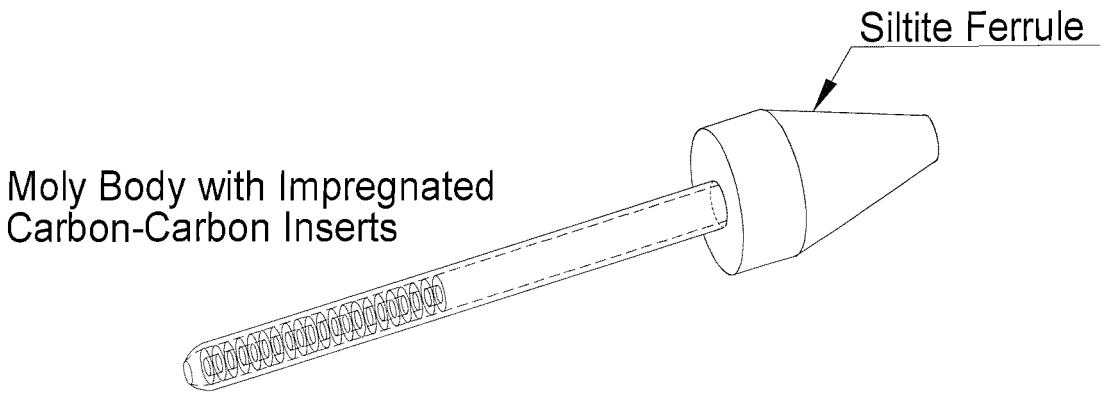

Fig 3.6 Impregnated insert cathode body with ferrule

As has already been stated, the novelty of this device is in its small size, the use of a carbon matrix for the insert material, rather than sintered tungsten and the turned orifice. Other interesting design features which facilitate manufacture and deployment are the heaterless ignition capability, the molybdenum body, rather than tantalum, the

compression fitting of the insert and the simple swagelock adaptor for ease of mounting.

3.1.3.1. Insert Manufacture

Inserts impregnated with low work function materials have been shown to significantly improve the discharge voltage-current output for a hollow cathode. This improvement results from the increased emission of electrons from the impregnated insert during operation. Reactions at the insert surface result in a lowering of the work function of the surface. In conventional inserted hollow cathode systems the impregnated carbonates undergo a decarboxylation reaction during the impregnation process to become oxides. During cathode operation gaseous Barium oxide is driven off the insert which reacts with the Tungsten insert to produce compounds of tungsten, oxygen and barium, plus free Barium itself, which is the source of much of the electron emission from the cathode.

The final design required a series of inserts to be impregnated with the carbonate mixture for placement in the molybdenum cathode body. Initial tests were carried out on the fabrication of molybdenum inserts but these proved extremely hard to work at such small dimensions. This was due to the small scales' requirement for unusual fabrication techniques and the materials resistance to the erosive processes involved in powderblasting. Powderblasting was chosen to manufacture the inserts as it was the only available technique capable of manufacturing the inserts at such a scale with a high degree of accuracy, while other techniques were inappropriate or unavailable. Current hollow cathode technology uses much larger tungsten inserts. However, as Tungsten is harder than Molybdenum, it would prove even more difficult to fabricate at such scales. It was therefore decided that the inserts would be manufactured from a carbon-carbon matrix wafer which could then be tested in a novel small scale cathode. The carbon-carbon material is easy to work at small scales and has a high open volume fraction, ideal for a large uptake of the impregnant.

3. MICRO HOLLOW CATHODE

It is not known whether similar reaction processes will occur at the insert surface due to the use of carbon instead of tungsten. The cathode insert may produce carbon monoxide and carbon dioxide as the oxygen from decomposition of the BaO reacts with the carbon insert. As carbon monoxide and carbon dioxide are gases mass would be lost from the insert. This could result in early erosion of the insert surface; however, this may not be entirely detrimental. Tungsten oxides have been shown to block the pores of the insert, preventing the impregnant reaching the surface and the subsequent liberation of Barium [89]. By using carbon, the reaction is likely to produces gases which will not impede the flow of impregnant materials to the surface of the insert. Obvious downfalls are the unknown nature of the reactions taking place by using a carbon insert and increased erosion of the insert with time. The effect of erosion and the resulting change in geometry would change the operating characteristics of the device and is not easily quantifiable. Also, it should be noted that as this device would likely work at low currents, it is also likely to operate at low temperatures. This would mean that the thermal decomposition of BaO will be low, allowing only a small amount of free Barium and Oxygen to be liberated to take place in reactions. Operation at higher currents would increase the temperature and therefore the rate of thermal decomposition of BaO, but the small size will limit the current that can be drawn from the device.

The carbon wafer was powderblasted to produce 0.1mm deep toroids which would be stacked to produce the insert. The production process was carried out in the clean room and powderblasting facility at the Rutherford-Appleton Laboratory, with the assistance of Dr R Stevens. Initially, a series of insert templates were produced on AutoCAD and transferred to an acetate mask. Several Chromium coated glass plates were cleaned and any residual water was driven off by heating to 120^0C. The plates were coated with negative tone chemically amplified resist and exposed to ultra-violet light through the acetate mask. The exposed plates were placed in a reactive ion etcher to strip exposed resist from the plate using oxygen as the etching agent. This plate was then placed in a bath of Chrome etch solution and finally all excess resist was removed

using a stencil remover. The product was a high definition chromium-glass mask of the inserts as seen from above, 380μm exterior diameter, 200μm interior diameter.

Several 100μm thick carbon-carbon wafers were then cleaned and residual water was driven off by heating. A layer of SBX resist was then applied and left to dry. SBX is a commercially produced liquid resist emulsion which can be used to create a rubbery mask on a surface. Exposure of SBX to UV light cures the resist and unexposed areas can be washed off. The SBX layer on the wafer was therefore exposed to UV through the manufactured Cr/Glass mask. Figs 3.7 and 3.8 show the SBX mask after excess resist was removed by immersing the wafer in water for 20 minutes and lightly rinsed.

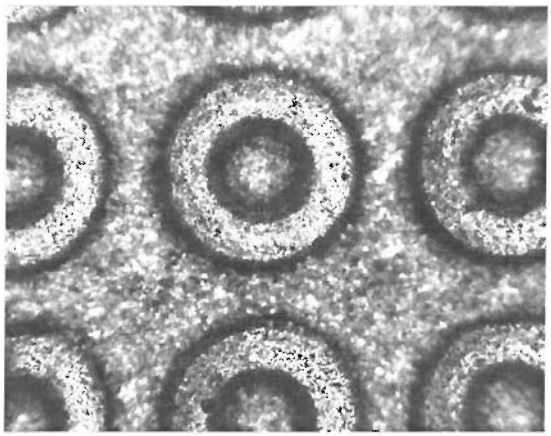

Fig 3.7 Insert mask x50

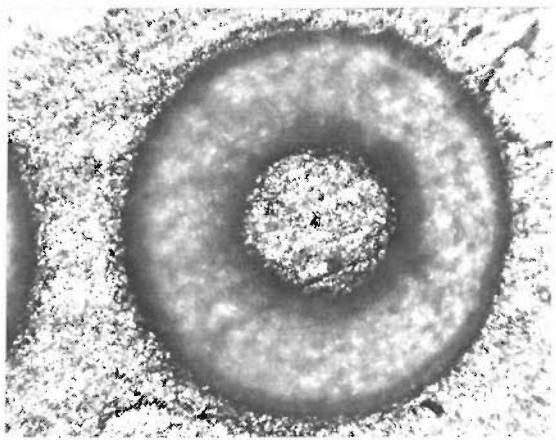

Fig 3.8 Insert mask x100

The wafer with the SBX stencil was then fastened to a silicon plate using adhesive and the plate was locked to a mount for use in the powderblaster. The mount was secured to a rotating table inside the powderblaster set to give an even blast across the whole wafer. The operating principle of this process was the mechanism of particulates bouncing from the elastic SBX whilst eroding the carbon wafer.

After approximately 6 hours of exposure to 1μm aluminium oxide (corundum) particles issuing at high speed from the gun, approximately 75% of the exposed wafer had been removed and the inserts located most centrally to the gun had very high

straightness. Stencil remover was added to deionised water in which the wafer was immersed. After placing on a hotplate at 40°C for thirty minutes both the adhesive and leftover SBX mask were completely removed. Inserts were then harvested from this solution and left to dry after thorough washing in more deionised water.

By threading the inserts onto 0.2mm diameter tungsten wire, a series of 100 inserts 10mm long ready for impregnation was produced. This kept the inserts in a regular shape and prevented the central channel from becoming blocked. Impregnation took place at temperatures in excess of 2500°C, above the melting point of the oxides, under vacuum conditions ($< 10^{-6}$ mBar) after which the insert was removed and all excess impregnant detached from its surface. The tungsten wire inside the insert stack was used to thread the insert into the cathode body and then removed. It was ensured the insert reached the extreme end of the body, by the turned orifice. Matching of the insert exterior dimension to the cathode bodies' interior gave a compression fit ensuring no movement.

3.1.3.2. Impregnation Process

Barium compounds have seen extensive use in lowering the work function, and thus improving the operation of cathodes. Coatings were found to generally have low lifetimes, especially at high currents, leading to the development of matrices to dispense the material [52]. Under heating during impregnation and under cathode operational conditions carbon dioxide is driven off both the impregnated carbonates to form oxide mixes. These oxides exhibit very low work functions, aiding electron emission. Local variations in the surface mixture are known to have a high effect on discharge current and when the impregnant is not in a dispenser matrix, but is surface coated onto components, the lifetime of such a coating is generally low [52].

3. MICRO HOLLOW CATHODE

The process of impregnating the barium carbonate, calcium carbonate, aluminium oxide mix was performed in an evaporation chamber equipped with heating elements. The carbonates undergo the decarboxylation reaction to form oxides which transfer into the matrix when melted. It is clear from table 3.1 that the impregnants significantly lower the overall work function of the cathode. Overall, a W-O-Ba compound mix has a work function of around 2.2eV [64]. The variation in the work function of the barium and calcium oxides is due to the difference each exhibits depending on the lattice structure formed when it was created. Different ratios of the impregnants result in different lattice structures, the reason for using a specific ratio.

Material	**ϕ, eV**	**T_{melt}, K**
Al	4.17	933.32
Ba	2.52	1000
C	5	4098[f]
Ca	2.87	1115
Mo	4.57	2896
W	4.6	3695
Al_2O_3*	3.77	2326
BaO*	1.7-3.4	2245
CaO	1.6-1.86	2572

Table 3.1 Work function and Melting Point of materials used in fabrication of hollow cathodes [79, 64*]

[f] Sublimation

The process of impregnating any of the components of the hollow cathode device must take place in an Evaporator system. This system is comprised of a bell jar in which a high vacuum can be maintained, containing refractory metal boats through which a current can be passed to heat the contents to temperatures in excess of 2500^0C.

Prior to evacuation, the components for impregnation were placed in the metal boat with the impregnant mixture. The gasket at the base of the bell jar and the surface

to which it adheres were thoroughly cleaned to ensure a good seal. The bell jar was then put in place with a surrounding Perspex implosion guard.

The system was evacuated to less than 0.1mBar. When the vacuum was stable the nitrogen trap was filled with liquid N_2 and the whole system left to evacuate further. The bell jar then reaches pressures of less than $1x10^{-4}$ mBar over a period of approximately one hour. Appendix A details the procedures for operating the evaporator system and other procedures relating to the fabrication and operation of the device.

The process of impregnation requires the metal boat to be connected across electrodes in the evaporation system at a pressure of less than $1x10^{-4}$ mBar. The current is then set in excess of 40A. Resistive heating of the boat increases the temperature of the mix to a point where it decomposes from carbonates to oxides which, when melted diffuse into the matrix of the hollow cathode inserts or surface coat the molybdenum body.

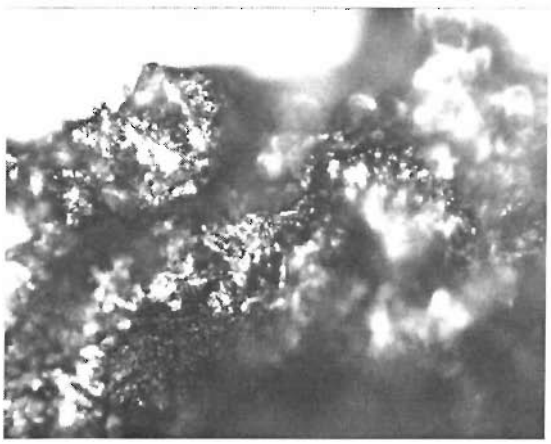

Fig 3.9 Impregnant mix after impregnation, x200

Fig 3.9 shows the impregnant after heating in the evaporator system. Prior to this the mix was a fine white powder, it now forms a relatively hard and brittle substance with regions which appear to have crystallised or even metallicised.

3.1.3.3. Heater System

Many hollow cathodes are pre-heated before use to facilitate initiation of the plasma discharge. When thermionic emission starts to take place the initiation voltage for the plasma drops drastically. It was felt that development of a heater system would allow a characterisation of this effect. By manufacturing a micro-engineered heater system the overall design constraint of keeping the cathode system at a low weight and volume could be maintained. The use of novel materials ensured that heat propagated more easily toward the cathode but was well insulated and bypassed the difficulties of directly building the heater onto the small body.

Experiments were carried out using the heater system on the temperature dependence of initiation voltage. The heater was developed from two ceramics, between which a tungsten heating element was wound. Both ceramics had good electrical resistance, preventing shorting. The exterior ceramic, Macor, had a high thermal resistance, the interior ceramic, Shapal-M, had a low thermal resistance. This promoted propagation of heat to the cathode at the centre. The interior ceramic was designed to make a good fit with the cathode, improving conductance. A thermocouple was located near the cathode tip for temperature measurement. Fig 3.10 gives a schematic of the heater system.

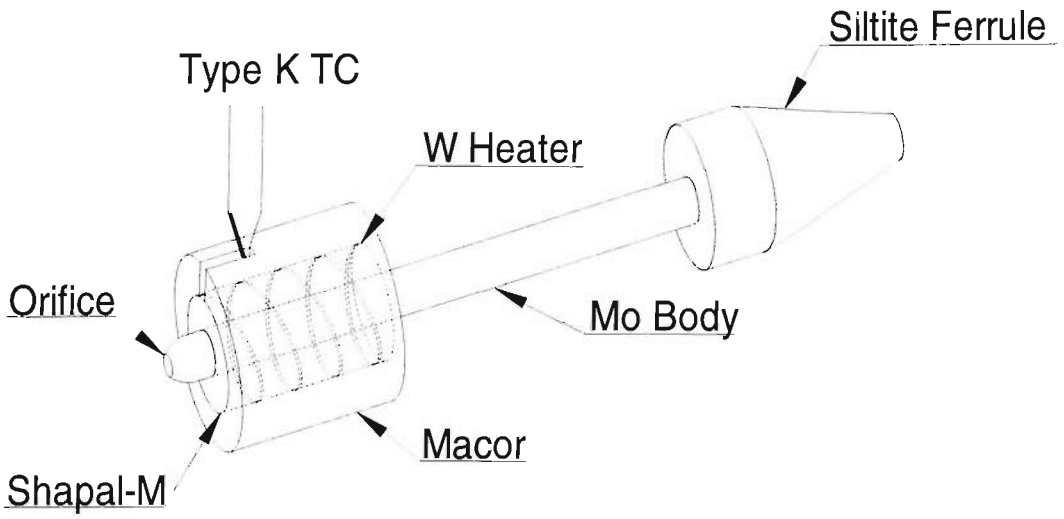

Fig 3.10Heater System (not to scale)

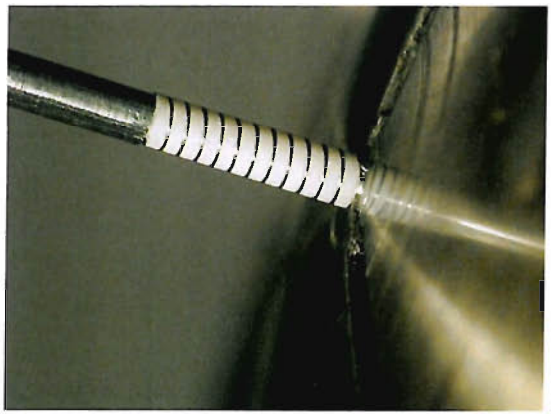

Fig 3.11 Shapal-M ceramic on mandrel

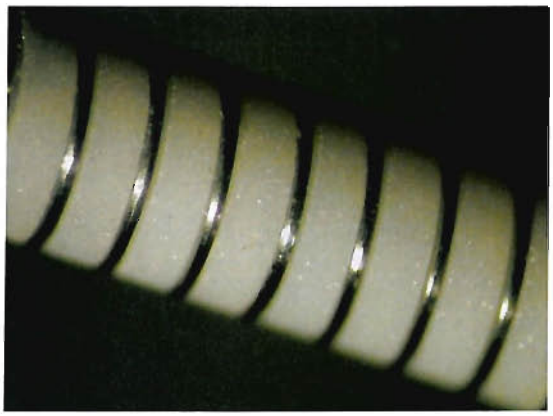

Fig 3.12 Shapal-M with W/Rh Heater

A 0.125mm groove was cut into the 2mm diameter, 10mm long Shapal-M cylinder and a 0.1mm W(0.75)/Rh(0.25) wire was wound into this groove and secured with Rocksett high temperature adhesive, seen in figs 3.11 and 3.12. Tails were chased out each end for electrical connection and the whole assembly was surrounded by a 5mm OD, 2mm ID Macor ceramic sheath, seen in fig 3.13. A type K thermocouple was then secured into a prefabricated slot in the Macor sheath close to the orifice end. The whole assembly was then cured in an oven overnight at 70°C.

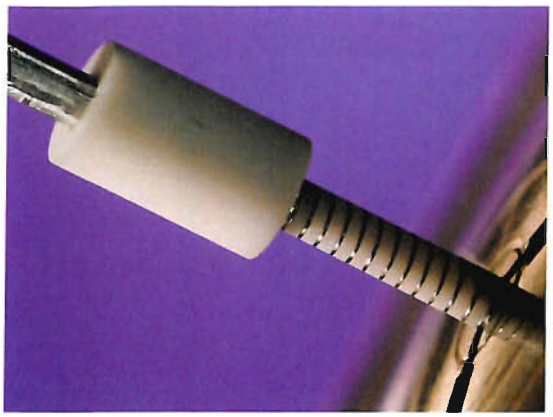

Fig 3.13 Macor collar surrounding heater

3.1.4. Keeper & Anode

The keeper was constructed from a 1mm thick stainless steel plate. Several 10mm diameter discs were produced from the plate and had a 1mm diameter central orifice drilled. Examples were checked for flatness and orifice regularity and the best was directly attached to a post, made of an insulator, in this case Macor, and mounted by the cathode.

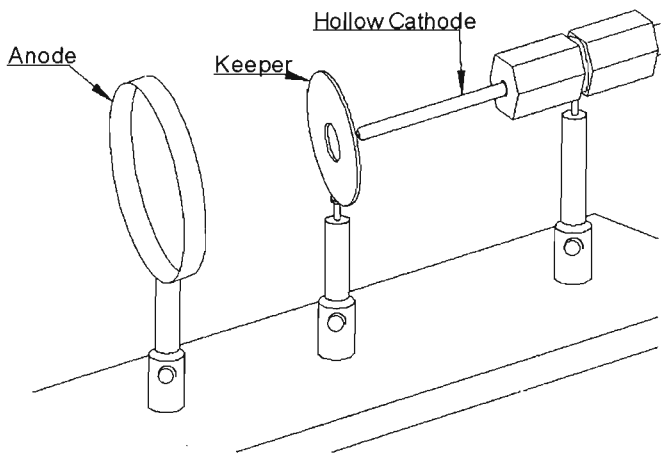

Fig 3.14 Cathode, keeper and Anode

3. MICRO HOLLOW CATHODE

The anode was a simple 200μm thick tantalum ring, 10mm in depth, 25mm diameter. This was mounted on a Macor insulating post and placed in a Melles Griot post holder on the mount plate downstream of the keeper. The anode was not used after testing showed that the discharge could not be maintained at the higher currents. The cathode was therefore operated in a simple diode configuration using the keeper only. It should be noted that the separation between the cathode and keeper is known to have a significant effect on the operating parameters of the device. Various values of keeper-cathode separation were therefore investigated, with results being presented for the same cathode under the same flow conditions at different separations.

Chapter 4

Experimental Apparatus & Procedures

4.1. Apparatus

The experimental apparatus simulates operational conditions for the hollow cathodes under development, and provides the environment necessary to generate a stable plasma. The experimental apparatus can be divided into several distinct areas:

- Cathode setup
- Vacuum system
- Power supply system
- Propellant feed system

4.1.1. Cathode Setup

The micro hollow cathodes, discussed in the previous chapter, and their associated components require a versatile mount system inside the vacuum chamber. The mount

was developed to allow adjustment of key components, permitting a wide range of experiments to be performed and repeated accurately.

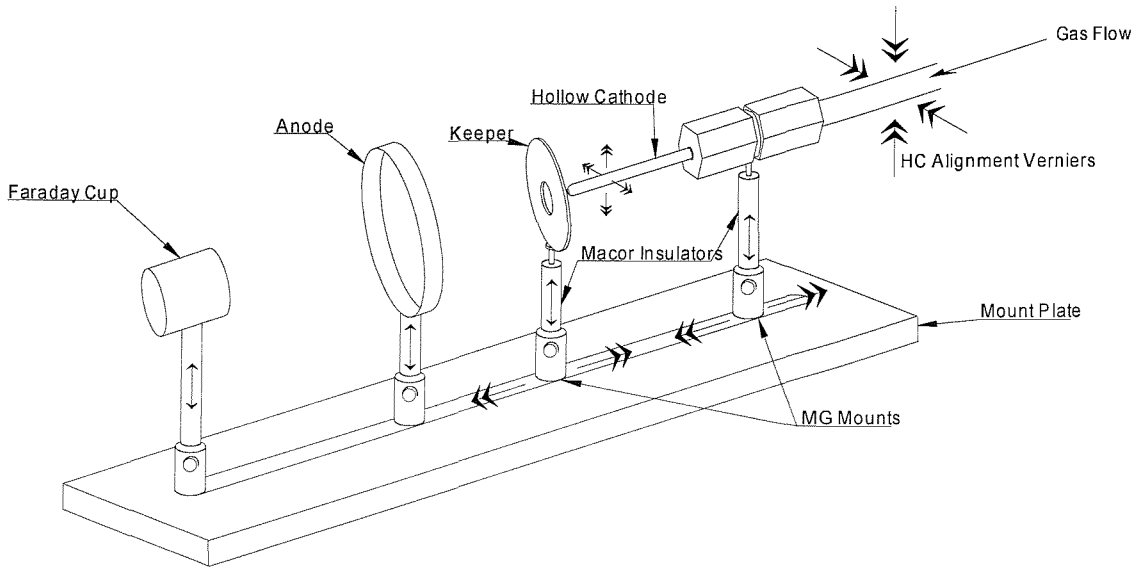

Fig 4.1 Component Mount System

The cathode with ferrule is mounted in a swagelok body on the mount plate. The position of components, such as the keeper and detector, could be easily altered to allow a range of conditions to be reproduced. Crucially, at the beginning of each measurement run the keeper-cathode separation was checked due to its central role in the operating characteristics of the cathode. Melles-Griot optical mounts attached to the mount plate hold Macor posts to which components are mounted. Component supports are manufactured from Macor as it acts as an insulator between the charged device components and the mount plate. An unshielded Faraday cup was also used to determine the properties of the plasma produced by the device. After a period of initial systems testing, improvements were made to the cathode and component mount system. These included:

- Decreasing the width of the keeper mount to ensure a more consistent and radially regular setup
- Altering electrical connections to allow closer spacing of components

- Improvement of the axial straightness of cathode components, ensuring a uniform plasma plume

4.1.2. Vacuum System

The cathode and mount are connected to a vacuum system made up of three key subsystems:

- Vacuum chamber
- Pumping system
- Pressure sensors

Figure 4.2 shows the setup of the vacuum system used to test the micro hollow cathodes, which also includes a retarding potential analyser (RPA) which could be used to investigate the plasma.

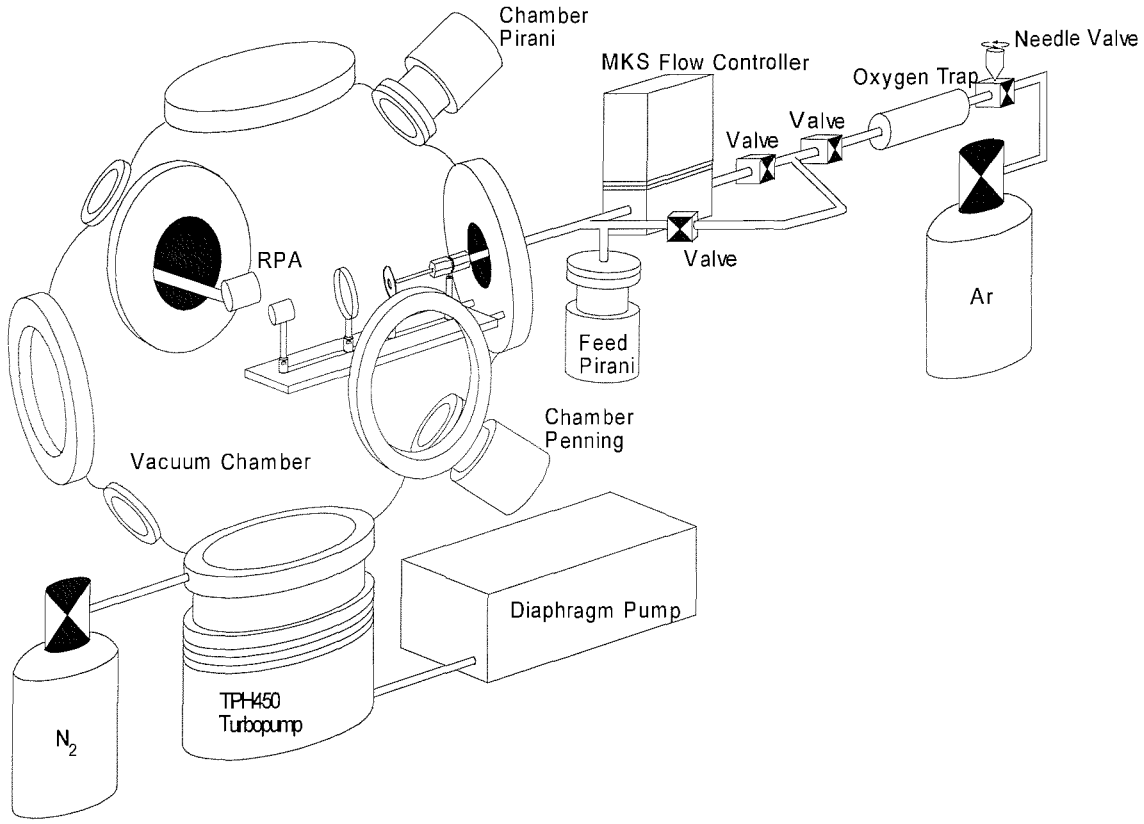

Fig 4.2 Experimental system setup

Residual atmospheric contaminants must be flushed from the cathode and chamber to ensure operating conditions mimic those seen in space. The whole system is therefore left under vacuum for 24 hours before cathode operation to ensure contaminants have been removed, approaching the 10^{-8} mBar range. Further, a dry nitrogen system is used to reduce contamination of interior surfaces during periods when the system must be opened. By flooding the chamber with N_2, surface adsorption of contaminants is reduced, particularly oxygen and water vapour. The flange with the attached cathode assembly could be difficult to fit and care had to be taken to ensure that the gasket was placed properly. Poor seals were evident as the final pressure would be substantially higher than expected, which would normally approach 10^{-8} mBar after 24 hours. If the pressure was in this region, typical for this kind of vacuum chamber, the external leaks from the atmosphere were considered to be negligible in comparison to the mass flow through the cathode. When in operation, the cathode raised the background

pressure of the chamber by a factor of 1000 or more. The effect of outgassing after a 24 hour period of exposure to high vacuum was also considered to be negligible in comparison to the flow rate of Argon through the cathode and the measured pressure. Frequent checks were also made during vacuum system operation on pump speed and coolant water supply as occasional problems had been observed in these areas.

4.1.2.1. Vacuum Chamber

The vacuum chamber is a stainless steel, spherical chamber, approximately 0.6m in diameter, with a number of ports of various sizes (5xCF16, 1xCF12, 6xCF8 and 4xCF4). These ports are used to connect:

- Pumping system
- Cathode and component mount system, including propellant feed
- Electrical connections
- System internal pressure sensors
- Retarding potential analyser
- Observation windows

The component mount system was connected directly to a flange which included mass flow and electrical feeds.

4.1.2.2. Pumping System

The vacuum chamber was evacuated using a two-stage system. At high pressures, a diaphragm vacuum pump with a nominal pumping rate of 3 cubic meters per hour was used. At low pressures, a Pfeiffer TPH450 turbopump, with a volumetric flow rate of 450 litres per second was employed. Frequent Checks on the blade rotational frequency

(optimally 720Hz) and turbopump temperature were performed to ensure the system was operating properly.

The high-pressure diaphragm pump evacuated the chamber to approximately 1mBar over a period of approximately five minutes. Pressure gauges trigger operation of the turbopump which lowers pressure to 10^{-6} mBar range within 30 minutes, 10^{-7} mBar range beyond 30 minutes and 10^{-8} mBar range within 36-48 hours. The turbopump required a water coolant system, with a flow rate of at least 0.3 litres per minute, and had a thermal shutoff circuit should the pumps integrity be threatened by excessive thermal load.

4.1.2.3. Pressure Sensors

Pressure sensors were necessary to several aspects of operation of the vacuum system. The turbopump required a low pressure before it could operate or it would suffer damage. A Pirani sensor was therefore linked directly to the turbopump controller. The Hollow Cathode itself required low pressure for operation, as well as a sufficient period of outgassing at low pressures to expel atmospheric contaminants. These low pressures were monitored using a Penning sensor. Flow rates through the Hollow Cathode were also checked using data collected from the Pirani pressure sensors. Finally, integrity of the vacuum seals was also tested using the pressure sensors, a pressure of 10^{-7} mBar or below indicated minimal leakage

High pressure (1000mBar – 1.8×10^{-3} mBar) measurement was provided using a Leybold AG Pirani sensor (SN: 61329) and a Combivac CM31 meter. The meter was set to the mBar range and had a calibrated 0-10V output. Low pressure (6×10^{-3}mBar – 1×10^{-8} mBar) measurement was provided using a Balzers IKR 020 penning sensor (SN: BG G12 530/13042) and a Balzers TPG 300 meter which was also set to the mBar range and had a calibrated 0-10V output. As Penning gauges have been shown to be unstable when

operated for long periods, these would be turned off during pumpdown and other periods of inactivity.

4.1.3. Power Supply System

A series of electrical supplies provided power to various parts of the system including the cathode heater, keeper disc, anode and detectors, seen in fig 4.3.

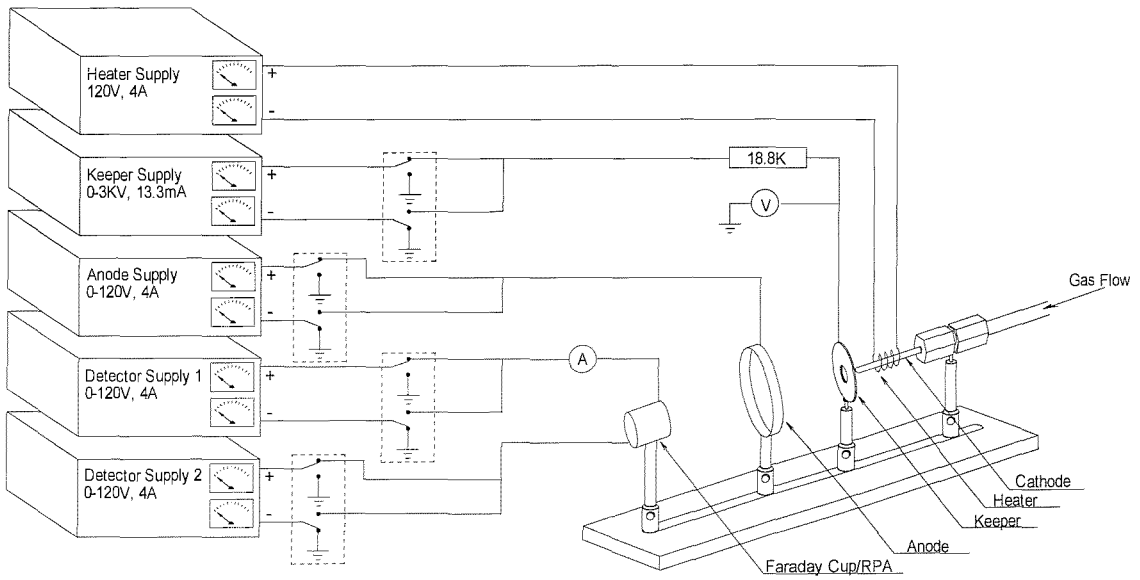

Fig 4.3 Power supply system

All power supplies were current regulated, direct current and are denoted at their maximum range. Switches indicate that the polarity of the supply could be changed dependent upon the operational conditions. To prevent any damage to the power supplies or to the cathode itself, supplies were powered up and down at 0V and 0mA.

Probably the most important property in defining cathode operation was the keeper supply characteristics. Other cathodes have been shown to operate under conditions of a positively biased cathode and a grounded cathode. The voltage on and current to the positively-biased keeper is instrumental in dictating the operating

parameters of a hollow cathode. The supply had a voltage range of 0-3KV and a controllable current range of 1.5-13.3mA to allow plasma initiation and operation under a variety of conditions. While the highest available current from this supply is low, the size of the cathode would likely limit the maximum available current, and this supply could be used for an initial testbed for the device. Appendix A details the procedure for discharge initiation and operation. The resistor in the keeper supply line limited current during plasma initiation; the voltmeter read the voltage at the keeper disc after initiation. As the resistance of the gas prior to initiation is much greater than that of the resistor, the potential between the keeper and cathode is effectively equal to the voltage measured at the supply.

The cathodes were predominantly deployed in a heaterless configuration but did have its initiation voltage investigated under heating and saw more extensive employment in discharge initiation for the second impregnated insert device. A 120V supply with current limit operated the heater at 4.5 to 6 Watts. An anode is required in a full electron bombardment ion thruster. However, during characterisation of the hollow cathode in the vacuum chamber it was not a critical component, and was generally left floating.

A Faraday cup and Retarding Potential Analyser (RPA) were placed in the vacuum system to perform any required analysis of the plasma. The RPA required two supplies as the biased aperture used to retard charged particles must also be supplied with a voltage. In both cases one or two 120V supplies were used. All supplies had an internal ammeter, but the small currents measured by the detector required a high sensitivity ammeter.

4.1.4. Propellant Feed System

Accurate flow control through a cathode is important for several reasons. In characterisation of the cathode, knowledge of the flow rate is necessary to determine its relationship to output current and initiation voltage. Flow rate can also determine the mode (spot or plume) of plasma production in the hollow cathode. Further, when designing an ion thruster it is also necessary to consider flow control when defining the internal pressure of the thruster's ionisation chamber.

Residual contaminants must be flushed from the cathode and propellant feed system as these would adversely effect cathode operation. All valves, including the mass flow controller are opened midway through the pumpdown cycle to ensure all contaminants are expelled. An Agilent OT1-4 oxygen trap was also included in the feed line to scrub any oxygen from the supply gas (either as a contaminant or due to leaks) and leaks were minimised by maintaining a positive pressure with respect to atmospheric in feed lines up to cathode flow controllers. Feed lines were manufactured from swagelok ¼" stainless steel tubing and were cleaned with pressurised air before use expunging any particulates that would affect the cathode, flow controller or valve operation.

The propellant feed system was made up of a combination high flow/low flow system, used with argon feed gas. Argon is substantially cheaper than Xenon, while having similar, if slightly poorer, properties for cathode operation. It is therefore useful for initial characterisation and life testing of cathode devices. Low flow rates, less than 4.5×10^{-7} kgs^{-1}, were provided using a MKS 1179A mass flow controller with associated PR4000 control electronics. Higher flow rates, exceeding 4.5×10^{-7} kgs^{-1} were achieved using a needle valve and monitored using several pressure sensors linked to a data acquisition system. In this case the needle valve was set and flow rate calculated later.

Pressure sensors and other measurement devices were connected to a data acquisition system. This allowed data to be collected simultaneously on an accurate timescale. The 16-channel data acquisition system was connected to the parallel port on a computer running "Windmill" software. The software package had a timestep minimum of 100μS, though was nominally operated over timesteps of 0.1 to 1 second. As the system was limited to a maximum of 30000 data points (10,000 per channel in the configurations used) there was a threshold on the total time it could be deployed. The hardware was also limited to a 10 volt range with a current maximum of a few μA. Usefulness was therefore restricted to measurement of pressure, temperature via a type-K thermocouple and current measurements on a picoammeter.

4.2. Measurements

Cathode operation is dependent on a number of variable physical characteristics beyond geometry and materials used in the construction of the device. The equipment used to measure the system's operational properties covered both physical variables and the properties of the plasma produced by the cathode. Measurements were made on cathode:

- Electrical properties
- Gas pressure and flow rate
- Temperature
- Plasma properties

Experiments were carried out according to procedures designed to facilitate system use and ensure repeatable conditions. All data was input and processed through Excel.

4.2.1. Electrical Properties

Before mounting the keeper-cathode separation was measured using a micrometer. After a pumpdown period of 24 hours, the flow rate was set, using either the mass flow controller or the needle valve and left to stabilise. The external keeper voltmeter was isolated from the circuit as it could act as a current sink before discharge initiation and checks were also made on the continuity of electrical feeds. After mounting, the cathode was kept at ground potential and the keeper supply voltage was increased until plasma formation occurred.

Verniers were employed to fine tune the y-z alignment of cathode before and during the initial discharge initiation of a run. Observation windows were used first to align the cathode in the y-z plane by eye. If required, after initiation, the verniers were moved until an axially symmetric plume was formed, indicating that the cathode was in a central position. Experiments were only performed after any adjustments had been made, which may have been required after minor disturbances to the cathode during mounting of the flange to the vacuum system.

Initiation voltage, keeper voltage and keeper current were of primary interest. Voltage measurements on the system were carried out using internal meters on supplies and Fluke 75 multimeters where appropriate. The initiation voltage could be noted from the supply at the point of discharge formation. As the keeper supply was in current-limited mode the voltage immediately fell from its value at initiation to a level dependent on a number of factors, the most important of which were current, flow rate and cathode design.

Measurements on keeper voltage were only performed after a period of stabilisation subsequent to initiation while the cathode reached an equilibrium point. A stable voltage was considered to have instant fluctuations of less than 0.25% and long timescale deviations of less than 0.5% min^{-1}. Keeper current and mass flow rate were set

to their desired values and were measured and verified using a multimeter, keeper voltage was also checked using a multimeter. Variation of these values allowed a series of experiments on the dependence of discharge voltage on current and flow rate for the micro hollow cathodes to be performed. The anode was left floating throughout tests as when used the current drawn was too much for the cathode and the plasma would rapidly extinguish then reform continuously.

4.2.2. Gas Pressure and Flow Rate

Pressure and flow rate measurements are central to the characterisation of the hollow cathode. Discharge current is highly dependent on the ambient pressure in the cathode and flow rate through the cathode. Pressure sensors were placed in the cathode propellant feed system and downstream in the vacuum chamber described in section 4.2.3. A mass flow controller and needle valve controlled flow rate.

Initially, after the flange with cathode components was mounted on the vacuum system, checks were made on the quality of the vacuum seal connecting the flange to the chamber. The flow rate was set prior to measurement runs, and could be altered during measurement runs.

The flow rate was set using one of two procedures, dependent on desired level: At low flow rates, below 4.5×10^{-7} kgs^{-1}, the MKS mass flow controller was used to set the flow rate. The mass flow controller had a range of 9×10^{-9} to 4.5×10^{-7} kgs^{-1} Argon, an accuracy of 1% maximum flow rate (4.5×10^{-9} kgs^{-1}) and a repeatability of 0.2% (9×10^{-10} kgs^{-1}). Flow rates were accurate to 1.5×10^{-10} kgs^{-1} according to the calibration certificate supplied with the device. A gas correction factor for Argon was input into the control electronics to account for the gas flow properties in comparison to Nitrogen, which the manufacturers used as the baseline. For Argon, MKS quote a correction factor of 1.39, which with the measurement method (flow rate) and units (SCCM) were input into the

PR4000 control unit. This value is derived from an equation supplied by MKS which relates the properties of a gas to diatomic nitrogen (used in their calibration process).

At high flow rates, in excess of 4.5×10^{-7} kgs^{-1}, the needle valve was slowly opened to desired values of up and downstream pressures, known to coincide with a specific flow rate (seen from prior checks on the operation of the valve). The apparatus is then left to stabilise. The data acquisition program was then run under a unique identifier and data was later interpolated to give flow rates. Checks were continually made against the stability of the flow through the cathode, both in high and low flow rate modes.

Several methods exist to determine the flow rates from pressure measurements associated with the cathode. The gas density beyond the downstream end of the cathode can be multiplied by the effective pumping rate of the turbopump system to give the mass flow rate. The effective pumping rate is the total flow rate taking account of turbopump speed and the conductance of its connection (a measure of the permittivity of an orifice to gas flow). Flow measurements could be verified through rates predicted using equations describing flow through the micro hollow cathode. Flow equations could not be used as the primary method for determining flow rate as several variables could affect measurements which have large associated uncertainties, including exact knowledge of the pressure differential across the orifice, temperature, and minor variations in the cathode geometry. While methods that rely on such factors are inherently inaccurate, they simplify the system design and several can be verified against other to give some confidence in the results. A full discussion on mass flow measurements is given in chapter 5.

4.2.3. Temperature Measurement

Thermal measurements were required to determine the temperature dependence of plasma initiation voltage when using the heater element. Temperature measurements on

the cathode tip were made using a pyrometer and Type-K thermocouple. The Type-K thermocouple, made of Alumel and Cromel wires, operated up to approximately 1250°C and used an AD595 cold junction compensator, calibrated for type K inputs, as a reference point. The pyrometer had a temperature range of 800 to 1800°C, and works on the correlation of metallic luminescence to specific temperature values.

When making temperature based measurements on the cathode system the heater was mounted 2mm upstream of the cathode tip. The cathode is then heated at a power of 4.5 to 6 watts. Temperature is measured using either the thermocouple, mounted near the orifice or the pyrometer with reference to the 2mm exposed cathode body by the orifice. Measurements on initiation voltage and voltage-current properties are then made in the same manner as described previously.

4.2.4. Plasma properties

Measurements were also conducted on the plasma plume using an unshielded Faraday cup and a retarding potential analyser (RPA). This allowed a determination of the plasma potential, electron temperature and number density, giving an insight into the plasma conditions within the cathode. During collection of electrons and ions by detectors, voltages were noted using the meter on the supply and detector current measured using a Keithley series 7000 picoammeter. To prevent any possible damage to the apparatus a procedure for powering down the system was also devised. However, the large uncertainties associated with the surface area of the cup interacting with the plume, and lack of success with the RPA has decreased their importance. These measurements and their outcomes are therefore discussed in appendix B.

Chapter 5

Experimental Results & Analysis

5.1. Introduction

This chapter presents the results and analysis of a range of experiments made on the micro hollow cathodes developed in this project. The goal was to investigate novel methods of miniaturising electron emitters that could be used in ion microthrusters thrusters. Measurements on the hollow cathodes designed to meet the requirements cover a range of parameters relating to the physical conditions of the discharge. Key elements include initiation voltage as a function of mass flow rate and the Voltage-Current relationship.

The initiation voltage and voltage-current relation of a hollow cathode are some of the principal factors determining suitability of a device to a role as an electron source for ion propulsion. Low initiation voltages put less demands on the system as a whole and cause less damage to the device resulting from arcing. The voltage-current relationship is instrumental in establishing the power required and hence efficiency of the device, as well as the characteristics of the plasma discharge.

Cathodes were operated in a diode configuration at high and low flow rates and at a variety of discharge currents and voltages. Currents ranged from 1.2 to 13.3mA at flow

rates of argon in the 10^{-7} and 10^{-6} kgs^{-1} range. Discharge voltages were typically several tens to hundreds of Volts. The cathode-keeper separation ranged from 0.5 to 1.2mm. When in use, the cathode internal pressure was typically above ten mBar, while the chamber pressure generally lay in the 10^{-3} mBar range. Analyses were performed using formulae seen in chapter 2, useful for the identification of system parameters giving a greater understanding of the operation of the device.

5.2. Initiation Voltage

The discharge initiation voltage is a key factor in the operation of the device. The initiation voltage is primarily a function of electrode separation, local gas pressure or mass flow rate and temperature, and must be optimised. Low initiation voltages ease constraints on the electrical system, reduce arc-induced erosion and may conserve propellant during the startup sequence.

A description of the results of tests on mass flow rate is presented first, followed by results of performance tests on the four cathodes. This covers the discharge initiation properties of the simple Molybdenum tube hollow cathode, the surface impregnated Molybdenum hollow cathode and the impregnated carbon-carbon insert Molybdenum hollow cathode, without the presence of the heater, which is discussed in a separate section.

All experiments were carried out using Argon as a seed gas. While Argon does not perform as well as Xenon, it is inexpensive and has been extensively used as a substitute. Testing of each impregnated insert cathode exceeded 160 hours operation with over 400 startup sequences. This is not on the same scale as large cathodes that may be tested for tens of thousands of hours, but was did demonstrate variations in the micro hollow cathodes performance.

5.2.1. Mass Flow Calculations

The continuity equation states that the mass flow rate into and out of a system must be equal. Under steady state conditions there should be no accumulation of gas in any part of the system when an equilibrium point is reached. Assuming that leaks are negligible, the mass flow rate through the valves and mass flow controller will equal that through the orifice of the cathode which will in turn be equal to that through the pumping system.

An MKS type 1179a mass flow controller was used at mass flow rates below 4.5×10^{-7} kgs^{-1}. This device had been calibrated against a known standard to an accuracy of 2% of flow rate, or a maximum of 9×10^{-9} kgs^{-1}. At flow rates in excess of 4.5×10^{-7} kgs^{-1}, the upper limit for the mass flow controller, quantification of the mass flow rate relied on measurements of pressure and volumetric flow rate as flow through the vacuum pump must equal the flow rate through the cathode, neglecting leaks.

The mass flow rate through the cathode is equal to the volumetric pumping speed, Q, multiplied by the gas density in the vacuum system, ρ:

$$\dot{m} = \rho Q \qquad 5.1$$

Density can be determined directly from pressure measurements assuming knowledge of the gas temperature. Cathode operation at high temperatures will affect this measurement. Salhi and Turchi state that for a first order approximation the gas temperature can be assumed to be equal to the wall temperature across the cathode internal radius [36].

As only a very small part of the cathode is at a high temperature and the vacuum chamber itself is at room temperature we can generally assume the gas to also be at room temperature, certainly around the pressure sensors and within the pumping system. The pumping speed was also determined through measurements of pressure, as well as on

mass flow rate and verified using other system parameters. These were necessary as the quoted volumetric pumping speed of a turbopump is that for an idealised case. In reality the connection to the chamber lowers the throughput of gas, dependent on the system design.

As stated, several methods were employed to increase confidence in mass flow rate measurements. This was due to the potentially high uncertainties associated with mass flow rate calculations at flow rates outside the operating range of the calibrated mass flow controller. The primary method of determining the pumping speed was to match a calibrated flow against the ambient pressure in the chamber. As long as the ambient pressure was significantly larger than the baseline pressure when there is no leak, the equilibrium point between inflow and outflow allows calculation of the pumping speed. Equation 5.2 shows the volumetric pumping speed of the vacuum system in terms of the flow rate into the chamber and the ambient pressure:

$$Q_{Pump} = \frac{5.62x10^{5}\dot{m}}{P_{Chamber}} = \frac{0.01685\dot{m}(SCCM)}{P_{Chamber}} \qquad 5.2$$

The volumetric pumping rate, Q_{Pump}, is in liters per second, the chamber pressure, $P_{Chamber}$, is measured in mBar and the mass flow rate in both kilograms per second and standard cubic centimeter per minute SCCM (SCCM for Argon = $3x10^{-8}$ kgs^{-1}). Fig 5.1 shows the dependence of the ambient chamber pressure at equilibrium to the flow rate through the cathode measured by the penning gauge when the calibrated mass flow controller was in use. Beyond six sccm or $1.8x10^{-7}$ kgs^{-1} the relationship is approximately linear, corresponding to a mass flow rate out of the chamber directly proportional to chamber pressure.

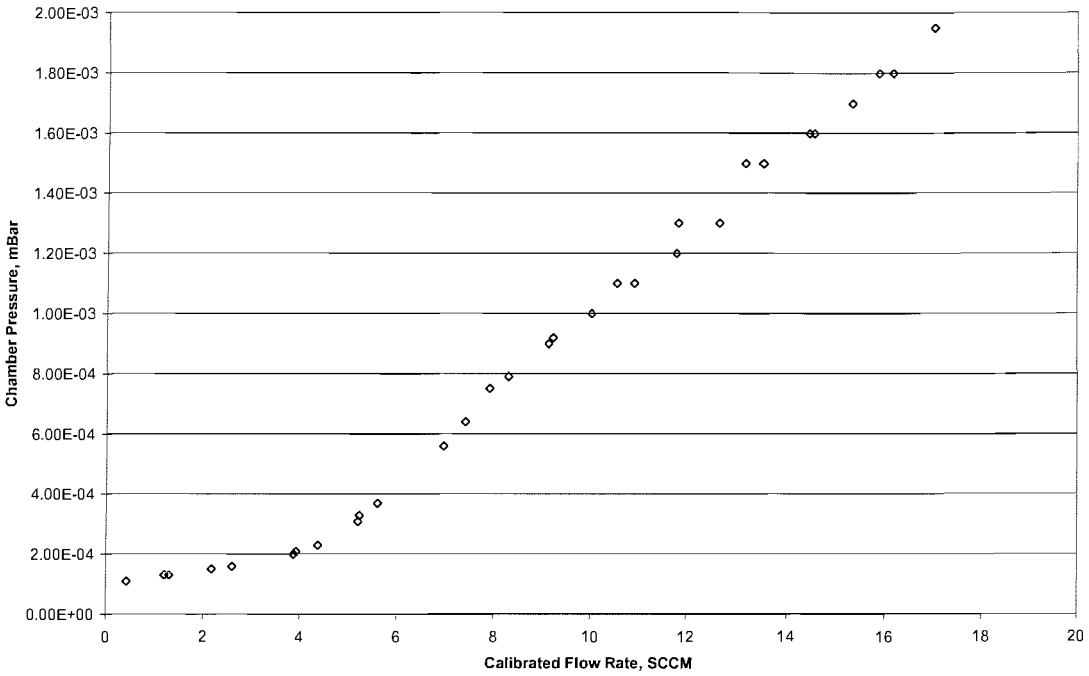

Fig 5.1 Correlation of Flow through Calibrated MFC to Equilibrium Chamber Pressure

The uncertainty associated with the Penning pressure gauge in the vacuum chamber is large, at 21.9%. This value was calculated by calibrating the output of the penning gauge against the pirani gauge at higher pressures, adding the maximum systematic errors associated with the needle valve and pirani sensor in quadrature. However, as the gauge was used at the high end of its scale, the uncertainty will be lower than the maximum as the accuracy is known to improve at higher pressures, particularly above 10^{-4} mBar. The calculations of mass flow rate could then be verified using what was expected from pressures at known flow rates. While the errors associated with flow rate are likely to be large this is not too important in cathode research. This however is not true in thruster development when mass flow rates through the cathode must be well defined.

Applying these results seen in fig 5.1 to equation 5.2 gives the system volumetric pumping speed as a function of the flow through the calibrated mass flow controller and thus cathode, seen in fig 5.2 below. At low flows this shows high variability, but at

higher levels, above 10sccm, the pumping speed appears relatively stable, in the region of 150ls^{-1}.

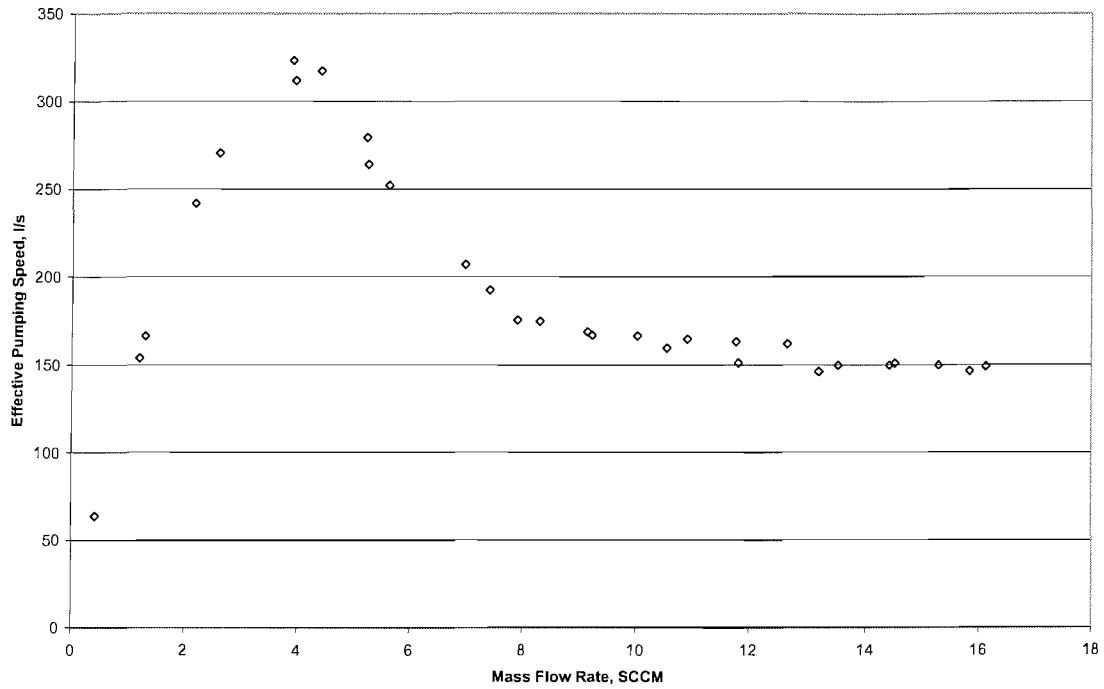

Fig 5.2 – Volumetric Pumping Speed as a function of Flow Rate

A second method of determining the mass flow rate through the system, which can be used to verify other methods, relies on the time required to pump the system down between two known pressures.

$$Q_{Pump} = \frac{V_{Chamber}}{t_{Pumpdown}} \ln\left(\frac{P_A}{P_B}\right) \qquad 5.3$$

$V_{Chamber}$ is the chamber volume, $t_{Pumpdown}$ is the time it takes to pumpdown between two known pressures, P_A and P_B. Advantages are that pressure does not have to be defined to an absolute value and can be measured in arbitrary units as the equation relies on the ratio only. The chamber volume was measured at approximately 63.2 liters. Tests carried out at initial pressures of $1.8\text{x}10^{-3}$ and $2.2\text{x}10^{-3}$ mBar showed the pumpdown

speed lay between 135 and 189 ls^{-1}, agreeing with previous measurements and increasing confidence in the calculations of flow rate. For this method to be viable, the final pressure must be lower than 1% of the initial to account for outgassing effects and is only viable in a free molecular flow regime, where collisions between gas molecules are negligible. In a vacuum system a gas can exist in either a viscous or free molecular state, or in a transitional state between the two. When the mean free path of the molecules is small in comparison to the dimensions of the containing vessel the flow is viscous. Viscous flow can be either turbulent or laminar. In a laminar regime the flow speed has a regular variation, increasing from the wall to a maximum at the centre of the containing vessel. In a turbulent flow regime, the flow is characterised by large variations of pressure and velocity and exhibits unstable vortices. The flow regime that a gas will occupy is dependent on its density and speed (and therefore temperature) as well as the dimensions of the containing vessel. At low pressures the mean free path of the gas molecules is much larger than the dimensions of the containing vessel, the flow is in a free molecular state. In this state the behaviour of the molecules are governed by molecular phenomena and their velocity is essentially random. Between viscous and molecular flow regimes lies a transition region. In this case the mean free path is of the same order as the dimensions of the containing vessel. The Knudsen number allows a calculation of which state the gas inhabits, either viscous or free molecular flow [108]:

$$Kn = \frac{\lambda_{MFP}}{L_{Char}} \qquad 5.4$$

A Knudsen number greater than one signifies that the flow is in a free molecular regime. Between 0.01 and 1 the flow is transitional, and viscous below 0.01. λ_{MFP} is the mean free path between molecular collisions and L_{Char} is the characteristic length, directly related to the dimensions of the system or the region of interest. The mean free path is described by:

$$\lambda_{MFP} = \frac{1}{n\sigma} \qquad 5.5$$

Where n is the number of particles per unit volume and σ is the collisional cross-sectional area of the particles and the total cross-section for argon is approximately $3.5\text{x}10^{-21}$ m^2 [78]. At an internal chamber pressure of $2\text{x}10^{-3}$ mBar, the number density is $1.972\text{x}10^{18}$ m^{-3} and the mean free path is 144.8m. This is far in excess of the characteristic length meaning that the Knudsen number is greater than one and the system is in a free molecular flow regime. While the Knudsen number helps define transition between laminar and free molecular flow, the Reynolds number helps define transition between turbulent and laminar flow. The transition from laminar to turbulent flow takes place when the flow speed, gas density or pipe diameter are increased. The Reynolds number is defined by [109]:

$$\text{Re} = \frac{\rho UD}{\mu_V} \qquad 5.6$$

ρ is the gas density, U is the flow speed, D is the pipe diameter and μ_V is the dynamic viscosity, equal to $22.9\text{x}10^{-6}$ Pa.s for Argon. In this case, the relatively low density and diameter of the hollow cathode tube act to keep the Reynolds number low, well below the point where turbulent flow occurs in a pipe (> approximately 2300) [110]. At 20mBar, the Reynolds number in the cathode is 39.2, in feed tube it is around 1000, still below the transitional region. The flow in the system is therefore laminar in the feed tube and hollow cathode, then goes through a transition to a free molecular flow regime downstream in the vacuum chamber. The determination of mass flow rate using the chamber pressure, volume and pumpdown time is therefore still valid as measurements are made in the vacuum chamber which inhabits the free molecular flow regime.

At the orifice, the flow will reach sonic speeds when the critical pressure ratio condition is met, seen in equation 5.7 [111].

$$\frac{P_{Down}}{P_{Up}} = \left(\frac{2}{\gamma+1}\right)^{\frac{\gamma}{\gamma-1}} \qquad 5.7$$

This evidently places a limit on the gas velocity at the orifice. The value of γ is the ratio of specific heats and is equal to:

$$\gamma = \frac{C_P}{C_V} = 1.667 \text{ for Argon} \qquad 5.8$$

The critical ratio for Argon is 0.487. To reach sonic speeds, the gas pressure must therefore drop to just less than half its upstream value over the region concerned. Note that the sonic speed for an ideal gas is given by [112]:

$$v_S = \sqrt{\frac{\gamma RT}{W}} \qquad 5.9$$

Where R is the universal gas constant, T is the temperature and W is the molar weight. For Argon this would be equal to $320ms^{-1}$ at room temperature, reaching $670ms^{-1}$ at $1000^{o}C$. The gas temperature is therefore important in understanding the flow speed.

Each of the micro hollow cathode devices was not observed to glow except at the lowest flow rates ($2.4x10^{-7}$ kgs^{-1}). Under these conditions the discharge voltages were extremely high, around 250V and increased with increasing current. The cathode therefore generally operated at below a temperature $800^{o}C$ where the body would be observed to luminesce. Measurements using the thermocouple showed that the cathode operated above room temperature, but these measurements were hampered by failure of the thermocouple and its placement outside the inner ceramic sheath. The few measurements made, at around 350K, are therefore very likely to be significantly lower than the actual temperature of the cathode wall, which is likely be increased by processes such as ion impact and arcing between matrix grains.

The contributions to flow speed from ionisation modify the Boltzmann equation. The equation for the flow speed at the orifice, U_{or}, becomes [31]:

$$U_{or} = \sqrt{\frac{kT_i}{m_i}\left(1+\alpha\frac{T_e}{T_i}\right)} \qquad 5.10$$

k is the Boltzmann constant, m_i is the ion mass, T_e and T_i are the electron and ion temperatures respectively and α is the degree of ionisation. The low currents and relatively high flow rates that the micro hollow cathodes were operated at, mean that ionisation was low. Even at high electron temperatures the flow speed in the orifice would be dominated by the neutral's motion. Flow speed is therefore largely dependent on the sonic velocity and hence temperature and molar weight if the critical pressure condition is met.

A final method of verifying the volumetric pumping speed of a system relies on determining the gas flow conductance of the connections from the vacuum system to the turbopump. Conductance is a measure of the resistance of an orifice to flow through it and is dependent on the dimensions of the orifice. It decreases rapidly with diameter with a lesser dependence on length. In a free molecular flow regime, the conductance of a short, round orifice is given by [113]:

$$C = \frac{v_{Avg}}{4} A_{pipe} \qquad 5.11$$

where v_{Avg} is the average molecular velocity and A_{pipe} is the cross-sectional area of the vacuum line.

The average molecular velocity is described in terms of temperature, T_0, and atomic mass, m_n:

$$v_{Avg} = \sqrt{\frac{8kT_0}{\pi m_n}} \qquad 5.12$$

Equal to 394.4ms^{-1} for Argon at 293K. Obviously this will change at higher temperatures, but again if it is assumed that the gas is at room temperature when going through the pump system this method can be used. To determine the overall pumping speed of the system, the pumping speed of the vacuum system must be added in parallel to the overall conductance of the orifices leading to it. The conductance of each connection between the chamber and the vacuum system must also be added in parallel [113a]:

$$\frac{1}{Q_{Pump}} = \frac{1}{Q_{PS}} + \frac{1}{C_1} + \frac{1}{C_2} + \frac{1}{C_3} \ldots \qquad 5.13$$

Q_{PS} is the manufacturers quoted pumping speed; C_n is the conductance of connection *n*. From the chamber to the turbopump, there are 5 interconnecting orifices. The chamber neck, a step-down orifice (from 250mm diameter to 150mm diameter), a gate valve, a CF to ISO adaptor and the neck of the turbopump itself. Using information on the conductance of various orifices of specified dimensions it was possible to calculate the overall conductance and thus the pumping speed of the system. For air, the solution to equation 5.13 gives a pumping speed of 180ls^{-1}. However, flow rate is inversely dependent on dynamic viscosity. The dynamic viscosity of Argon, at 22.9μPa.s, is greater than air at 18.5μPa.s. Factoring in this difference gives a theoretical pumping speed of 145ls^{-1}, which agrees well with both the previous methods. This further backs up previous calculation on pumping speed and therefore mass flow rate.

To ensure measurements on flow rate were correct, checks were made on potential leaks in the system. Tests were performed on the leakage of connections in mass flow feed to the cathode during operation. Fig 5.3 shows the downstream pressure as a function of upstream pressure for cathodes with open and closed orifices.

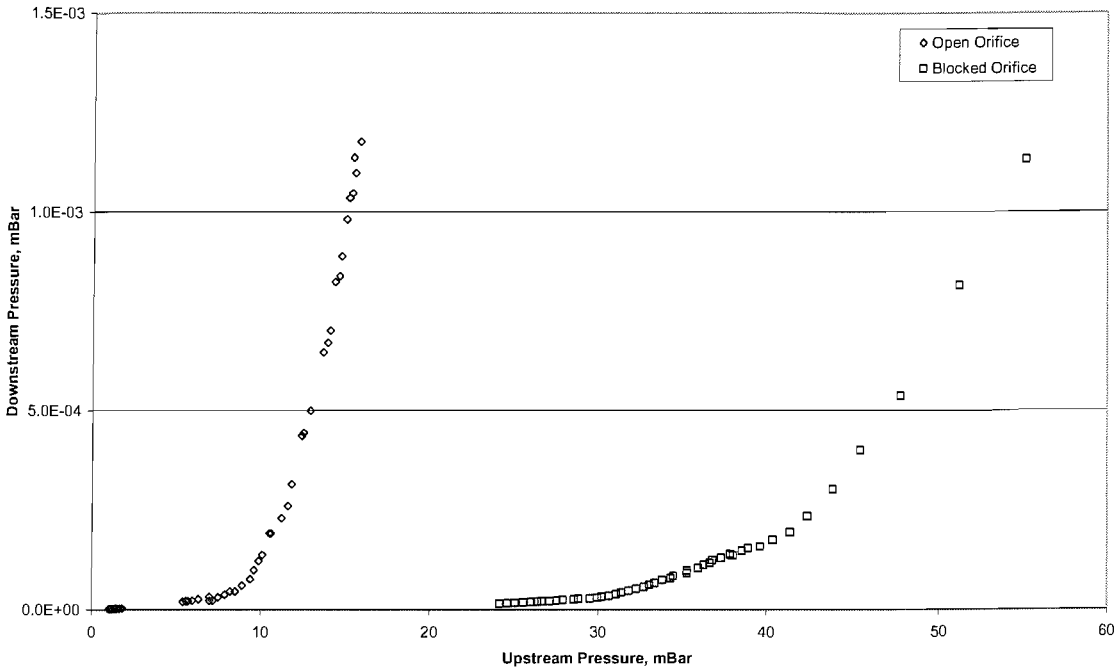

Fig 5.3 Cathode Leak as a function of Pressure

The upstream pressures required to achieve the same downstream pressures (indicating a similar flow rate) through leaks alone are around 3.6 times larger than when the orifice is open. It has previously been shown that flow rate through the system is approximately linearly dependent on downstream pressure. The flow rate through leaks when the cathode orifice is blocked is significantly lower than that through an open orifice as can be seen through the much higher pressures required to attain the same downstream pressure and hence flow rate. There is therefore a small amount of leakage through connections to the cathode body, but it is small in comparison to the flow through the cathode orifice. Further, the hollow cathode is not operated at these higher pressures where leakage becomes significant, allowing any effect due to leaks to be discarded. The flow rate into the chamber as a result of leaks in the cathode feed line is therefore assumed to be negligible in comparison to the flow the orifice itself. The continued good performance at high vacuum during pumpdown (10^{-8} mBar range) implied that external leaks were negligible. Leaks would reduce the apparent performance of the device as higher internal pressures would be required to achieve the same operating characteristics and would also raise the uncertainty associated with mass flow measurements, reducing confidence in the results.

These experiments have shown that a simple knowledge of the surrounding conditions enables the mass flow rate through the novel micro hollow cathode to be established and the bulk of the gas has been shown to flow through the orifice.

5.2.2. Initiation Voltage as a function of Mass Flow Rate

One of the main factors affecting initiation voltage is the gas conditions between the keeper and cathode body. The pressure of the gas between these two electrodes is a major influence the initiation voltage. However, pressure variations downstream of the cathode orifice are extremely hard to measure. Fluid dynamics states that for a mass flow into a vacuum system, the pressure drops from its upstream value to ambient over approximately one orifice diameter downstream [29]. The orifice geometry, upstream pressure, temperature and cathode internal surface roughness will all affect the local pressure. Paschen described the relationship between initiation voltage and the product of the gas pressure and the cathode-keeper separation. Describing this relationship is not a trivial matter due to the dynamic nature of the flow conditions in the region between keeper and cathode, as well as the non-uniform geometry of the device, which is likely to result in further microscopic pressure differentials dependent on the geometry of the orifice. It is therefore useful to compare initiation voltages in terms of mass flow rate as this can be measured more easily and is more critical to propulsion systems.

As the region close to the orifice is at a much higher pressure than the region close to the keeper the pressure dependence of the initiation voltage will dominate over the dependence on distance. As stated, the pressure drop-off from the cathode interior to chamber ambient occurs over approximately one orifice diameter. Therefore at very low separations, less than 0.2mm, the pressure between the electrodes per unit length will be significantly higher than when the electrodes are at greater separations. This makes

calculations of the pressure-distance relation, used by Paschen extremely difficult. This is further complicated as the gas is flowing rather than static, and undergoes a pressure drop downstream of the orifice, with the highest pressure variation seen near to the orifice [29].

An easier method of comparing initiation conditions is to use mass flow rate at constant cathode-keeper separations. For ion thruster operation this is a crucial factor as it is desirable to minimise the mass flow rate in terms of initiation voltages to conserve fuel. The uncertainty of the flow rate below $4.5x10^{-7}$ kgs^{-1}, when the mass flow controller was in use, was quoted at $9x10^{-9}$ kgs^{-1}. Above this level, when flow rate values depended on calculation, the uncertainty was calculated at 21.9%, and resulted from the uncertainty in the pressure measurements ($>1x10^{-4}$ mBar). The same uncertainties can be applied to all measurements seen in this section and to all measurements of flow rate. Fig 5.4 shows the cold-start initiation voltage curve for the simple molybdenum cathode with associated uncertainties, low at low flow rates and high at higher levels. Boundaries on the initiation regions have been approximated showing areas below the curve where initiation will never occur, around the curve, where initiation will sometimes occur and above the curve where initiation always occurs. Initiation voltage measurements were generally carried out under cold-start conditions where the cathode was at room temperature to allow a good comparison between the cathode types, as uncertainties in cathode tip temperature were high when using the heater system.

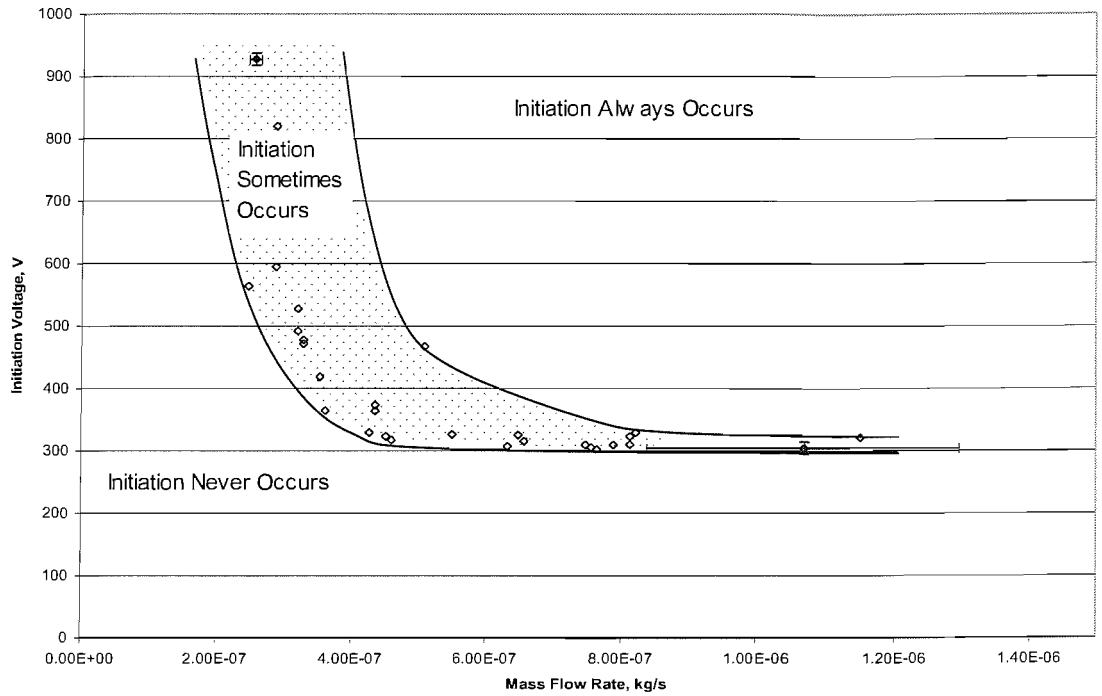

Fig 5.4 Initiation Voltage as a function of Mass Flow Rate, simple Molybdenum cathode, 0.9mm keeper-cathode separation

At low flow rates, below $5x10^{-7}$ kgs^{-1}, the initiation voltage is highly variable (between 300 and 1000V), a result of the unstable nature of the factors determining the initiation voltage. Such factors include the local pressure, temperature, electrode separation and orifice geometry, which is known to change with time due to erosion of the orifice. Above this level, the initiation voltage is observed to stay at an approximate minimum of 300V and is much more stable. These results are similar to early measurements made on mercury hollow cathodes [114].

Fig 5.5 shows the initiation voltage as a function of mass flow rate for the surface impregnated hollow cathode. These measurements show the lowest initiation voltages for any of the cathodes tested. The dependence follows that expected, with decreasing initiation voltages for higher flow rates to an approximate steady state just below 300V. The keeper-cathode separation for this experiment was lower than that for the simple molybdenum cathode. Measurements are therefore not directly comparable. However, if

different cathode-keeper separations are relatively close and substantially greater than the orifice diameter, they can be assumed to be in the same range as the average pressure per unit length between the electrodes is similar. This is evidently not the case when comparing high to very low keeper separations where the average pressure per unit length can be vastly different.

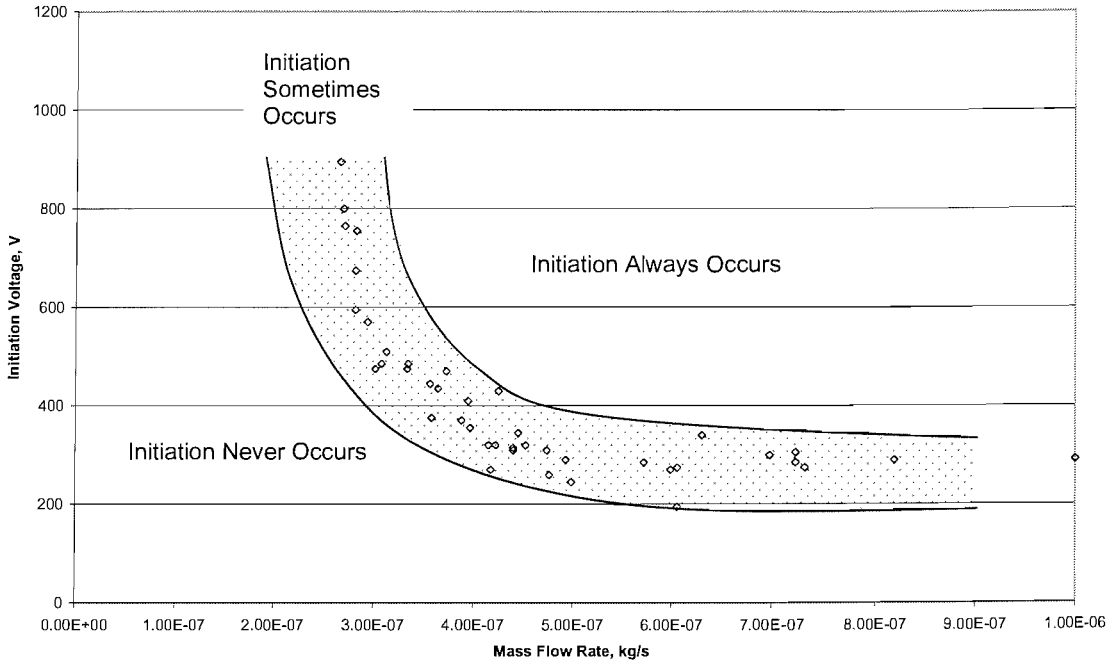

Fig 5.5 Initiation voltage as a function of mass flow rate, surface impregnated cathode, 0.5mm keeper-cathode separation

The initiation voltage for the surface impregnated cathode is similar to that seen for the simple molybdenum cathode, but performs slightly better, with lower initiation voltages at similar flow rates, most obvious at the lower flow rates. This is likely a result of the lower work function as well as the lower electrode separation used when testing the surface impregnated cathode, which was duplicated in tests on the impregnated insert cathode. It may also be affected by non-uniformities introduced through the impregnation process, which may locally enhance electric fields. There are a number of points where initiation took place at voltages lower than expected, widening the band at

higher flow rates where initiation sometimes occurs. However, initiation voltage under these conditions is neither easily modeled, or particularly repeatable.

Fig 5.6 compares the initiation voltages for the impregnated insert hollow cathode performed at different cathode-keeper separations to try to demonstrate the effect that altering the electrode separation has on initiation voltage. It should be noted that the large uncertainty in the high end mass flow rate arises primarily from a systematic error. This does not therefore affect analysis of the relative performance of the three cathodes.

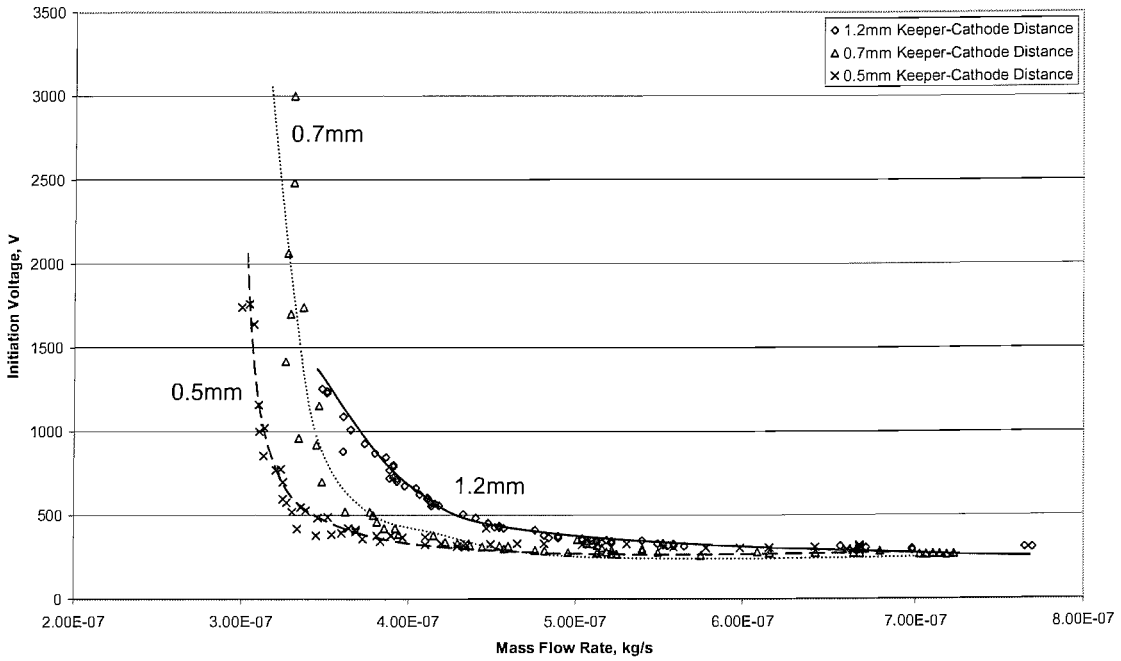

Fig 5.6 Initiation voltage as a function of mass flow rate, impregnated insert cathode, different keeper-cathode separations

The lowest separation shows the lowest initiation voltages, however, the difference is minor except when the mass flow rate is below $5x10^{-7}$ kgs^{-1}. At higher flow rates the initiation voltage stabilises around 300V for all keeper separations. According to Paschen, the initiation voltage reaches a minimum at a certain point dependent on the product of gas pressure and electrode separation (P.d). Lower *or* higher values of P.d result in increased initiation voltages. Therefore increasing the

electrode separation from zero at a given pressure will first result in a decrease, followed by an increase in initiation voltage. As stated, modeling this for a non-planar surface under differing pressures and flowing conditions is difficult. Measurements at low flow rates suggest the initiation voltage inhabits the right side of the Paschen curve, where decreasing electrode separation results in lower initiation voltages. On the right side of the minimum on the Paschen curve the electron mean free path in terms of the inter-electrode gap is short. At very high values of P.d the mean free path, and thus time between collisions decreases. The amount of energy an electron can gain by being accelerated in the electric field therefore falls, decreasing ionisation. This results in an increase to the voltage required for gas breakdown to initiate the discharge. On the left side of the Paschen minimum the electron mean free path exceeds the inter-electrode gap and vacuum breakdown occurs as ionisation of the gas is small and does not aid breakdown [115]. However, as the Paschen curve models planar geometries and static gas conditions, the decrease in initiation voltage at lower separations cannot be directly attributed to this effect. Another significant effect of altering electrode separation is on the electric field density between the non planar electrodes, complicated by various material types in different parts of the cathode which could be subject to different fields dependent on the electrode configuration. It is therefore very difficult to predict the initiation behaviour of hollow cathodes. Initiation voltages are approximately equal above $5x10^{-7}$ kgs^{-1} for cathode-keeper separations between 0.5 and 1.2 mm. This is satisfied by the postulated reduced dependence on electrode distance at larger separations (in comparison to a high variation seen at low separations) and the relatively large uncertainty in measurements. The keeper-cathode separation must therefore be optimised to decrease the initiation voltage where possible, but must also permits the plasma to pass through it and be configured to sustain the lowest possible voltages during discharge operation, improving efficiency.

Fig 5.7 illustrates initiation voltages for the three cathode types. The keeper-cathode separation for the simple molybdenum cathode was greater than for the other two, so is not directly comparable at higher flow rates, but serves as a guideline. There are only minor variations between all three cathode types, seen primarily at low flow

rates. Overall there is a general concurrence between all three types at higher flow rates with the surface coated showing slightly lower voltages overall. At lower flow rates the impregnated insert device performs the worst; the simple and surface coated bodies perform similarly. It would be expected that the impregnated devices would show the lowest initiation voltage if lowering the work function of the insert plays any role in determining the initiation voltage. It is therefore believed that the breakdown path is from the orifice to the keeper edge, which is the shortest path from areas likely to have the greatest amounts of surface irregularities and therefore intense localised electric fields. This is backed up by the fact that overall the surface impregnated cathode performed better overall as the impregnant coating was across all of the cathode surfaces, including at the orifice where breakdown was likely to initiate. Fig 5.6 also showed that at the highest flow rates the initiation voltage was independent of keeper-cathode separation. The concurrence of the simple cathode and impregnated insert initiation voltages at high mass flow rates, and their poorer performance in comparison to the surface coated cathode further suggests that breakdown occurs from similar areas, presumably at the cathode orifice.

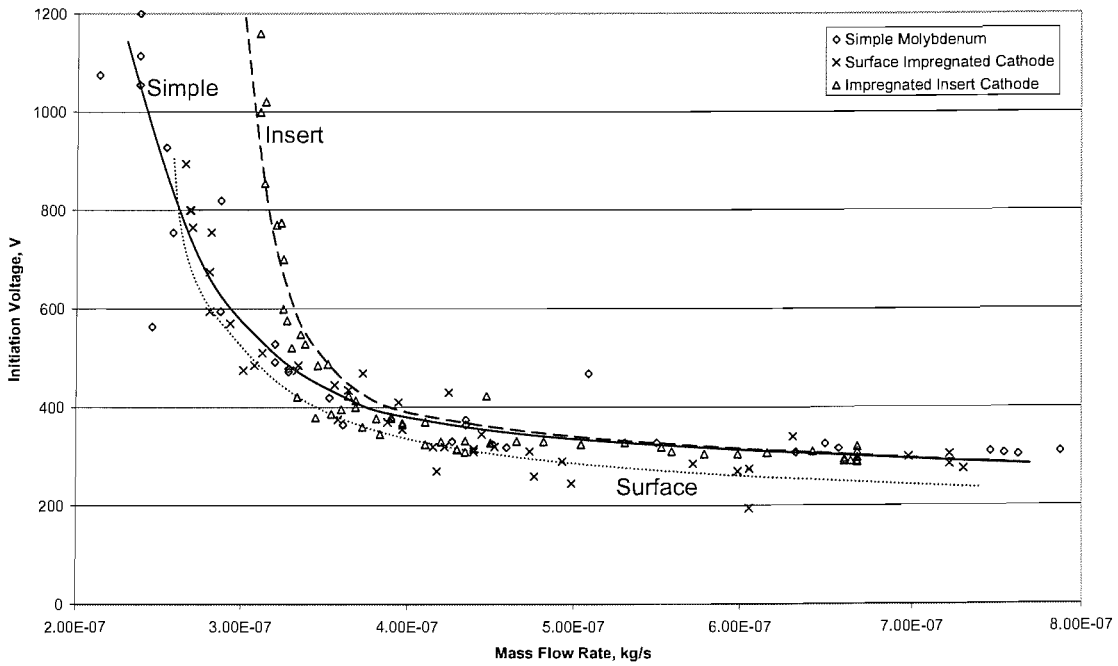

Fig 5.7 Initiation voltage as a function of mass flow rate for 3 cathode types

The variability of the results for the simple molybdenum cathode is attributed to erosion of the device seen in initial testing. Tip erosion primarily arose from arcing seen during optimisation of the electrical system. This resulted in an uneven orifice, which altered pressure and electrical differentials in the inter-electrode region. The surface impregnated and impregnated insert cathodes were subject to lesser erosion over their lifetimes due to improved power supply and initiation procedures. Section 5.4 shows images of erosion induced failure in the simple molybdenum cathode.

The highest initiation voltages were exhibited by the impregnated insert model. This may be due to the devices' smaller internal diameter upstream of the orifice, altering the pressure differential downstream of the orifice. At higher flow rates (in excess of $5x10^{-7}$ kgs^{-1}) initiation voltage is independent of both cathode type and keeper separation, within the limits seen. During initiation, the likely breakdown path was the shortest one, from the inside of the turned orifice to the keeper edge. This would enhance erosion and likely was instrumental in shortening lifetime. The insert will not initially play a role under cold-start conditions other than in altering the dynamics of the gas flow. Irregularities on the surface impregnated cathode and its lowered work function could therefore play a minor role in decreasing the initiation voltage. Variations in tip geometry will also arise from micromachining techniques used in fabrication of such devices as working at such small scales can lead to significant proportional variations in the overall geometry. These experiments have shown that cold-start initiation is a viable method of initiating the plasma in this novel micro hollow cathode device.

There are several methods of improving the initiation voltage performance of a hollow cathode. Optimisation of the geometry and utilisation of low work function materials would increase the electron emission current prior to discharge initiation, lowering the required voltage. Increasing the ambient pressure between the electrodes using, for example, an enclosed keeper would lower the required flow rate to reach a specified initiation voltage. Finally, heating the cathode would increase thermal emission of electrons, resulting in greatly reduced initiation voltages beyond a minimum temperature around $800^{o}C$.

5.2.3. Thermal effects on Initiation Voltage

The effect of increasing temperature on initiation voltage is marked. This section attempts to explore this relationship for the impregnated insert cathode. Tests were carried out using the impregnated insert cathode with Argon seed gas and at a cathode-keeper separation of 0.7mm. Temperature measurements were made using a disappearing filament pyrometer and a Type K thermocouple. The pyrometer had a significant associated uncertainty in its measurements but operates over a wide temperature range, though cannot function below the threshold for luminescence for a material. The thermocouple worked at lower temperatures, but failed at higher levels. Photographs of the cathode operating in a thermal emission regime can be seen in section 5.4.

Fig 5.8 shows a rise in initiation voltage as a function of tip temperature at around 1000°C. Above 1000°C the initiation voltage falls, consistent with thermionic emission, eventually to a level three times lower than that at room temperature at 1250°C. There may also be thermal effects on the chemistry of the impregnant mix, altering the surface work function. The exposed end of the heater near the keeper was seen to glow during heating. This would cause thermionic emission of electrons which would be attracted to the keeper and affect the field experienced at the cathode tip. This is believed to be the reason for the increase in initiation voltage at around 1000°C when the heating filament would be emitting copiously. At higher temperatures the increased emission from the cathode itself is sufficient to decrease the initiation voltage to below 150V.

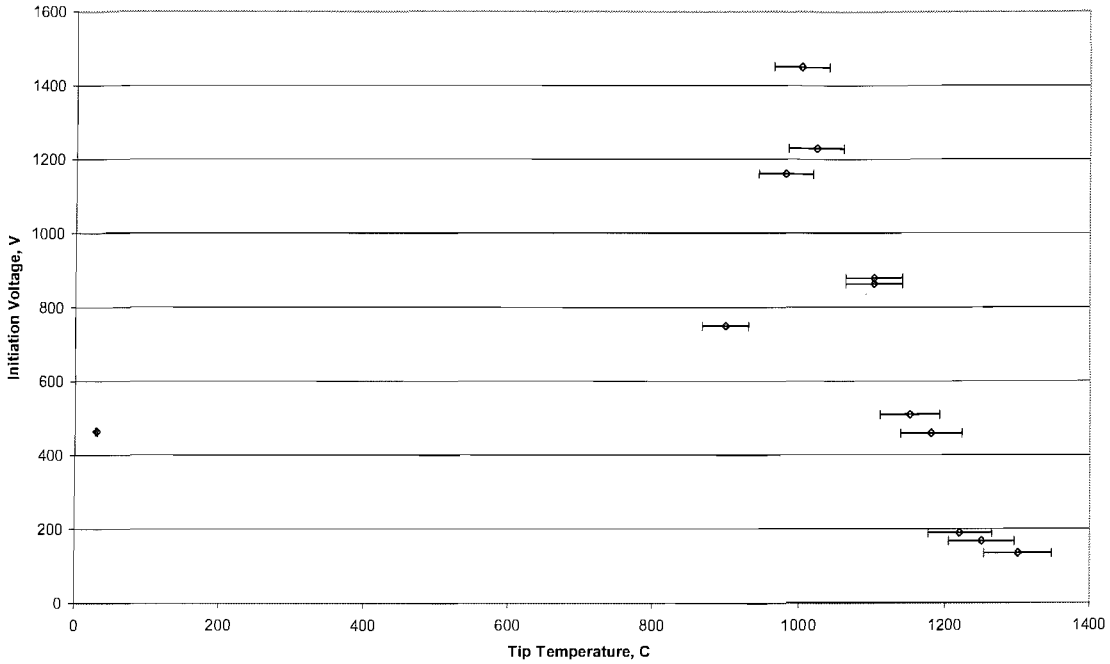

Fig 5.8 Variation of initiation voltage with tip temperature at 3.5×10^{-7} kgs^{-1}

The heater design would not allow this problem to be easily remedied and a redesign would be required. However, good cold-start operation meant this was not needed. Results may also be affected by the change in pressure distribution due to the rise in viscosity associated with the rise in the cathode wall temperature. The quoted uncertainty of the optical pyrometer was stated to be $\pm 50^0$C. There were no measurements between 20 and 900^0C as the type K thermocouple failed during tests and the optical pyrometer was limited to temperatures where the cathode was observed to glow.

Fig 5.9 again shows the variation in initiation voltage as a function of tip temperature, but this time at a much lower flow rate of 1.5×10^{-7} kgs^{-1}. Interference from the electric field of the heater has meant that once more the initiation voltage undergoes an increase until thermal factors dominate at high temperatures. At low flow rates the effect of increasing tip temperature is obvious and heating may be necessary under operational conditions where initiation voltage must be optimised. In this experiment the heater is operated at 4.5W for around 90 seconds to allow the tip to exceed 1000^0C. The

miniaturised hollow cathode will allow faster temperature increases than a traditional device due to the lower mass, and should therefore be more efficient in heating the cathode for discharge initiation. The relaxation time to drop from this temperature to ambient was just over 630seconds.

In this case the micro hollow cathode could not sustain the discharge at low flow rate (which would be desired in a neutraliser) and low current. Efforts to draw larger currents from the device using the anode, which would sustain the discharge at lower flow rates, were unsuccessful as a stable discharge could not be maintained, potentially due to the small size of the device limiting the maximum current density. Using the heater during initiation increases device lifetime as there will be less orifice erosion as the discharge is easily initiated, but heating could also increase the depletion of impregnants adversely affecting insert lifetime.

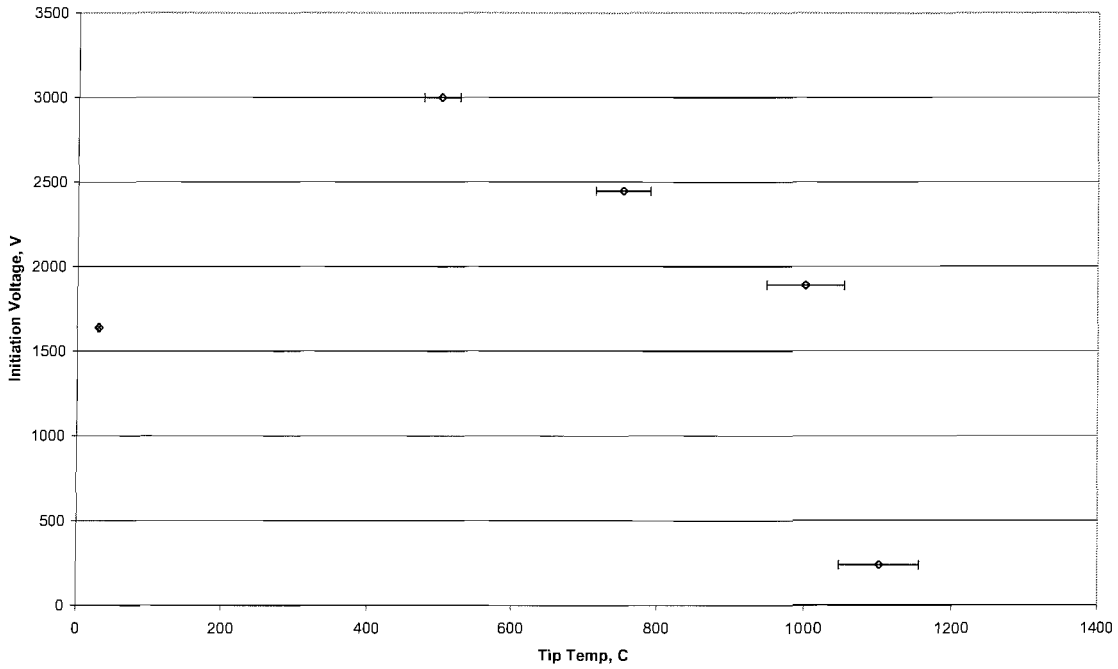

Fig 5.9 Variation of initiation voltage as a function of tip temperature at 1.5 x10^{-7} kgs^{-1}

5.3. Voltage-Current Relationship

The voltage-current relationship in a hollow cathode is the primary measure of cathode performance for a given mass flow rate. Mass flow rate is the primary factor in determining the discharge voltage at a given current for a given cathode configuration (gas, geometry, materials). The voltage-current relation should exhibit a negative resistance, with falling discharge voltage as current is increased across some portion of the operating regime of the cathode. Hollow cathodes operate in one of two modes, known as spot and plume. The mode of operation will significantly alter the discharge voltage. The spot mode is characterised by lower discharge voltages, higher luminosity in the region of the orifice and takes place at higher currents and flow rates. The transition from plume to spot mode is governed by a number of factors including the gas species and flow rate, the current and the orifice dimensions [35]. A likely explanation for spot mode operation is that the existing ionising events within the cathode are sufficient to maintain the discharge, whereas in the plume mode additional ionisation is required in the cathode-keeper gap, necessitating higher voltages [91]. Operation of a cathode at higher currents also increases back ion bombardment, this increases the temperature of the device and acts as an impedance to the flow. The resulting increase in pressure in the cathode will enhance emission for a given mass flow rate making spot mode operation more likely.

Discharge voltages should therefore decrease as both the mass flow rate of the seed gas and the current is increased. Applied discharge voltages are generally around 2 to 4 times the first ionisation potential of the propellant, or approximately 30-60V for Argon [79], though can be much lower for devices operated at high currents, the T6 cathode can operate as low as 4V at 20A using Xenon. The keeper current, measured here is the sum of the electron emission current from and the ion current to the cathode. Measurements on the electron saturation current using an unshielded faraday cup suggested that the electron current made up at least 70% of the keeper current (see fig

B.1 Appendix B) and was likely substantially higher, with quoted values for ion current at the orifice in hollow cathodes at 10% of total current [116].

This section looks at the performance of the three types of micro hollow cathode, focusing on a comparison of the surface impregnated and impregnated insert types. All cathodes were operated in a diode configuration in a constant current mode with variable discharge voltages. Measurements were made with the anode in a floating state, not at any applied potential; in some cases probes and heater were also present in a floating state. The cathode was allowed to stabilise for at least four minutes after initiation, and measurements were made when the discharge voltage deviated by less than 0.5% per minute. A period for stabilisation of the voltage was also allowed on alteration of the discharge current.

Experimental conditions were replicated as closely as possible between measurements on the different cathode types. Experiments were performed at comparable keeper-cathode separations and at a variety of flow rates over similar ranges. To minimise the effect of other variables on the voltage-current relationship all experiments were performed using high purity, 99.999%, Argon and the same keeper was used throughout. Also, cathode bodies were manufactured from a single Molybdenum tube and orifices were constructed with as close to uniform geometry as possible. These tests would determine if the impregnated insert cathode operated at lower voltages for similar currents over the other models.

5.3.1. Simple Molybdenum Hollow Cathode

Discharge voltage is a key factor in hollow cathode operation as it affects both the plasma properties, the power required by the cathode and the lifetime of the device. The power input to the cathode per electron output is instrumental as it defines the efficiency of the device. The simple molybdenum cathode was the first and most basic device

constructed. It consisted solely of a non-impregnated molybdenum body with turned orifice.

Fig 5.10 shows the minimum voltage needed to sustain the hollow cathode discharge at constant current of and varying mass flow rates. The keeper-cathode separation was 0.9mm ±0.05mm and the current was set at the maximum of 13.3mA. Low end flow rates, below $4.5x10^{-7}$ kgs^{-1}, were set using the MKS flow controller. Higher values were calculated using pressure measurements and flow balance relations, described earlier.

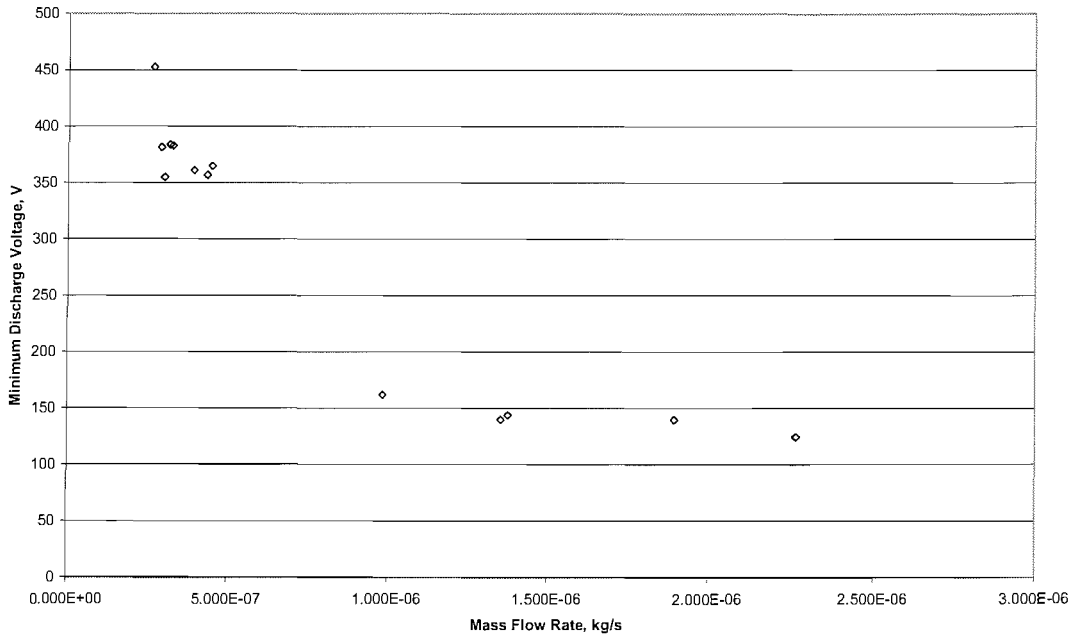

Fig 5.10 Minimum Discharge Voltage as a function of Flow Rate at 13.3mA, Simple Mo Cathode

In this case it is evident that mass flow rate has a lesser effect on discharge voltages above $1x10^{-6}$ kgs^{-1}. The uncertainty in the mass flow rate above $4.5x10^{-7}$ kgs^{-1} was calculated at 21.9%. Below $4.5x10^{-7}$ kgs^{-1} the uncertainty in the mass flow controller is stated as $9x10^{-9}$ kgs^{-1}. Uncertainties were therefore minor in comparison to

overall flow rates. The uncertainty in the discharge voltage and current was given as ±0.2 Volts from technical specifications and estimated at ±0.2mA for the current.

The minimum discharge voltage follows the same decreasing trend with increasing flow as that seen for initiation voltage. The minimum voltage observed was 125V at a flow rate of 2.25×10^{-6} kgs^{-1}, but was within approximately 10% of this level by 1.35×10^{-6} kgs^{-1}. This voltage is significantly higher than that seen in other cathodes developed for ion thrusters, by a factor of four or more. The simple molybdenum cathode is therefore unlikely to be particularly suitable for application to micro ion thruster design but does provide a suitable benchmark for comparison of the performance of later models. Fig 5.11 shows the voltage-current relationship for the simple molybdenum hollow cathode operated at a high flow rate of $1.7 \times 10^{-6} kgs^{-1}$ and a keeper cathode separation of 0.9mm.

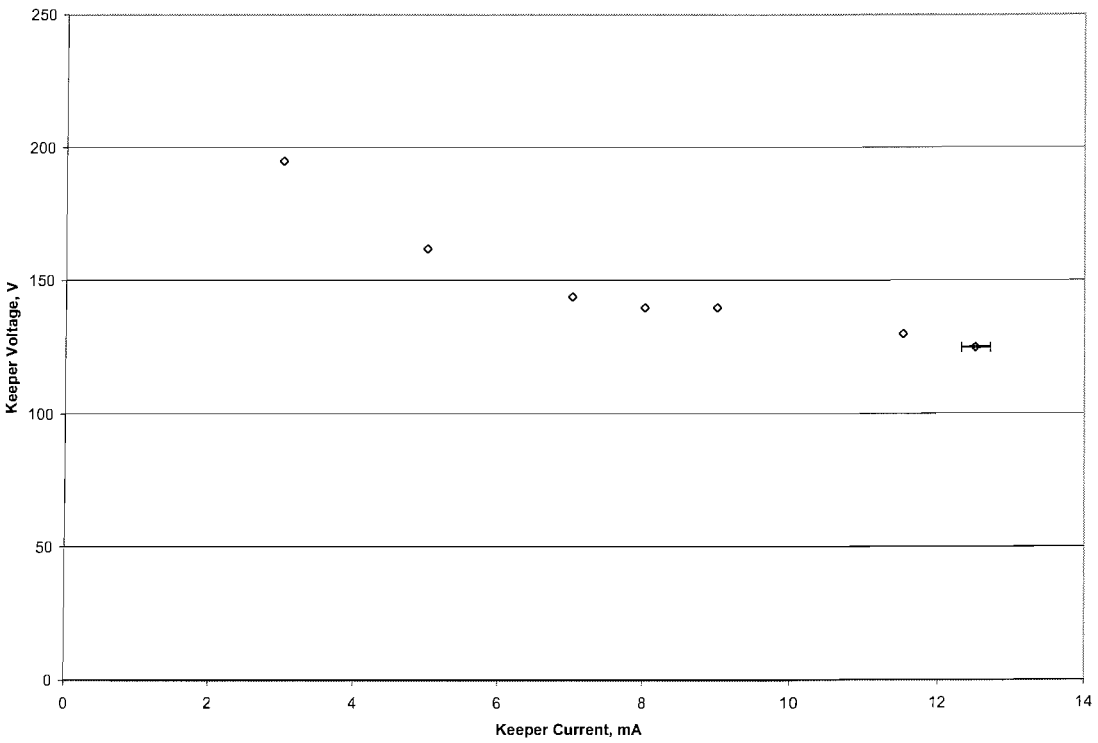

Fig 5.11 VI curve: Simple Molybdenum Cathode, 1.7×10^{-6} kgs^{-1}, 0.9mm k-c separation

At these higher flow rates the cathode was operating in the spot mode and the negative resistance trend is consistent with that expected from a hollow cathode device, though at higher relative voltages, from approximately 195V to 125V. These voltages are again too high to offer efficient operation in a practical device. Measurements could not be made on the voltage current relationship of the simple molybdenum cathode at low flow rates. This was due to the fact that the discharge would quickly extinguish as the current was reduced from its maximum. Note that the electrical supply was limited to a maximum current of 13.3mA. This was a limitation in terms of what would be required of a hollow cathode, even at such a small scale, and in conducting tests on the device, where we would wish to observe the cathode operating at higher currents. As stated, attempts to operate the cathode at higher currents met with failure, potentially due to the small size of the device.

The power input per mA output current for the simple molybdenum cathode under these conditions was between 0.14 and 0.22W/mA, assuming electron emission current is at 90% of keeper current, as in larger diameter cathodes [116]. This is better than FEEP cathodes at 0.6W/mA, but does not match large hollow cathodes, e.g. the T6 cathode at 20A operates at outputs of around 0.004W/mA.

5.3.2. Surface Impregnated Hollow Cathode

Impregnating the surfaces of the simple molybdenum body was the next step in development of the novel micro hollow cathode device. A wide range of tests were performed on this model, primarily for comparison with the impregnated insert device. Measurements were carried out at a cathode-keeper separation of 0.5mm at flow rates in the 10^{-7} and 10^{-6} kgs^{-1} range. As with the previous experiments, the uncertainty in the flow rate was greater at higher values, reaching 21.9% of the total flow rate value. Uncertainties in the voltage and current measurements and the cathode-keeper separation were small and a result of systematic errors in the measurement devices.

Fig 5.12 shows that the minimum sustainable discharge voltage for the surface impregnated cathode was approximately 75volts at a current of 13.3mA and a flow rate of $1x10^{-6}$ kgs^{-1} and had reached to within 10% of this at $5.14x10^{-7}$ kgs^{-1}. Stable conditions at higher voltages can be observed above the minimum due to the inherent variability in hollow cathode operation, especially at low flow rates when the cathode operates in the plume mode. At higher flow rates, around $1.8x10^{-6}$ kgs^{-1}, the discharge voltage dropped to 64Volts. This discharge voltage is within a factor of three of operating voltages for cathodes used in existing ion thrusters, still at a level where significant optimisation would be necessary for use in a propulsion system. The higher potential may be necessary across the orifice to extract the measured currents as the current density in orifice is very low and plasma conductivity to electrons may be much lower than in larger cathodes. At an electron emission current of 10mA the current density in the orifice is around $0.3Amm^{-2}$, considerably lower than the T5 cathode at on the Artemis mission at $34Amm^{-2}$ or the T6 cathode on the Bepi-Colombo mission at 12-$18Amm^{-2}$. The power consumed was low due to the low currents involved, between 0.33 and 0.85W.

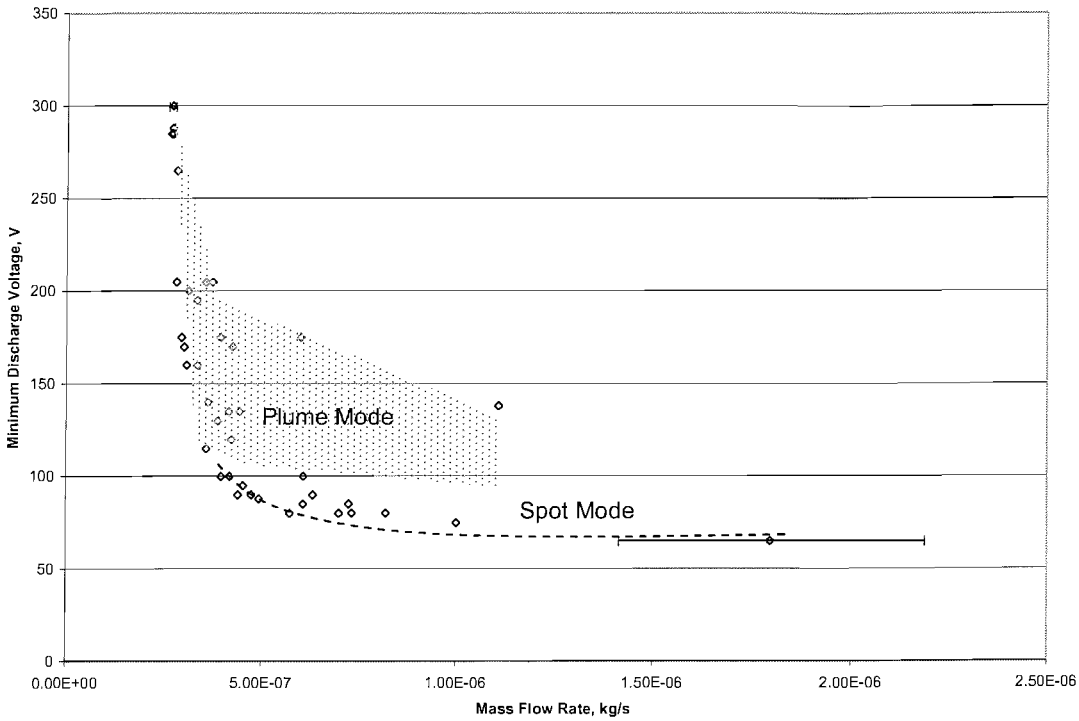

Fig 5.12 Minimum Discharge Voltage as a function of Flow Rate at 13.3mA, Surface Impregnated Cathode

The large variation in values of discharge voltage between $3X10^{-7}$ to beyond $1x10^{-6}$ kgs^{-1} indicates the presence of a transition region where the cathode would switch between spot and plume modes. Fig 5.13 shows a large variation in discharge voltage at the upper end of the current scale. This indicates a transition between the high voltage plume mode, and the lower voltage spot mode at this point.

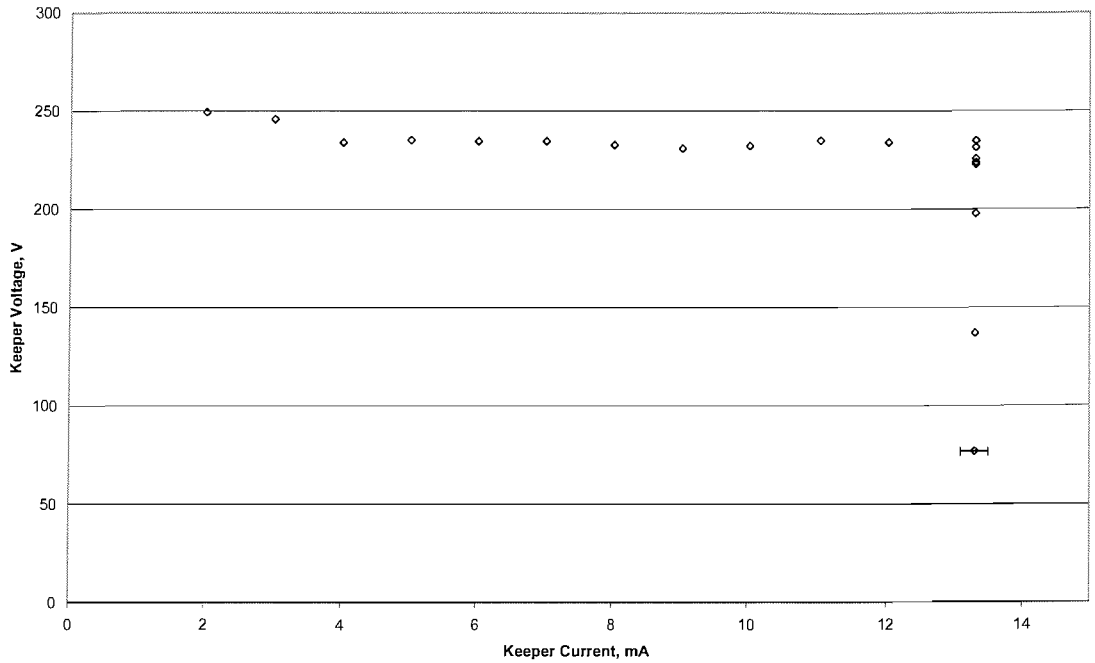

Fig 5.13 V-I Curve: Surface Impregnated Cathode, $1.1x10^{-6}$ kgs^{-1}

Transitions between the two modes were frequently observed for this cathode type, making measurement of the voltage-current relation for spot mode operation difficult to measure due to the highly varying voltages over short timescales. As stated, the electrical supplies were limited to a maximum current of 13.3mA, around the limit for transition between spot and plume modes for the surface impregnated cathode at this flow rate of $1.1x10^{-6}$ kgs^{-1}, which is a critical factor in determining the mode of operation.

Fig 5.14 shows the variation of keeper voltage with current for similar flow rates just below the $1x10^{-6}$ kgs^{-1} level. There is only a small variation between the keeper voltages for a specific current with the higher flow rate at a lower value of discharge voltage, as expected.

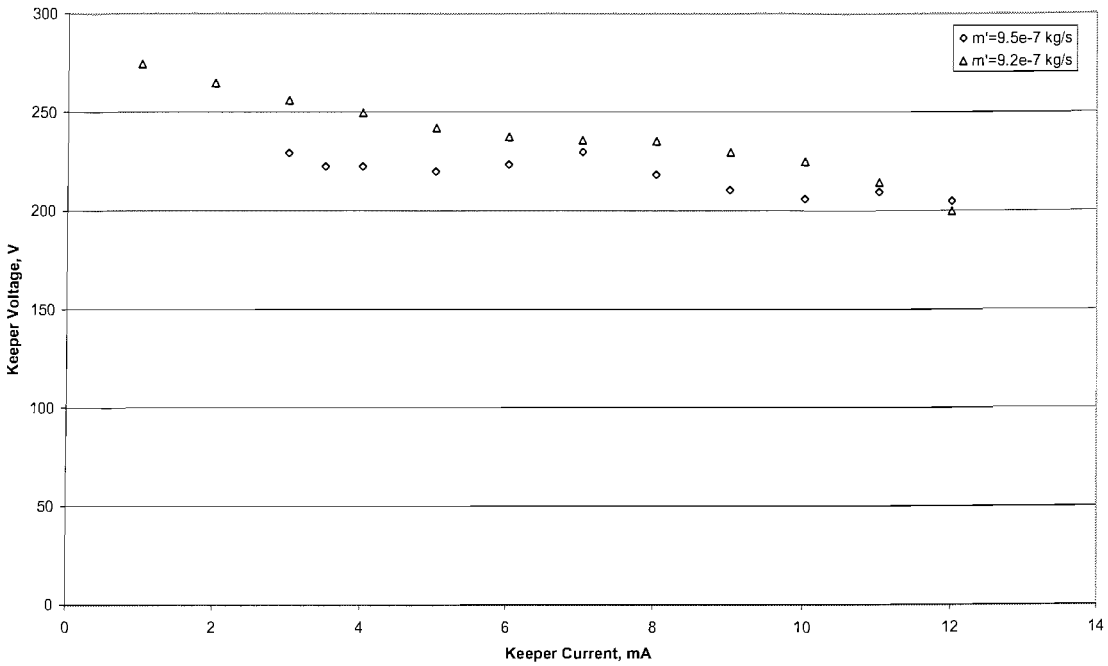

Fig 5.14 V-I Curves: Surface Impregnated cathode at $9.2x10^{-7}$ and $9.5x10^{-7}$ kgs^{-1}

Operation could not easily be compared at equal flow rates as above $4.5x10^{-7}$ kgs^{-1} flow rates could not be set prior to measurements, and had to be calculated after measurements had been made. The two measurement runs seen in fig 5.14 are also within the uncertainty quoted for mass flow rate and can therefore be considered to be approximately equal. This graph therefore shows the variation in discharge voltage as a function of keeper current for similar mass flow rates around $9x10^{-7}$ kgs^{-1}.

The Minor variations in voltage, such as points where the voltage increases as current is increased, or points where the discharge voltage is lower at the same current for a lower flow rate can be accounted for by the variation in voltage exhibited by a cathode in plume mode operation. Variations in the flow rate, erosion of the orifice, or variations in localised electron emission due to presence of the impregnant may also play a part. Variations in this mixture are known to have a high effect on discharge current, and the lifetime of such a coating is generally low in comparison to mixtures impregnated in a matrix [52].

At low flow rates all cathode types exhibit high keeper voltages. Fig 5.15 shows the similarity of the voltage-current relation for two measurement runs taken at $3x10^{-7}$ and $3.6x10^{-7}$ kgs^{-1} in the plume mode. In this case the high accuracy of the mass flow controller has allowed a comparison of operational characteristics at similar but distinct flow rates.

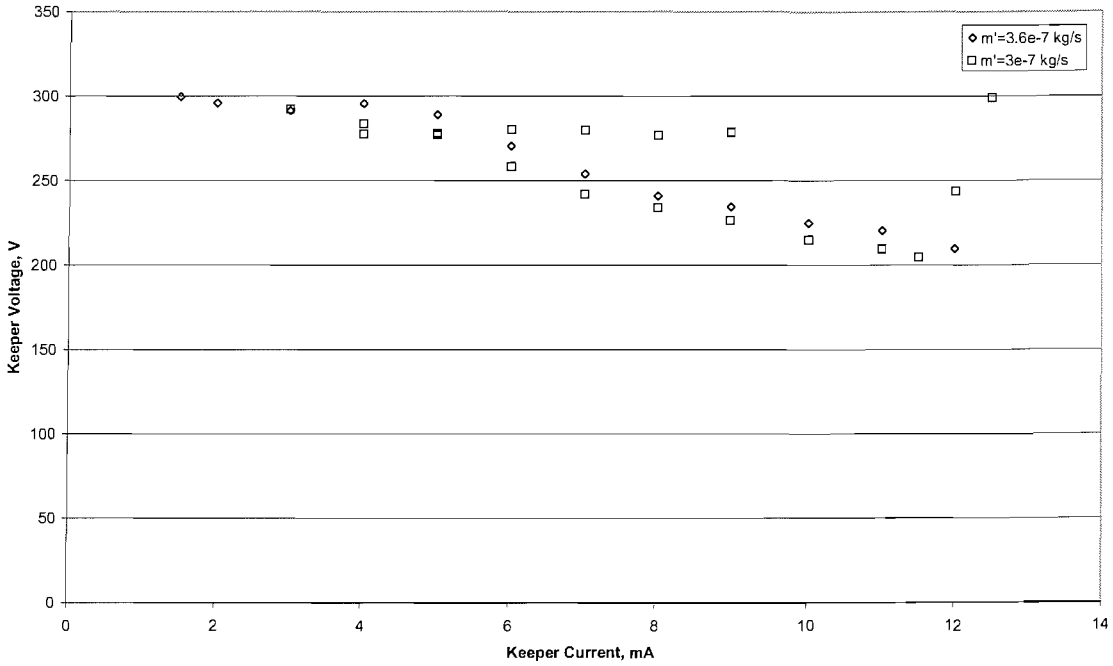

Fig 5.15 V-I Curves: Surface Impregnated cathode, $3x10^{-7}$ s and $3.6x10^{-7}$ kgs^{-1}

This graph shows that there is little difference in the voltage-current characteristics between measurements taken at close low level flow rates. Measurements taken at the lower flow rate of $3x10^{-7}$ kgs^{-1} actually show slightly lower discharge voltages than measurements taken at $3.6x10^{-7}$ kgs^{-1}. This may be a result of measurements being taken at different stages in the cathodes lifetime, with variations in geometry or impregnant concentration altering characteristics.

Fig 5.16 shows an expanded view of the hysterisis of the voltage-current curve seen in the previous graph. This phenomenon took place at a low flow rate in the plume mode and arrows signify decreasing or increasing current levels. Hysterisis phenomena

have been observed in other cathodes [95, 117]. Higher voltages than expected as the current is increased could be due to a time delay in the cathode heating up (thermal inertia) [95]. This could also account for the fall in voltage when the cathode is turned on.

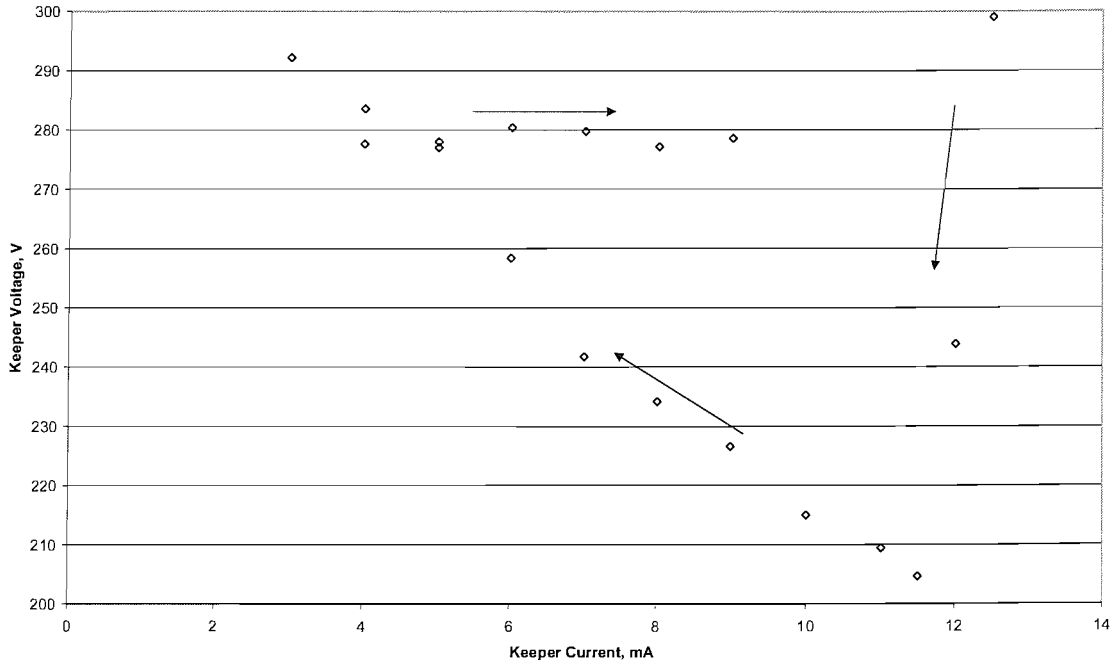

Fig 5.16 V-I Curve Hysterisis: Surface Impregnated cathode at 3 $x10^{-7}$ kgs^{-1}

After an initial drop in keeper voltage, there is an increase as the current is lowered. This then stays at a constant steady state as the current is increased. The discharge operates solely in the plume mode which is known to exhibit high voltage variations.

Fig 5.17 shows an interesting feature of specific voltage-current measurements. Measurements taken on the voltage-current characteristics of the surface impregnated cathode at $9.5x10^{-7}$ and $2.7x10^{-7}$ kgs^{-1} show the expected negative-resistance profile associated with hollow cathode operation, but with a peak in the trace at around 6mA.

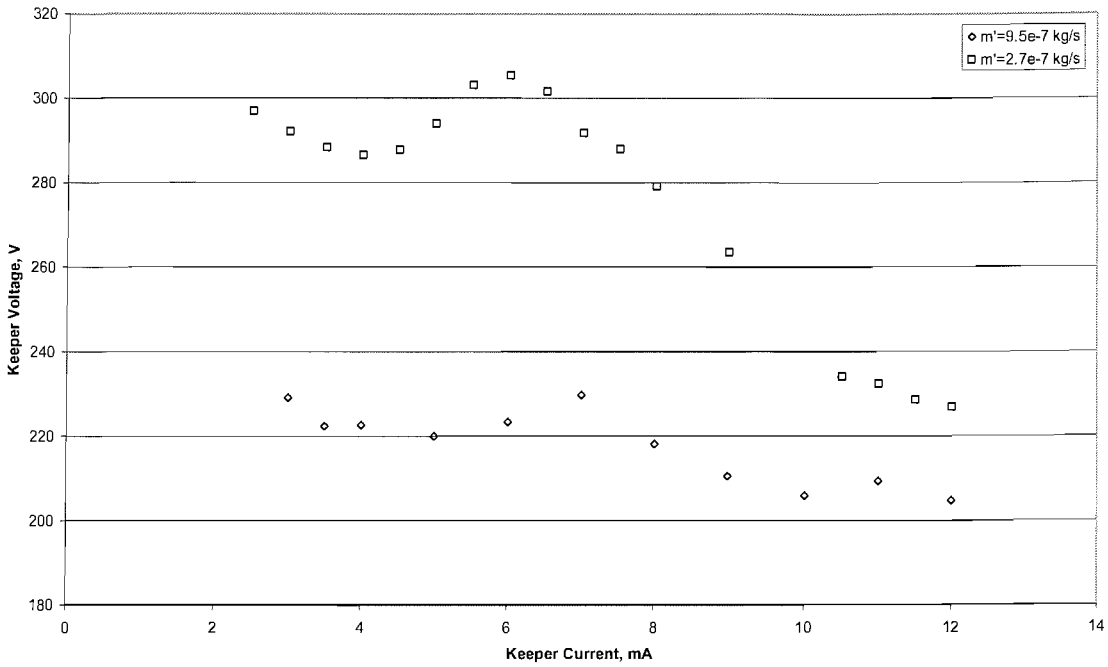

Fig 5.17 V-I Curves: Surface Impregnated cathode, $9.5x10^{-7}$ and $2.7x10^{-7}$ kgs^{-1}

Fig 5.17 shows an unexpected peak in the keeper voltage occurred when the current was altered while the cathode was operating in the plume mode. Electrons produced at these points will have a higher energy than those produced at lower keeper currents under the same conditions due to the higher voltages. This signifies a decrease in the efficiency of the emission process. These could not be accounted for, but could be a result of a number of phenomena. For example contamination, deposition and erosion are all detrimental to operation. Alternatively, it is possible that phenomena beneficial to plasma formation were taking place at the lower currents, resulting in a low current trough rather than a mid current peak.

In fig 5.18 measurements taken at the lowest flow rate of $2.4x10^{-7}$ kgs^{-1} do not show a negative-resistance trend, implying that the cathode is no longer functioning in the hollow cathode mode of operation and is emitting electrons in the Townsend mode. The Townsend mode exhibits very low current densities and has no quasi neutral plasma [118].

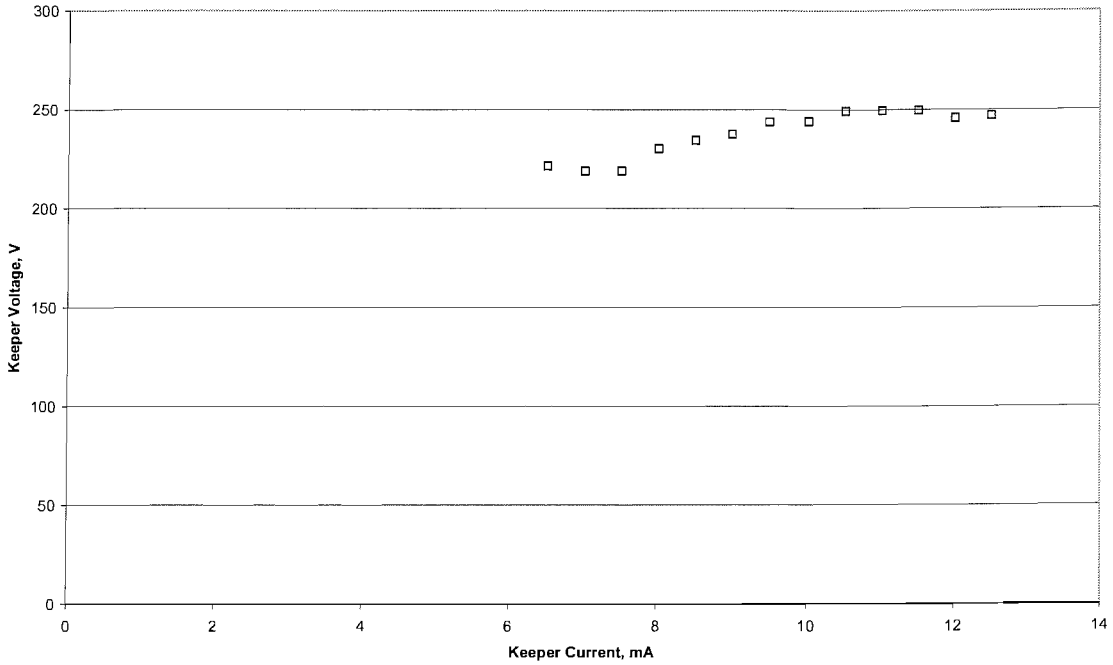

Fig 5.18 V-I Curve: Surface Impregnated cathode, 2.4×10^{-7} kgs^{-1}

After initiation at 13.3mA, the voltage remained approximately stable as the current was dropped, to 10mA, where the keeper voltage fell as current was reduced. The discharge could not be sustained below 6.5mA and showed significantly lower keeper voltages at low currents over other voltage-current curves at higher flow rates. The plasma was extremely diffuse and the cathode tip was observed to glow, suggesting thermal emission in the Townsend mode. Figs 5.19 and 5.20 show the cathode undergoing thermal emission at low-end flow rates of 2.7×10^{-7} kgs^{-1}. Fig 5.21 illustrates the cathode setup seen in the photographs. Using the optical pyrometer the luminosity equates to a temperature around 1300K. A small amount of thermal emission downstream of the orifice can be seen in fig 5.20.

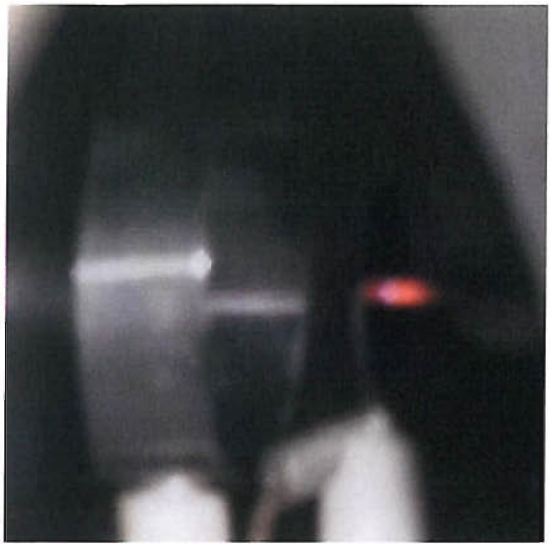

Fig 5.19 Thermally emitting cathode

Fig 5.20 Thermally emitting cathode with discharge

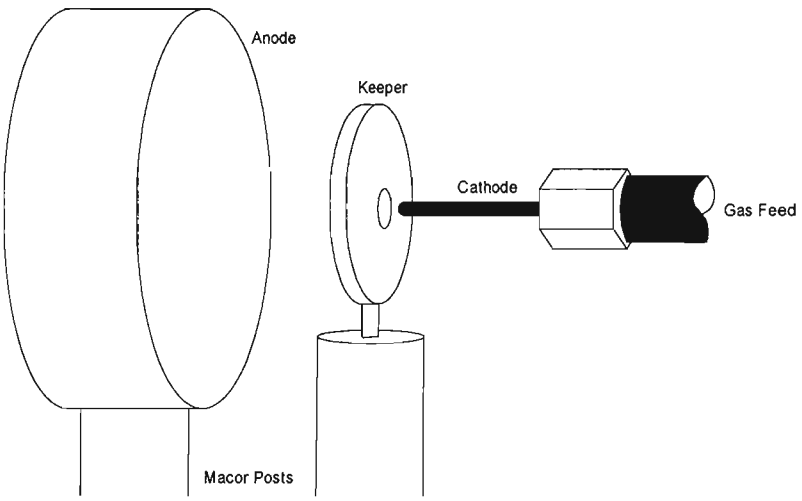

Fig 5.21 Cathode Setup

5.3.3. Impregnated Insert Hollow Cathode

The impregnated insert devices were tested at flow rates covering the operating range of devices used in the ionisation chamber existing, flight tested ion thruster systems, at a cathode-keeper separation of 0.5mm. Operation at the very low flow rates useful for

neutraliser operation (10^{-8} kgs^{-1} range) could not be achieved. Argon was used as the seed gas due to its due to its suitability, as an inert gas, and low cost. The devices were innovative in a number of aspects, all used to meet the requirements of miniaturisation. Aside from the easily manufactured body, the insert design used batch manufactured carbon inserts to dispense the low work function mixture. The application of Carbon as the insert material has advantages in it high melting point and high open volume fraction, ease of fabrication at small scales. Fig 5.22 shows the minimum discharge voltages for the impregnated insert cathode at the maximum current available from the supply of 13.3mA. A minimum discharge voltage of 54V was seen at a high mass flow rate of $2.2x10^{-6}$ kgs^{-1}. Voltages within 20% of this level could be attained at $4.5x10^{-7}$ kgs^{-1} and within 10% at $9x10^{-7}$ kgs^{-1}.

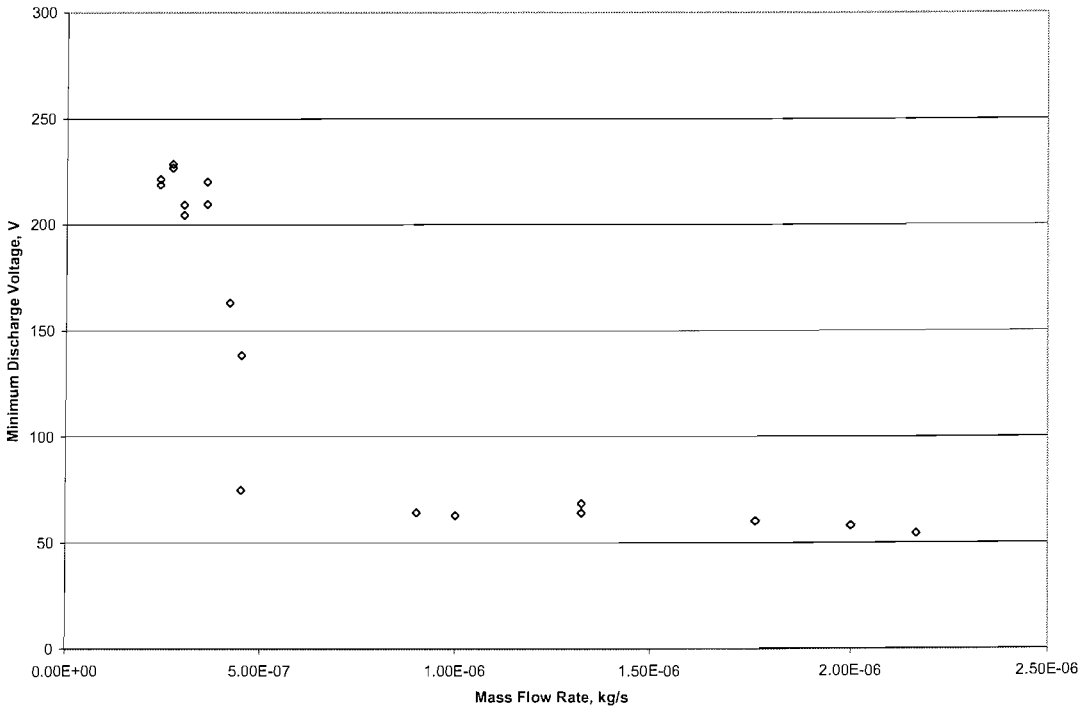

Fig 5.22 Minimum Discharge Voltage as a function of Flow Rate, Impregnated Insert Cathode

Above a transitional point around $4.5x10^{-7}$ kgs^{-1} mass flow rate variations evidently play a lesser role in determining keeper voltage. This point essentially

marked the boundary between spot and plume modes. Uncertainties in the flow rate result from the technique used to supply the gas and reach 21.9% above $4.5x10^{-7}kgs^{-1}$. Uncertainties in the measured discharge voltages are small at ±0.2V. Although the graph suggests a sharp drop in the discharge voltage at $4.5x10^{-7}$ kgs^{-1} this is just a result of more measurements being made around this point. It is believed that the transitional region between the modes would be wider, inhabiting the middle of the 10^{-7} kgs^{-1} range and could be varied by alteration of any of the factors which affect emission, such as temperature, work function, plasma potential as well as various microscopic processes.

The voltage-current measurements seen in fig 5.23 show the cathode operating in the spot mode, exhibiting a decreasing voltage with increasing current. Currents in excess of the maximum 13.3mA seen here would potentially result in even lower discharge voltages. The data shows a decrease in gradient at high currents suggesting that there may be a limit to the minimum possible discharge voltage.

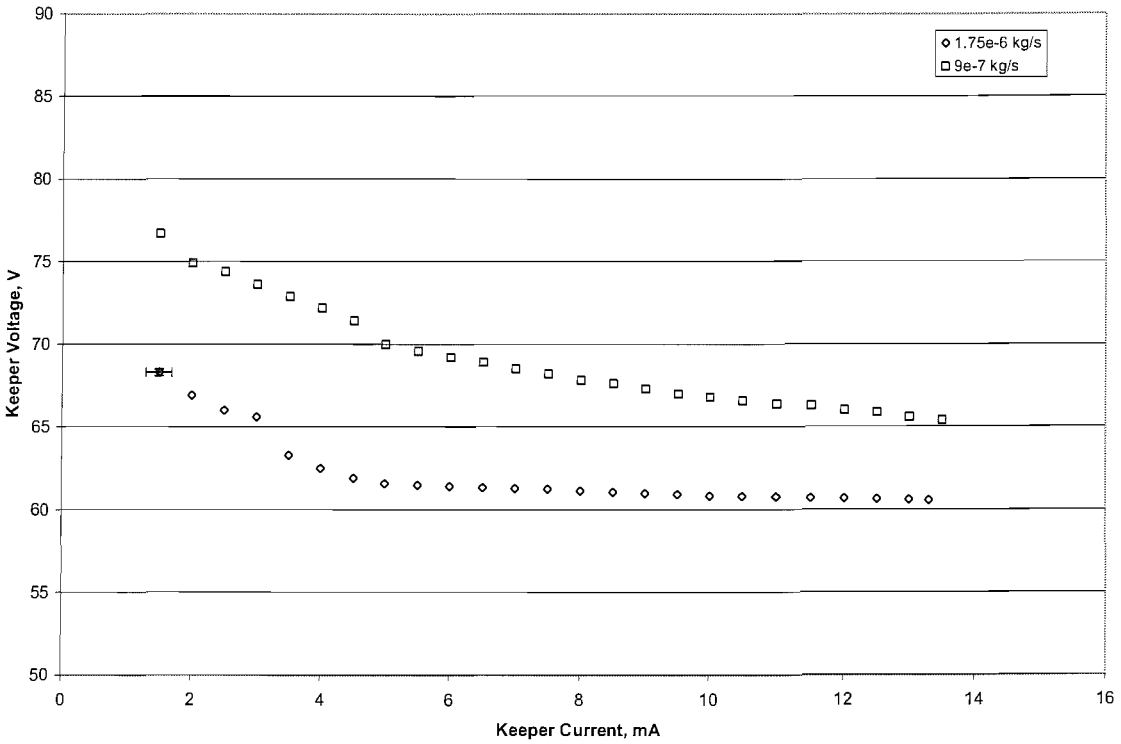

Fig 5.23 V-I Curves: Impregnated insert cathode, $9x10^{-7}$ and 1.75 $x10^{-6}$ kgs^{-1}

Increasing the mass flow rate by a factor of 2 has had a relatively small effect on the discharge voltage, decreasing it by between 5 and 9 volts. In both cases the cathode was operating in the spot mode. This amount, while significant, is not large in comparison to voltage decreases seen during mode transition in the cathode. The mode of operation is therefore more important to the performance of the cathode than the flow rate within that regime. These flow rates are quite high in comparison to the operating flow rates of larger cathodes which typically operate at between $5x10^{-8}$ and $1x10^{-6}$ kgs^{-1}.

Cathodes used in space-based applications must use their propellant efficiently as well as operate at a sufficiently low voltage and therefore power. The device must therefore be optimised to use a minimal amount of propellant while remaining in the spot mode. This graph suggests that the improved performance of the cathode at higher flow rates is outweighed by simply operating the cathode in the spot mode, with associated propellant savings. This is especially true if the cathode is being operated as a neutraliser, exterior to the thruster. However, the use of the hollow cathode at greater flow rates can be mitigated by using the excess gas flowing through the cathode as propellant gas in the thruster discharge chamber. The mass flow rate will therefore be selected to be a minimum based on current required from the cathode and consistent with operating mode.

Fig 5.24 shows an excellent example of mode transition for the impregnated insert cathode. The transition between spot and plume modes, a function of current and mass flow rate, takes place at 7-8mA. Minimum voltages are observed in the spot mode, above 8mA, whereas plume mode operation is seen at higher voltage and lower currents. In a second test under the same conditions mirrored voltages at high currents. At the transition point around 7.5mA this discharge extinguished. The discharge therefore ceased to operate in the spot mode at the same point in both cases, but could either switch to the plume mode or fail. This was due to instabilities at the transition point, making sustaining plume mode operation at low flow rates difficult.

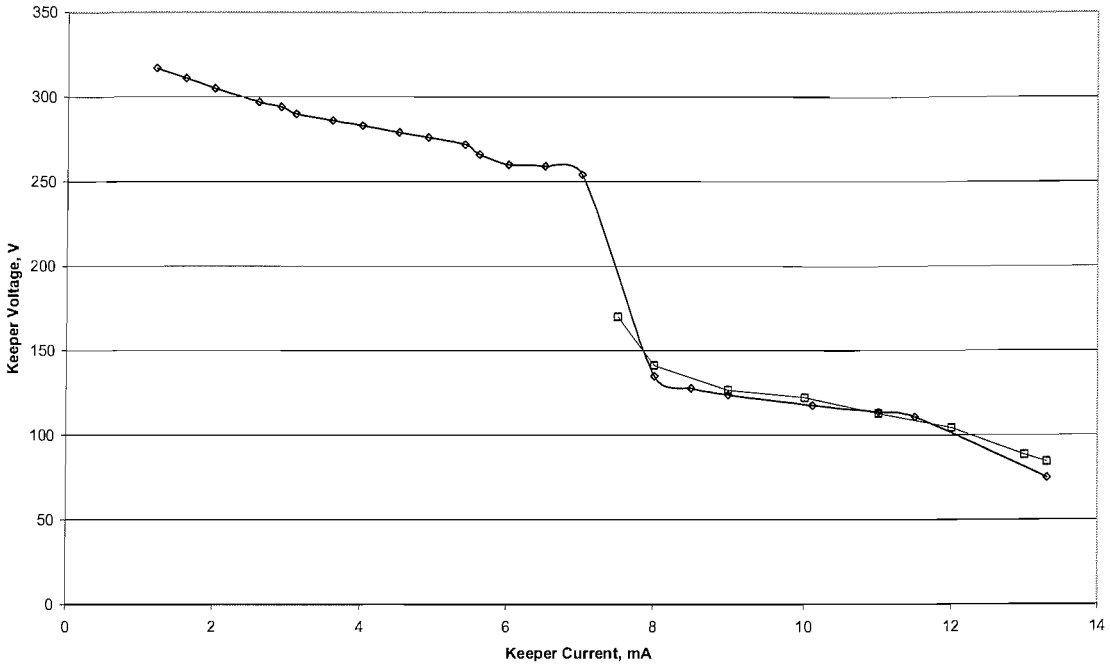

Fig 5.24 V-I Curves: Impregnated Insert cathode, Distinct Operating Modes, 4.5 $x10^{-7}$ kgs^{-1}

The transition between the spot and plume modes at $4.5x10^{-7}$ kgs^{-1}, seen in both figs 5.22 and 5.24, takes place at significantly lower flow rates and currents than that seen in the other cathode types tested as part of this project. Low flow rate operation in the spot mode is significant as it is under these conditions that the device could be best used as a plasma source for ion thrusters due to the decreased demands on power of this particular device. Spot mode operation took place from approximately 75 to 150 volts at 8 to 13.3mA, plume mode from 200-320 volts at 1.5-7.5mA. Once initiated, the discharge was approximately 3 cm long and had a characteristic violet glow. Plume mode luminosity was down at similar current levels in comparison to the spot mode and the integrated emission spectra appeared more blue signifying a change in the emission and therefore conditions in the plasma. Images in appendix C show the cathode operating in both the spot and plume modes.

Kaufman and Rehn formulated an empirical equation describing the conditions necessary for spot mode operation of a hollow cathode at a defined current [35]:

$$\frac{\dot{m}e\sigma_{ion}\sqrt{W}}{r_{or}m_i} \geq 2.78x10^{-17} \qquad 5.14$$

This shows the spot mode's dependence on mass flow rate, $\dot{m}$, the species' cross-section for ionisation, σ_{ion}, the molar weight, W, the ion mass, m_i and the radius of the orifice r_{or}. For Argon, this value is greater than or equal to $6.3x10^{-8}$ kgs^{-1}, for an orifice diameter of 0.2mm and electron energies between 20 and 100eV, where the cross section for ionisation is approximately invariant [78]. This relationship is simply a measure of the absolute minimum flow rate value to establish spot mode, further, the relationship is also dependent on individual device design, but does demonstrate the dependence of mode transition on gas, mass flow rate, orifice dimensions and plasma characteristics (through cross-section for ionisation).

For the impregnated insert cathode, the minimum conditions found experimentally for spot mode operation are:

- Flow Rate ~$4.5x10^{-7}$ kgs^{-1}
- Current ~8mA
- Cathode-keeper separation 0.5mm

The flow rate is significantly higher than that seen in larger cathodes, which typically show spot mode operation between $3x10^{-8}$ and $1x10^{-7}$ kgs^{-1}, however currents are much higher, typically 0.5 to 1A. Operation of the developed cathodes at higher currents would likely have continued to improve the power input per electron and the minimum sustainable flow rate for spot mode operation. However, the small size of the cathode limited the amount of current that could be drawn. Larger keeper supplies could not maintain stable operation, with the discharge rapidly initiating and extinguishing repeatedly. This was also true when operating the anode, where the discharge would continually expand to and contract from the anode.

Fig 5.25 shows the hysterisis effect observed on reducing current after measuring at high currents. In this case decreasing the current from its maximum does not exhibit an immediate increase in voltage as might be expected. Similar voltage levels can be maintained at significantly lower currents, decreasing the power consumption of the device. This could be an effect of thermal inertia, where efficient operation is maintained at lower currents as the cathode has not yet cooled to the level normally associated with operation at that current.

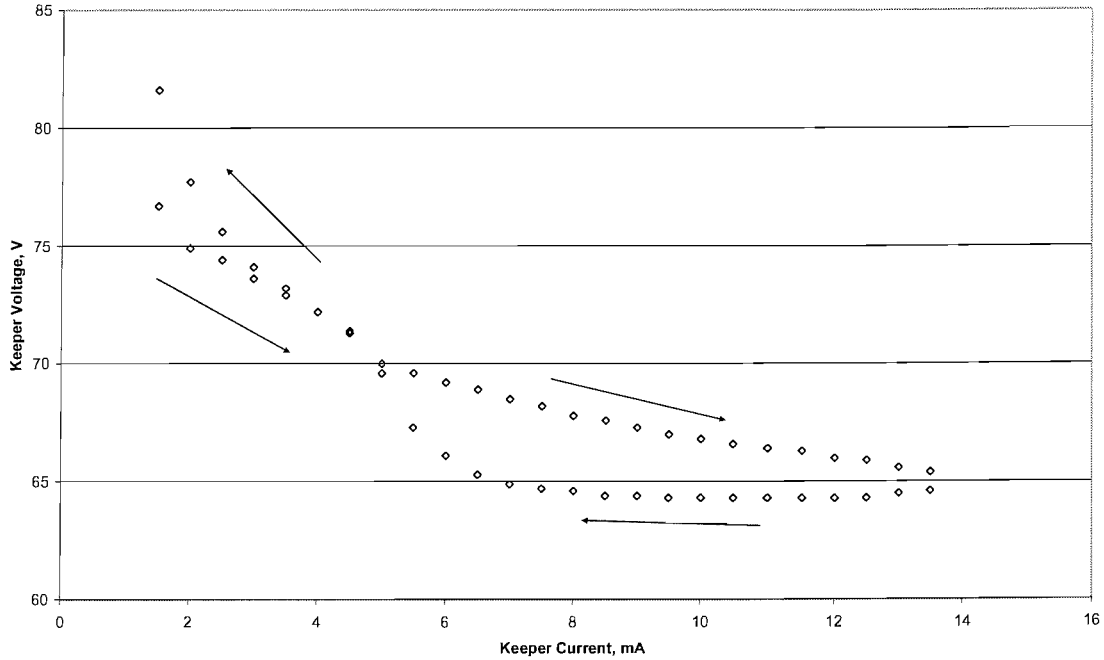

Fig 5.25 V-I Curve Hysterisis: Impregnated insert cathode, 9 $x10^{-7}kgs^{-1}$

There is a gradual decrease in operational voltage from 77V to a minimum just below 65V, as the current is increased. Decreases to the current show a stable low-level keeper voltage to 7.5mA, the keeper voltage then undergoes a rapid increase to a point in excess of 80V at 1.5mA. The initial increase in current from the minimum follows the expected decreasing voltage trend. Subsequent decreases to the current show a constant discharge voltage. This hysterisis effect has been observed in other hollow cathodes and is also apparent in the surface impregnated model tested in this study [119].

Fig 5.26 shows a further example of voltage-current hysterisis at a higher flow rate of $1.75 \times 10^{-7} kgs^{-1}$ for the impregnated insert cathode. The voltage falls from 68V to a below 61V, as the current increases. Subsequent decreases show a stable keeper voltage to 8.5mA, below which the keeper voltage steadily increases to around 68V at 1.5mA.

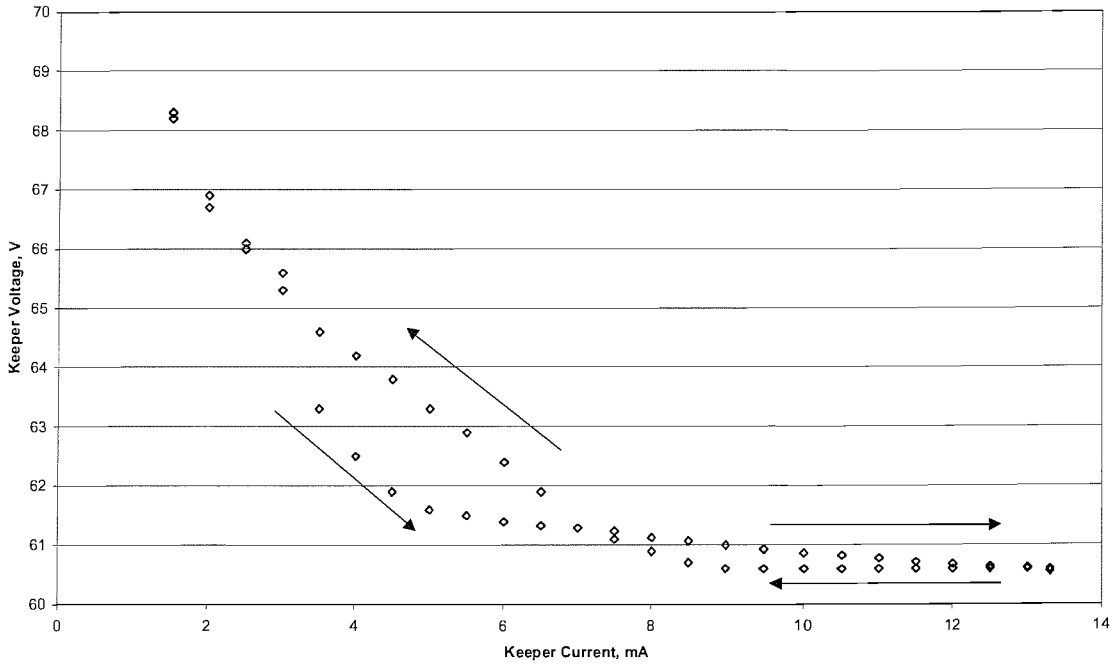

Fig 5.26 V-I Curve Hysterisis: Impregnated insert cathode, $1.75 \times 10^{-6} kgs^{-1}$

In both these graphs, when the current is decreased the keeper voltage remains fixed until reaching a point around 8.5mA when it starts to undergo a rapid increase in the required keeper voltage. Increases in current result in a steady drop of the discharge voltage. It is possible that further increases to the current would have resulted in greater drops in the discharge voltage, possibly even approaching levels similar to cathodes seen on flight tested ion thruster systems. Operation at higher currents was not performed due to problems with the stability and operation of higher current supplies.

The steady state values of keeper voltage at different currents could be the result from the establishment of an efficiently operating plasma through thermal inertia. As the

current is decreased, the demands on electron emission fall with respect to the required flux of electrons. The initial high current discharge acts as a self-sustaining point, increasing the efficiency of electron generation, allowing a stable voltage to be maintained.

Fig 5.27 shows the voltage-current curve for the impregnated insert cathode at a very high flow rate of 2.2×10^{-6} kgs^{-1}. The high flow rate and low discharge voltage suggest that the cathode is operating in the spot mode. The overall trend exhibits a negative resistance, but the profile is stepped for some reason. These transitions are not associated with mode switching due to the low overall variations in the discharge voltage and as has already been demonstrated, plume mode operation takes place at lower flow rates than those seen here. The very large flow rate and high internal pressure, coupled with a weakly ionised plasma in the very small device means that the physics of the device are hard to determine as it is significantly beyond well-characterised operating conditions.

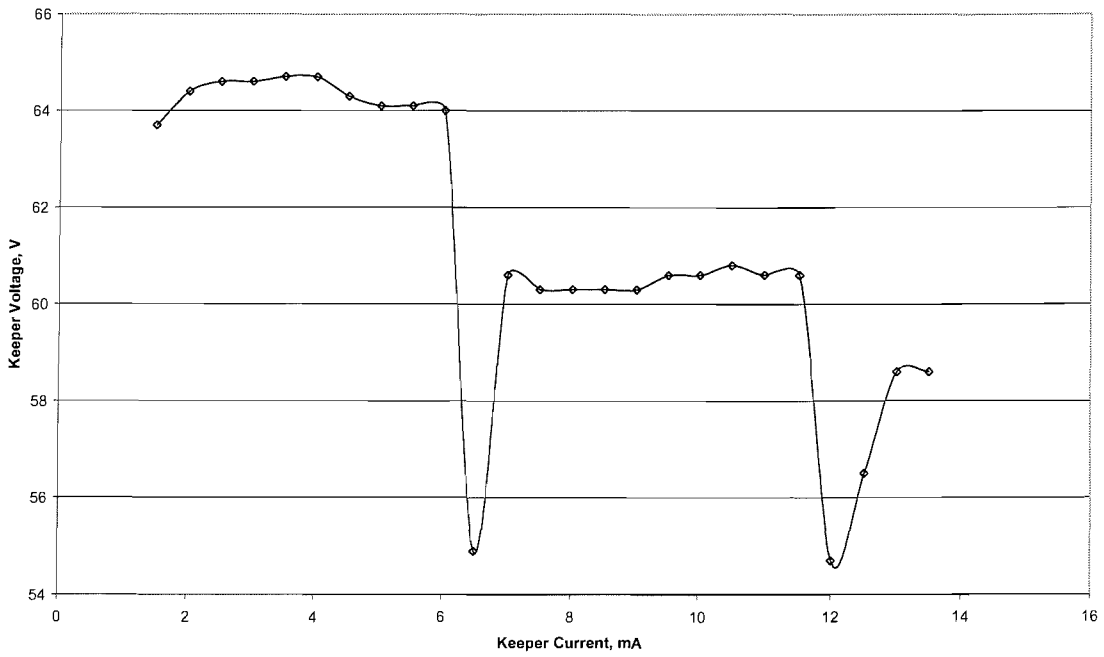

Fig 5.27 V-I Curve: Impregnated Insert cathode, 2.2×10^{-6} kgs^{-1}

The very low keeper voltages at 6.5 and 12 mA suggest transient phenomena, such as microfilament formation in the insert, sputtering or interactions between the carbon grains are taking place. Such processes result in increases in the current density, decreasing the keeper voltage in a current limited mode as the efficiency of electron emission is increased, resulting in a lesser demand on the required keeper voltage to maintain this level of emission. No further measurements were taken at this level as the mass flow rate was well beyond the operating range for a hollow cathode in an ion thruster. The lowest discharge voltages seen in fig 5.27 are the lowest operational voltages acquired with any of the cathodes under test. At approximately 55V it is much larger than that of the large hollow cathode devices seen in existing thruster systems such as the NSTAR and T5 thrusters which can operate at keeper voltages between 10 and 20 volts, though discharge voltages on the anode may be much higher at up to 40V. A plasma was also produced at zero flow rate in a static gas filled chamber. The discharge voltages did not approach the low end values of the flowing conditions and the pressures where a discharge could be initiated were disproportionately high at above 2mBar.

The impregnated insert cathode is a significant improvement in discharge voltage and power in comparison to the simple molybdenum and surface impregnated cathodes. The performance of the impregnated insert cathode cannot be expected to match that of an existing flight tested device as it is much smaller and is a prototype without performance-enhancing additions, such as an enclosed keeper. It does however demonstrate the potential to apply novel design and technologies to hollow cathodes, most especially in the potential of carbon for use as an insert material. Further investigation of the chemical processes taking place in the insert would be required to define the processes going on here. It is believed that the insert would act in the same manner as an oxide cathode, with emission only coming from the impregnant itself. Oxide cathodes have been shown to operate at low temperatures, below 700°C [103], which fits well with observations on cathode operating temperature. There is the potential for carbon monoxide production from the matrix as the oxides are reduced. Carbon dioxide, which would otherwise contaminate the cathode is unlikely to be produced due to the low amounts of oxygen and carbon monoxide has no detrimental

effect on cathode operation. The production of a gas rather than solid oxide wastes may also prevent blockages in the pores of the matrix which prevent the impregnant traveling to the cathode surface but will have an effect on the operating conditions of the device as the matrix is likely to erode significantly faster.

5.3.4. Discussion

This section discusses the effect of the novel aspects of the device on performance, especially the use of impregnated carbon inserts. As the surface impregnated and impregnated insert devices were operated under the same conditions and had the same body design, the viability of the carbon inserts could be evaluated. Hollow cathodes already come in a wide variety of sizes and configurations. The hollow cathode developed in the course of this project is novel in several aspects which will alter the voltage-current relation of the cathode:

- The size of the device is many times smaller than currently available models used in ion thruster systems
- Inserts are manufactured from carbon rather than tungsten

These features have both benefits and drawbacks. Construction is facilitated as molybdenum and carbon are easier to work than tungsten; thoriated tungsten also presents health hazards. The turned orifice eliminates the need for any welds, making the body easier to manufacture especially at such small scales. Drawbacks include the increased work function of the materials used in the manufacture of the device, the potential decrease in lifetime due to erosion of the thinner orifice wall and the unknown effect that the use of carbon as an insert material will play on the reaction processes that cause plasma production.

Spot mode operation for the impregnated insert device takes place at much smaller currents in comparison to existing large scale cathodes. It is, however, at

voltages around 5 to 10 that seen in these larger devices and at higher flow rates, around 2 to 10 times greater. It should be noted that the lower discharge voltage and flow rate in larger cathodes used Xenon which would improve performance in comparison to using Argon. The micro hollow cathode could therefore not be directly compared to larger existing, optimised devices. The comparative performance of the three cathode types was of more immediate interest as this enables the applicability of the novel techniques to be evaluated

The configuration that the device was tested in is similar to that used for neutraliser cathodes, but the device evidently requires much higher flow rates, similar to that used in discharge chamber cathodes. Therefore, due to its small size, lack of an enclosed keeper and prototype nature, direct comparisons with flight-tested devices do not tell the full story, it must be considered as a miniaturised experimental system. The voltage and current characteristics will however remain comparable and will therefore allow an evaluation of the overall performance of the device under test.

The data seen here represents a comparative study of the significant operating conditions seen in hollow cathode devices. Each graph is appended with information on flow rate and keeper-cathode separation. Unless stated otherwise, the discharge was initiated at the maximum current. Measurements then took place as the current was decreased.

Fig 5.28 shows the dependence of discharge voltage on mass flow rate for all three cathode types at a fixed current of 13.3mA. Early measurements on the simple molybdenum cathode were carried out at a separation of 0.9mm in comparison to the other two which were carried out at a separation of 0.5mm. The simple molybdenum cathode was not tested at a keeper-cathode separation of 0.5mm as early tests resulted in significant erosion of the cathode before further experiments could be performed. The cathode-keeper separation has an effect on the initiation voltage as emission is dependent on the electric field at the cathode as well as temperature and work function. However, the effect of cathode-keeper separation on discharge voltage is more difficult to define.

Emission from the cathode results from the intense electric field over the sheath between the plasma and insert surface. It is therefore a product of the plasma and cathode potentials and sheath thickness rather than the keeper voltage and separation. However, increasing the keeper cathode separation could have a number of effects on processes which determine the discharge voltage. Increases in the volume between cathode and keeper where ions can be produced which will impact the cathode, rather than be shielded by the keeper, will increase emission through heating as well as erosion. Also as enclosed keeper configurations have shown that pressure gradients in the cathode-keeper gap can have an effect on voltage, then increased separations in an open configuration will also have some effect. These effects should be relatively minor as ionisation is low at a fraction of the keeper current and it has been shown that the primary region of pressure variation lies within one orifice diameter of the cathode orifice [29], which at 0.2mm is upstream of the keeper under all conditions. However, alteration of the cathode-keeper geometry could also have an impact on how the plasma forms within the cathode body due to different electric field gradients which would not be easy to account for. Data for the simple molybdenum cathode cannot therefore be directly compared with the other two cathode types but does show the same profile as the other cathode types and suggests that the simple cathode is inferior to the other devices.

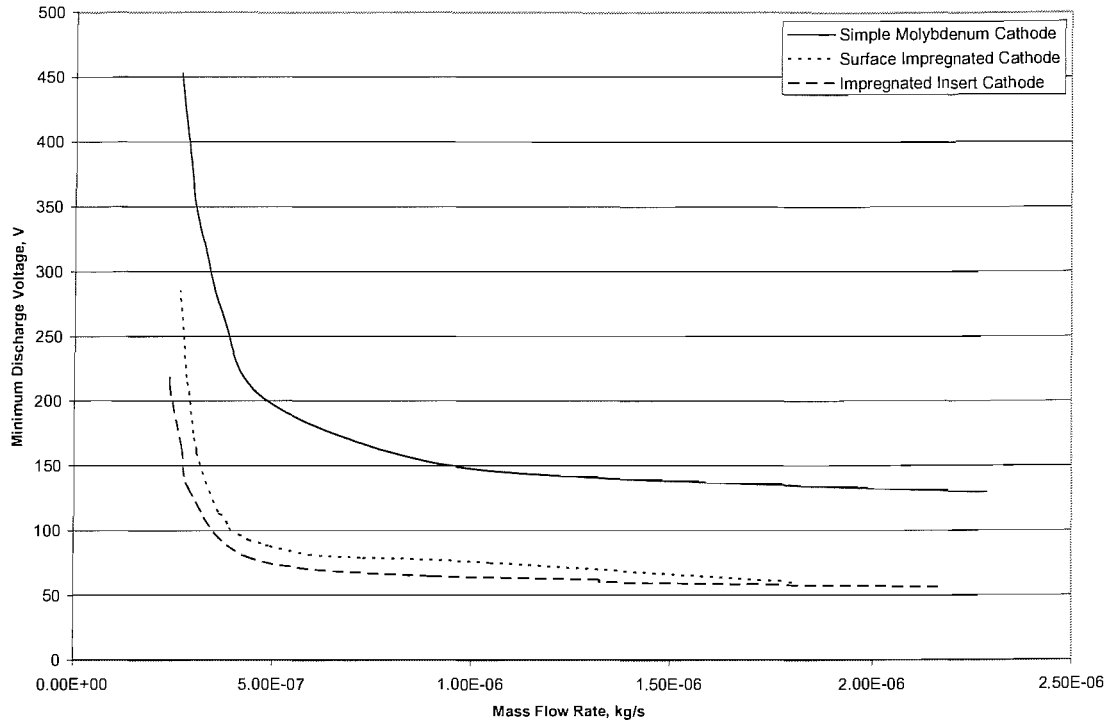

Fig 5.28 Minimum observed voltages for different cathodes, not adjusted for distance

This graph shows the relative performance of the three cathode types as a function of the mass flow rate. Spot mode operation is characterised by the horizontal part of the traces. Plume mode operation takes place when the trace has a high gradient. The impregnated insert cathode performs consistently better than the surface impregnated model, requiring the lowest discharge voltages for a given flow rate to sustain similar discharge currents. As the current is constant at 13.3mA, voltage is a direct measure of the power consumed and thus efficiency of the device at a specific mass flow rate assuming similar electron emission currents. Alteration of the cathode-keeper geometry could also have an impact on how the plasma forms within the cathode body due to different electric field gradients. The use of an impregnated carbon insert therefore apparently enhances the efficiency of the device, promotes establishment of the spot mode and is a viable method of improving output. As expected, all three cathode types show similar profiles throughout their respective ranges. Uncertainties vary throughout the range of operation of the device. Combining the uncertainties in the cathode-keeper separation to that in measured voltage, results in an overall variation of

±4.4% in minimum discharge voltage. The uncertainty in the flow rate results from the method of measurement, $\pm 9 \times 10^{-9}$ kgs^{-1} below 4.5×10^{-7} kgs^{-1}, ±21.9% above. The large uncertainty in the mass flow rate above 4.5×10^{-7} kgs^{-1} covers an inaccuracy common to all measurements. The measurements still therefore demonstrate the improved performance of the impregnated insert device. The best power output per mA of emitted electrons (at 90% of keeper current), at 0.05W/mA is between that of a FEEP neutraliser (0.6W/mA) and a large scale hollow cathode (~0.004W/mA) as might be expected.

In fig 5.29 the shaded areas represent the areas on the voltage-current graph inhabited by the surface impregnated and impregnated insert cathodes at a low flow rate of 4.5×10^{-7} kgs^{-1}.

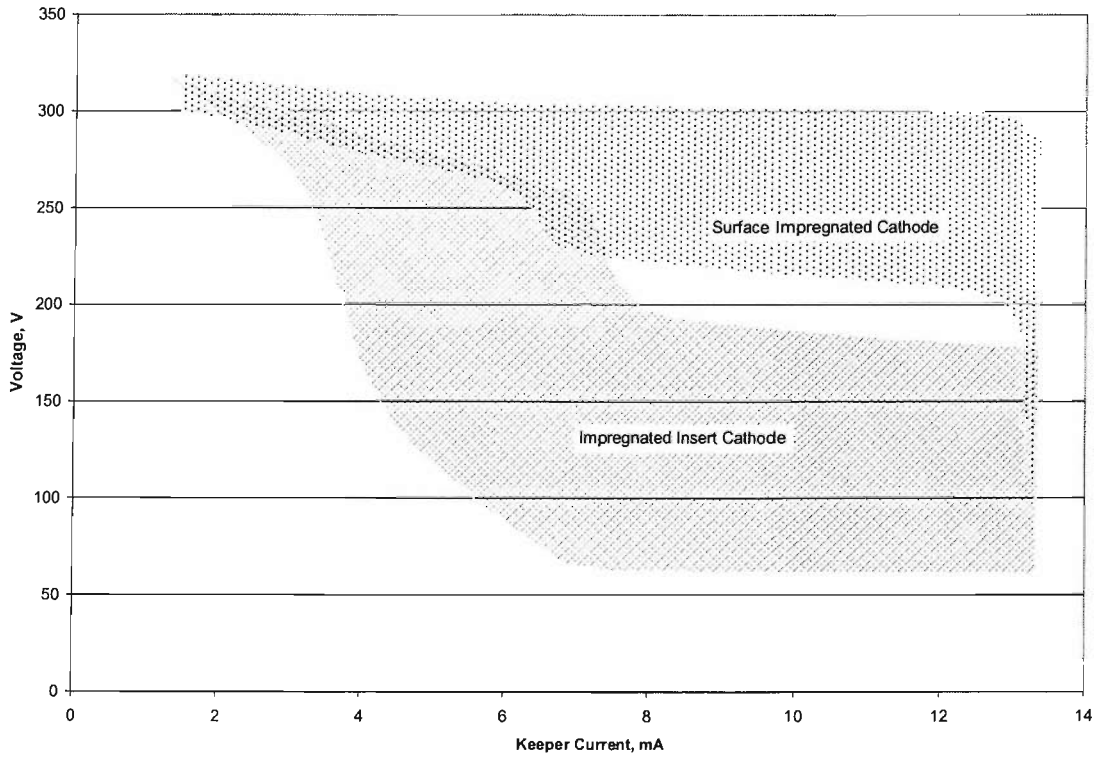

Fig 5.29 Comparison of VI Curves for different cathode types, 4.5×10^{-7} kgs^{-1}

This graph demonstrates the similarity in the discharge voltage between the two cathode types at very low flow rates in the plume mode. The impregnated insert cathode

performs more efficiently at low flow rates, transiting to spot mode at currents as low as 6-8mA. The Surface impregnated cathode was only observed to operate in the spot mode at the highest currents, around 13mA, at this low flow rate and was highly unstable at this point.

In fig 5.30 the shaded areas again represent the areas on the voltage-current chart inhabited by the surface impregnated and impregnated insert cathodes, this time at $9x10^{-7}$ kgs^{-1}. At this level the impregnated insert cathode is consistently operating in the spot mode, while the surface impregnated cathode operates in the plume mode except at the highest currents around 13mA.

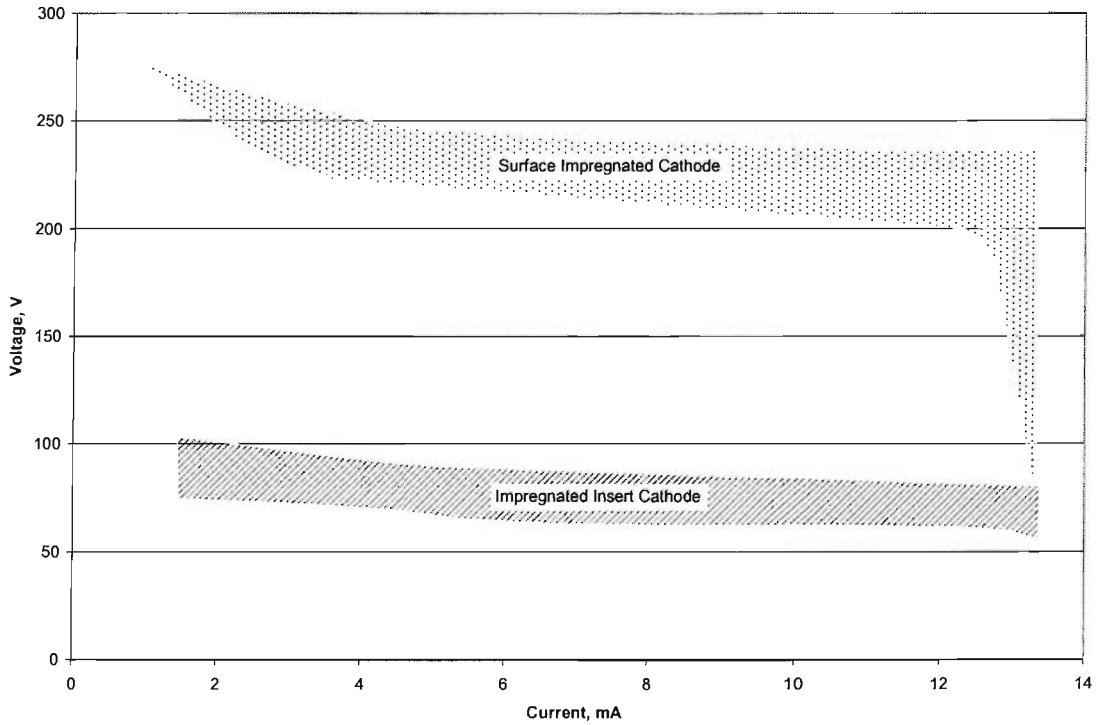

Fig 5.30 Comparison of VI Curves for different cathode types, $9x10^{-7}$ kgs^{-1}

The performance of the impregnated insert cathode is much better than the surface impregnated model, with significantly lower discharge voltages resulting from earlier establishment of the spot mode. The stability of the operation of the impregnated insert cathode was also considerably better, with a much more defined point for the spot-

plume transition, as seen in fig 5.24 for a lower flow rate of 4.5×10^{-7} kgs^{-1}. It is believed that successively larger currents would continue to give lower voltages. However, problems with the impregnated insert design could potentially arise from scaling laws which state that the smaller the insert diameter, the smaller the maximum available current [35].

The Richardson-Dushman equation, covered in chapter 2, gives the thermionic emission current density in terms of effective work function and cathode temperature:

$$J_{Th} = A_R T_C^2 \exp\left(-\frac{e\phi}{kT_C}\right) \qquad 5.15$$

The actual temperature of the cathode insert will be affected by other processes such as ion bombardment and could be higher than that exhibited by the cathode walls. However, if the temperature of the device is just below the threshold for luminescence, around 800°C, the upper limit for thermionic emission current density would be 0.124Amm^{-2} assuming a very low work function of 1.5eV for the cathode insert (as in an oxide cathode). At a work function of 1.7eV around that in a dispenser hollow cathode this drops to 0.014Amm^{-2}. As the optical disappearing filament pyrometer is limited to use when the device is incandescent, or glowing, there is a lower limit to its range around 800°C. The micro hollow cathode device developed as part of this project was not observed to glow during operation, so the device was therefore operating at less than 800°C during plasma production. This is consistent with other larger hollow cathodes when operating at low currents, which exhibit decreasing temperature [120]. Existing devices used in large ion thrusters have shown operating temperatures between 750 and 1200°C [28], at currents from a few hundred milliamps to 35 amps.

Definition of the emission area of the cathode insert surface is difficult. Other investigations have suggested that the amount of insert surface involved in emission is about half the internal diameter of the cathode in length directly behind the orifice [116]. Based on this assumption the emitting surface area of the insert of a 0.2 mm internal

diameter cathode is around 0.06mm^2. If the electron emission current is 90% of the keeper current the electron emission current density is equal 0.2Amm^{-2}. There will be an effect on the emission area due to surface roughness, though this would be hard to quantify and is neglected here. This is evidently above the upper limit for thermionic emission of 0.124Amm^{-2}. Markings on other hollow cathode interiors from ion bombardment have been reported to show the extent of the emission area, giving emission current densities around 0.5Amm^{-2} [64] which would suggest that the inserted micro hollow cathode would be unlikely to exceed 30 or 40mA in total current if electrical supplies were altered to allow this.

The presence of electric fields will enhance emission from the insert surface. The work function, ϕ, becomes the effective work function, ϕ_{eff}, equal to:

$$\phi_{eff} = \phi - \sqrt{\frac{eE_C}{4\pi\varepsilon_0}} \qquad 5.16$$

This requires a definition of the electric field at the cathode surface. The plasma potential was measured at around 75V by the unshielded Faraday cup (see appendix B). Assuming that this is invariant throughout the plume, believed to be the case in spot mode operation [91], and that the sheath thickness is between 5 and 10 times the Debye length, which from measurements made on the electron temperature is believed to lie around 9 microns (see app x), the electric field at the cathode surface is between 8x10^{-5} and 1.6x10^6 Vm^{-1}. The maximum contribution to the surface work function is therefore a drop of 0.05eV. This will aid emission but is not enough to account for the difference in cathode and thermionic emission currents.

Emission will likely take place in the field-enhanced Schottky mode, due to the high electric fields, which can account for a further increase to electron emission.

$$J_S = J_{Th} e^{0.4389\frac{\sqrt{E_C}}{T_C}} \qquad 5.17$$

Substituting an electric field of $1.66 \times 10^{6} Vm^{-1}$ into the above equation shows that thermionic emission will be enhanced by a factor of 1.7 at a temperature of 800°C. Schottky emission can also be enhanced if sharp points exist in the region where the discharge is initiated due to enhancement of the electric field. If the cathode insert operates in the same way as a dispenser hollow cathode and has a work function around 1.7eV this is not enough to account for the postulated current density and other mechanisms such as impact by metastables, and photoelectric emission may be taking part. It is believed that the cathode insert will operate more like an oxide cathode rather than a dispenser cathode with oxygen vacancies in the oxide acting as sites promoting electron emission and lowering work function rather than through dipole effects as in dispenser cathodes (as in a tungsten insert hollow cathode). Oxide cathodes exhibit slightly lower work functions in comparison to dispenser cathodes and therefore start to emit at lower temperatures, below 800°C, but can be easily poisoned by background gases. Emission current densities of the order of $0.15 Amm^{-2}$ have been reported in standard models of this type of device [121], similar to the levels seen here, with the lower work function more easily allowing low temperature operation. It is also concluded that this size of micro hollow cathode is around the size limit for development of a traditional metal body cathode, due to both the difficulties in fabrication at smaller scales and the difficulties in establishing an efficient discharge in such devices, which is capable of low currents only. There may be scope to develop microfabricated arrays of hollow cathodes, but application to ion propulsion systems would be difficult due to the requirements on performance. It has also been shown that a carbon matrix insert material is a viable means of dispensing the impregnant material. The inserted device showed improved performance over the simple and surface impregnated models, particularly in respect of transition to the spot mode at low currents and flow rates.

5.4. Other Observations

During the course of experiments on the micro hollow cathodes a variety of conditions arose where the discharge deviated from normal operation. Generally, all of these phenomena occurred at the end of the test life of the cathode.

Figs 5.31 to 5.33 show the formation of a visible plasma plume on the cathode side of the keeper disc at varying degrees of severity for the first of the impregnated insert cathodes. This was indicative of erosion of the orifice, and was therefore undesirable. Fig 5.35 shows plasma formation perpendicular to the simple molybdenum cathode body.

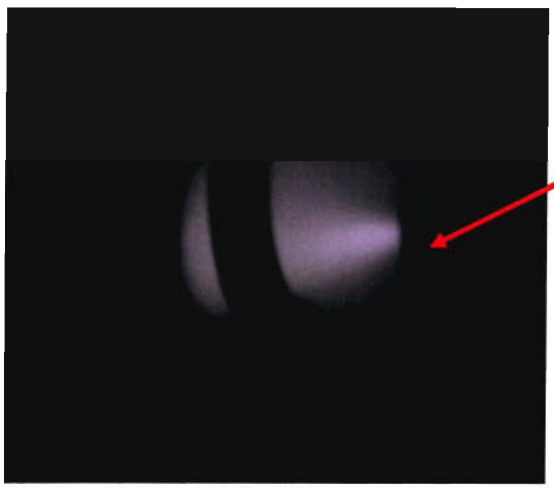

Fig 5.31 Plasma formation upstream of keeper

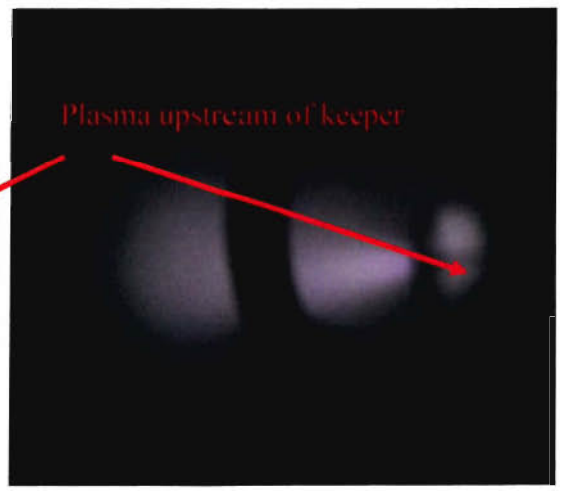

Fig 5.32 Increased plasma formation around keeper

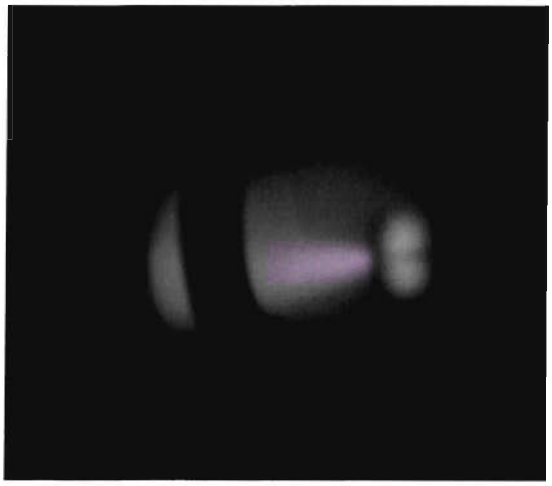

Fig 5.33 Significant upstream plasma formation

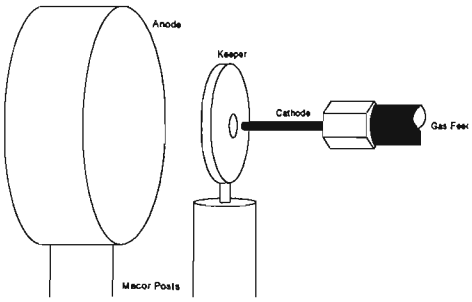

Fig 5.34 Cathode Setup

Fig 5.35 Erosion has caused discharge
to couple to chamber wall

In fig 5.35 substantial erosion has caused the discharge to stream out of the side of the cathode. The limiting factor in the lifetime of the device therefore appears to be orifice erosion as no significant change in the discharge voltages was observed over cathode lifetime. The final impregnated insert cathode used showed lesser erosion, the only difference to the first model being more extensive use of the heater, rather than using cold-start capability. More benign initiation procedures therefore lower erosion during initiation, which has proved a key factor in the life of the micro hollow cathode.

5.5. Review of Results

Commercially available hollow cathodes used in flight tested thruster systems, of similar inserted designs are typically at least 5 times the diameter of the ones developed here and run at higher discharge currents, generally in a closed keeper configuration at generally lower flow rates, from similar levels to a factor of 5 lower.

To obtain the best performance from the micro hollow cathodes, operation should take place in the spot mode, due to lower discharge voltages and more stable operation. The impregnated insert cathode was much better at reaching spot mode operation at lower flow rates and currents in comparison to the simple molybdenum and surface impregnated cathodes. Conditions required to attain spot mode operation for the impregnated insert device showed minimum flow rates of 4.5×10^{-7} kgs^{-1} at currents in excess of 8mA and at a keeper-cathode separation of 0.5mm.

As stated, the cathode internal diameter must be in excess of several times the Debye length for formation of a stable plasma. Otherwise the diameter of the cathode is so small that the plasma sheath exceeds the internal diameter, therefore stopping the discharge from penetrating the cathode and forming the internal plasma. As the impregnated insert device exhibited the best power outputs in comparison to the other cathode types, it can be inferred that the matrix is taking part in the discharge and the plasma penetrating the cathode interior.

Stability of the discharge is also affected by emission mechanisms, the Schottky effect is not the only phenomenon producing high current densities from the internal surfaces. Photoelectric emission and electron emission under impact of metastables may also play a factor. The imperfections in the interior of the carbon inserts also increase surface area and non-uniformities may contribute localised higher current densities due to field fluctuations.

The potentially high plasma potential in the micro hollow cathode, due to operation at low currents means that there is likely to be a statistically significant amount of multiple ionisation. This should be minimised to extend lifetime. Operation at higher currents would remedy this problem to some extent; however, as the electrical supplies could not reliably and stably achieve these higher currents experiments were only performed at low currents. It is also known that depletion of impregnants and depositions on the insert surface are other major contributors to lifetime considerations. Minimising sputtering in the device may therefore enhance the overall lifetime.

Only minimal variations in the operational characteristics of the second impregnated insert device were observed over operational timescales of hundreds of hours. This device also showed the least erosion around the orifice of all the cathodes tested. Therefore, while the micro hollow cathode has not been fully lifetime tested, neither is it operated at the demanding levels seen in other cathodes and could potentially operate for the thousands of hours required to be practical in a working ion thruster. The lesser amount of erosion seen in the second impregnated insert cathode resulted from better startup procedures and confining testing to well within normal cathode operating conditions. The high open volume fraction and low sputter yield of the carbon inserts should allow it to operate in this or another cathode well beyond this time, making it a potential alternative to sintered tungsten.

In conclusion, operational values lie closer to the desired range of a hollow cathode used as an ion thruster electron source than known existing micro hollow cathodes [22, 99]. Carbon matrix inserts have been demonstrated as a performance enhancing part of the system and a potential alternative to sintered tungsten inserts. The requirement for an alternative to tungsten arises from the difficulty in working it, especially at small scales. The weight of tungsten parts is also a consideration, making carbon a potential weight saving option. Further, the availability of carbon in extremely high open area volumes, in excess of 60% open, may allow even greater amounts of impregnant to be taken up per unit volume. The different chemistry of the device will

undoubtedly alter emission, but the postulated current densities and comparison with the surface impregnated device suggest that the impregnated insert is operating efficiently.

Other novel solutions applied to the orifice and heating element showed scope for development in these areas. The turned orifice did act to hold the insert in place and allowed the plasma to form in the cathode body. This can be seen through the lower power levels that the impregnated insert devices operated at. However, erosion was a problem and resulted in early failure of the simple molybdenum cathode. Erosion can be reduced by optimising the initiation conditions for the device using high flow rates and heating.

The heater system facilitated discharge initiation, increasing lifetime. The novel design allowed the same heater system to be used on both impregnated insert cathodes. The use of ceramics with varying electric and thermal properties, combined with precise machining to fit the cathode body ensured good propagation of heat to the cathode. Such a system could be further developed for use in test systems, but would likely be too bulky and expensive to produce in bulk to be useful in a thruster. Shielding the electrical connections into the ceramics to prevent electric field effects and thermal loss would improve the capabilities of this device.

Further application of the novel techniques and design used here may therefore allow development of an efficient electron source for use in an ion microthruster system.

Chapter 6

Summary & Conclusions

6.1 General Remarks

Many of the characteristics of a hollow cathode have been thoroughly investigated over the years. The effects of different propellants, geometries, keeper configurations and inserts have been studied [122]. Development and evaluation of micro hollow cathodes has been relatively minor in comparison to research on larger cathodes, which typically have external diameters of millimeters [98]. This chapter summarises important points in the development and investigation of the impregnated insert micro hollow cathodes which were designed and built to test the effect of novel materials for use in small scale devices. Table 6.1 shows the device's main physical parameters.

Size, mm	0.2 internal, 0.5 external diam
Flow Rate, kgs^{-1}	$2.7x10^{-7}$ to $2.2x10^{-6}$ kgs^{-1}
Discharge Current, mA	1.5 to 13.3
Discharge Voltage, V	54 to 220
Power, W	0.33 to 2.93

Table 6.1 Impregnated Insert Cathode Major Parameters

All experiments were carried out using Argon at flow rates between $2.4x10^{-7}$ and $2.2x10^{-6}$ kgs^{-1}. Argon was used as it was inexpensive and performs suitably as a propellant. Discharge currents were low, at between 1.5 and 13.3 mA. Discharge voltages varied between 54 and 220V, dependent on flow conditions.

6.2 Cathode Design

Scaling down the body and impregnated insert of a hollow cathode to produce a miniaturised device introduced a number of problems. Manufacturing at such small scales required novel techniques and materials. Three different designs of micro hollow cathode were fabricated; dimensions were consistent throughout the three models. The first design consisted solely of the molybdenum tube with a turned orifice, fitted into a ferrule and mounted in a swagelok fitting. Flow tests showed that leakage through the ferrule was much less than the flow through the main body. Molybdenum was used instead of tungsten or tantalum as it is easier to work and was available in prefabricated tubes of the desired size. A tapered orifice with an internal diameter of 0.23mm and a radius of curvature of approximately 0.14mm was formed by turning the body. Larger designs often use complicated manufacturing techniques to connect an orifice plate to the body, even more difficult to apply at smaller scales. The turned orifice solution simplifies production and effectively secures an insert in place when in use. The keeper used in all of the hollow cathodes developed was constructed from a 1mm thick stainless steel plate with a 1mm central orifice mounted on a Macor insulating post.

The second model consisted of the same molybdenum body but had its surfaces coated with a low work function $BaCO_3$:$CaCO_3$:Al_2O_3 mixture. This was used for comparison with the impregnated insert design. Surface coatings on cathodes have been shown to have a limited lifetime [52] and difficulties in evenly impregnating their surface cause variation in initiation voltage, discharge voltage and the relation between flow rate and upstream pressure.

The final design was made from the same uncoated molybdenum body, but had impregnated inserts made from a novel carbon matrix material. The carbon matrix is made of pulverized graphite, ground to a specific grain size and pressed into wafers. The graphite crystals are randomly oriented within the matrix, giving uniform bulk properties but non-uniformities are apparent at microscopic levels. Carbon has the advantage of being much easier to work at low scales, is hard to erode and has a high open volume for uptake of the impregnant, in excess of 60% in some cases. This design will have a number of differences to the surface coated model. Upstream pressure as a function of flow rate will be altered through lowered diameter and surface friction from insert roughness, resulting in different plasma conditions in the insert. The insert will also reduce the diameter of the plasma production volume, reducing the active area from which electrons are emitted, though lifetime of the emitting surface in contact with the plasma may increase due to the matrix holding more impregnant and dispensing it evenly. Two of the more complex carbon matrix inserted cathodes were built for comparison and redundancy. Impregnation was performed in an evaporation chamber for both designs that utilised the carbonate/oxide mix.

Mass flow rate was controlled by needle valves at flow rates above 4.5×10^{-7} kgs^{-1}, relying on pressure measurements, and by a high accuracy MKS mass flow controller at flow rates below 4.5×10^{-7} kgs^{-1}. The latter system is more precise; however, it is also too heavy and large for use on a nanosatellite. Varying the flow rate using valves is subject to a relatively large combined error. Improvements to either system would be required for application to a viable thruster system for use on small scale satellites.

A removable heater system was also employed to investigate discharge initiation at high temperatures. It was manufactured from two ceramics with good electrical resistance with a tungsten heating element between. The exterior ceramic had a high thermal resistance, the interior a low thermal resistance, promoting heat propagation to the cathode at the centre. The interior ceramic made a good fit with the cathode to improve conductance. A pyrometer was used to measure the temperature of the device, limited to above 800^0C when the cathode starts to luminesce.

6.3 Discharge Characteristics

At flow rates in excess of $5x10^{-7}$ kgs^{-1} initiation voltages of 300V were apparent, typical for a cold-start cathode [34]. Deviations in the initiation voltage between cathode types appeared to be a result of flow variations and local deformations around the orifice, thought to result from surface impregnation or erosion of the orifice. Erosion was especially evident in initial tests on the simple molybdenum cathode due to arcing during electrical system optimisation. The impregnated insert cathode had the poorest cold discharge initiation characteristics of the three devices. This could be a result of altered pressure differentials in the orifice region created by different internal geometries. The higher initiation voltages could be mitigated by employing the heater system or initiating at slightly higher flow rates.

Temperature tests showed that above 1300K the initiation voltage fell to around 100V, three times lower than at room temperature, presumably due to increased thermionic emission and effects on the impregnant chemistry. The heater was operated at 4.5W for 90 seconds to reach this temperature. Using the heater during initiation increases the lifetime of the device as orifice erosion will be reduced, but heating will also increase the depletion of impregnants affecting insert lifetime. Also the application of a bulky and power consumptive heater system to a design used on a microthruster is not feasible. Application of a heater to a thruster cathode would therefore require optimisation of mass, size, cost and electrical shielding on the heater.

After initiation the discharge was around 3 cm long with a violet glow when operating in the spot mode. In the plume mode luminosity was lower at similar currents and the integrated emission spectra appeared more blue signifying different conditions in the discharge plasma. Table 6.2 shows the minimum discharge voltage for the various cathode types at different flow rates and at a discharge current of 13.3mA.

Flow Rate, kgs^{-1}	Minimum Discharge Voltage, V		
	Simple Mo 0.9mm (Keeper Dist)	Surface Impregnated 0.5mm	Impregnated Insert 0.5mm
$4.5x10^{-7}$	355	91	78
$1x10^{-6}$	160	75	63
$1.8x10^{-6}$	142	64	58

Table 6.2 Minimum Discharge Voltage as a function of Flow Rate and Cathode Type

Operating voltages for the impregnated insert cathodes were consistently lower in comparison to both the surface impregnated and simple molybdenum cathode, though the different cathode keeper separation for the simple molybdenum cathode means that it cannot be directly compared. Numerous transitions between the spot and plume modes were evident at low flow rates, especially for the simple and surface impregnated cathodes, which were less likely to consistently show spot mode operation. The impregnated insert cathode exhibited mode transition at lower currents and at a lower voltage for comparable conditions and was more stable.

For the simple molybdenum cathode, the voltage-current relation showed a negative-resistance trend over the current range, where resistance decreases with increasing voltage. The discharge voltage fell from approximately 195V to 125V between 1.5 and 13.3mA at a high flow rate of $1.7\ x10^{-6}\ kgs^{-1}$ and at a keeper separation of 0.9mm. This equates to a power of 0.3 to 1.66W and power:current ratio of 0.14 to 0.22W/mA if the emitted electron current is equal to 90% of the keeper current [116].

For the surface impregnated cathode, the discharge voltage reached a minimum of 63V at $1.8x10^{-6}\ kgs^{-1}$ but was within 20% of this value at $1x10^{-6}\ kgs^{-1}$. Low voltage spot mode operation for the surface impregnated cathode was generally only observed at the highest currents and at flow rates in excess of $9x10^{-7}\ kgs^{-1}$. At a flow rate of $9x10^{-7}\ kgs^{-1}$ the voltage was observed to vary between 250 and 77V over the 1.5 to 13.3mA range (0.375 – 1.02W). The surface impregnated cathode could operate in the spot mode at lower flow rates, but would only do so sporadically and for limited times. This was

also true for the simple cathode. Power consumption per mA was from 0.09 to 0.27W/mA, similar to the simple molybdenum cathode, but was operated at half the flow rate. At a similar flow rate as the simple molybdenum cathode, the surface impregnated device had a power:current ratio of 0.06W/mA, half that of the simple molybdenum cathode. Operation at this level starts to approach what is required for a device that could be used in a viable thruster system, either as a discharge or neutraliser cathode, but further optimisation and lifetime testing would be required.

For the impregnated insert cathode, discharge voltages between 77 and 65V were observed across the 1.5 to 13.3mA current range at a flow rate of $9x10^{-7}$ kgs^{-1}. This equates to a power of 0.11 to 0.86W with a ratio of 0.06-0.09W/mA if the emission current is 90% of the keeper current. This is a substantial improvement over the surface impregnated model under the same conditions. The impregnated insert device allows spot mode operation at much lower flow rates and currents in comparison to the simple molybdenum and surface impregnated devices. Operating the cathode in the spot mode is desirable as it reduces discharge voltage, and hence required power, decreasing the cathode's electrical demand as well as reducing multiple ionisation. The minimum discharge voltage that was observed for the impregnated insert cathode was 54V at a very high flow rate of $2.2x10^{-6}$ kgs^{-1}. This equates to a power of 0.72W and a ratio of 0.05W/mA an improvement on the other two devices at similar high flow rates. At a low flow rate of $4.5x10^{-7}$ kgs^{-1}, the transition from plume to spot mode was observed at low currents of 7.5-8mA which are the minimum conditions for impregnated insert cathode operation in the spot mode at a keeper-cathode separation of 0.5 mm.

In comparison to larger flight-tested devices, discharge voltages for the impregnated insert micro hollow cathode were around 40 to 45 volts higher at significantly lower currents (~1%) and similar flow rates to a discharge chamber cathode (neutraliser cathodes operate at much lower flow rates in the 10^{-8} kgs^{-1} range) [91]. The available current is lower than that seen in practical ion thruster applications and was limited by the electrical supplies and potentially by the size of the cathode. Testing at higher currents for extended periods would be beneficial to determine if the devices

discharge voltage could be lowered further and would allow the lifetime of the inserts to be checked.

Cathode lifetime is an important consideration as it affects the applicability of a device to flight systems. The lifetime for the first impregnated insert cathode was in excess of 160 hours operation with over 500 startup sequences and the lifetime for the second model was in excess of 200 hours operation with over 400 startup sequences. Only the latter model, which had showed less erosion, was still performing well at the end of the test period. The deciding factor in respect of the cathode's lifetime appeared to be orifice erosion. The second impregnated insert cathode was subject to little erosion over its lifetime, a result of a more benignly designed electrical system and improved startup procedures.

The carbon matrix insert is unlikely to operate in the same manner as a tungsten insert cathode. This enhances emission through the formation of dipoles on the surface as the oxygen forms a layer between the tungsten insert and the barium atom in the oxide. A more likely explanation is that the matrix operates in the same fashion as an oxide cathode, where vacancies in the structure resulting from oxygen loss promote emission as sites which trap electrons that can easily be excited to emit. Byproducts of chemical reactions in the device may produce carbon monoxide (in preference to CO_2 due to lack of oxygen) which is not detrimental to cathode operation.

Based on the assumption on the length of the emission area in a cathode the current density of the cathode surface is around $0.2Amm^{-2}$, this is relatively close to larger cathodes which have current densities of around $0.5Amm^{-2}$. The current density in the micro hollow cathode can be accounted for by Schottky emission alone if the cathode temperature is around 800°C with a work function of 1.5eV (as in an oxide cathode). 800°C is around the threshold for luminescence, and the cathode was observed to glow at the lowest flow rates. If the device has a higher work function or lower temperature then emission enhancing effects such as metastable impact and excitation by UV photons

must take place to account for the emission current density, assuming the emitting area is correct.

Measurements on cathode wall temperature were made during operation using an optical pyrometer. Operation in the spot mode at a flow rate of 1.1 $x10^{-6}$ kgs^{-1}, a keeper voltage of 70V and a discharge current of 13.3mA showed no visible luminescence around the cathode tip, demonstrating that the cathode body was below ~1100K. The temperature during operation could not therefore be easily defined. Tests using the thermocouple showed readings around 350K, demonstrating that the device was undergoing heating, but the lack of knowledge on the propagation of heat to the thermocouple through part of the heater body and its early failure meant that a definitive measurement could not be made.

Measurements made using an unshielded Faraday cup gave an approximation for the electron temperature at around 90000K and plasma potential at 75V. The electron temperature is substantially higher than in larger hollow cathodes, which have electron temperatures of around 1eV or less (11,604K) but can be accounted for by the lower current. An estimation of the electron number density, at ~$5x10^{18}$ m^{-3}, and Debye length, at 10μm, can be made using the electron temperature assuming that it is invariant in the plume. The number density is similar to that seen in large cathodes, and while the Debye length is longer, it is still short enough to allow formation of a sheath and plasma in the cathode body. The plasma potential at 75V is around what would be expected as plasma potentials are generally close to the keeper voltage [30].

6.4 Significance of the Work

The smallest electron bombardment ion thrusters under development today are around 3cm in diameter [123]. There is therefore a requirement for miniaturised cathodes suitable to application in similar and smaller devices. The goal of this project has been to design and test a cathode that explores potential solutions to the problems of

miniaturisation of electron sources. Novel materials and manufacturing techniques have been used to fabricate miniaturised inserted hollow cathodes which have undergone testing to determine their relative performance.

The project has seen the development of a working inserted hollow cathode significantly smaller than existing impregnated insert cathodes. Carbon inserts demonstrated their improved performance over surface impregnated design and shown themselves as a as a potential alternative to sintered tungsten. The inserts showed no significant reduction in performance over 200 hour lifetime, though the turned orifice requires optimised initiation conditions to reduce erosion. The novel ceramic heater also demonstrated its usefulness as a test system. Other features of interest include the compression fitting of inserts and the simple swagelock adaptor for facility in mounting. Hollow cathodes are expensive to produce and the use of off the shelf parts and batch processing techniques therefore also reduces costs.

The final prototype operates more efficiently than other known examples of micro hollow cathodes for use in ion micropropulsion [22]. However, operational values lie outside the desired range of hollow cathodes used as ion thruster electron sources. With optimisation it is believed that the device performance could come significantly closer to that of efficient commercially available thruster cathodes. It has also acted as a successful test bed for novel technologies, showing that the carbon insert material is a viable method for increasing performance and that miniaturised bodies and orifices can produce plasmas in the spot mode, but may be limited in their total output current.

6.5 Suggestions for Future Work

A number of areas that would benefit from further study were encountered during the development and characterisation of the impregnated insert cathode. The most interesting field for investigation would involve the carbon insert technology. Studies that could progress development of carbon insert technology include:

- Application of carbon matrix inserts to existing cathode designs: a direct comparison with tungsten inserts
- Characterisation of reactions for impregnated carbon insert
- Long term behaviour of carbon as an insert material

Application of carbon insert technology to existing designs would demonstrate any performance variation in comparison to sintered tungsten and would allow larger currents from the device, due to the scaling laws governing maximum available current as a function of orifice and insert diameter [35]. Testing the performance of the device and carbon insert technology using a Xenon, rather than Argon propellant would also likely further improve performance. Matrices with larger open volume fractions could allow even greater uptake of impregnant, which may have an effect on lifetime. Characterisation of the reactions occurring in and at the surface of the impregnated carbon insert would allow the work function and long term behaviour of the device to be predicted, which could then be determined in life tests. A mass spectrometer could easily be used to measure for presence of carbon monoxide and other potential waste products to help determine chemical processes going on in the cathode.

Other novel aspects of the design which could be applied in other circumstances include the use of other micromachined parts, such as the heater and body. These would require more extensive changes. The heater has the benefit of using novel materials to improve heat propagation to the cathode and thus efficiency. However, the size, mass and ease of manufacture would have to be improved to meet the requirements for a working device. The prefabricated body and turned orifice were a cost effective solution, but were not robust in early experiments. This could be mitigated by using a thicker-walled body and optimising the initiation conditions.

Appendix A

Procedures

A.1. General Remarks

Procedures relating to the process of impregnation and operation of the hollow cathode device are given here. Impregnation and operation of the evaporator system and discharge initiation are discussed.

A.2. Impregnation Process

This section describes the procedures followed when operating the evaporator system to impregnate cathode parts. Processes for priming the evaporation system, impregnating parts and turning off the system are given.

Evaporator system preparation

1. Place parts for impregnation are in metal boat with impregnant
2. Connect boat across terminals
3. Ensure bell jar seals are clean
4. Put bell jar and implosion guard over apparatus
5. Switch on coolant water to diffusion pump

6. Switch on rotary pump
7. Switch on diffusion pump
8. Open roughing line to evacuate bell chamber
9. Close roughing line
10. Open backing line, evacuating to < 100μmHg
11. Close backing line
12. Open roughing line, evacuating to < 100μmHg
13. Close roughing line
14. Open backing line, evacuating to < 100μmHg
15. Fill trap with liquid N_2, refill every few hours
16. Open high vacuum valve, start slowly, if all OK open fully
17. Evacuate to < $1x10^{-4}$ mBar

Backing and roughing lines should not be open simultaneously. Lines can be closed and bell jar removed and replaced, allowing alteration of boats and parts for impregnation without fully powering down system.

Impregnation Process

1. Before placing parts in mix, thread onto 0.2mm diameter wire to ensure that central orifice holes do not become blocked and that carbon discs are kept in a linear array to ensure they will slide into cathode body
2. Connect boat across electrodes in evaporator system by moving turntable
3. Ensure that systems is evacuated to less than $1x10^{-4}$ mBar
4. Set filament selector to 3
5. Set power switch to LT
6. Increase rotary regavolt to required current (just in excess of 40A)
7. Resistive heating decomposes carbonates to oxides
8. Allow several minutes for impregnant to diffuse into matrix

Note that the melting point of the metal boat must exceed the temperature at which the mix calcinates and impregnates the insert or body.

Evaporator System Off Procedure

1. Ensure power to chamber filaments is off
2. Turn off liquid N_2
3. Close high vacuum valve
4. Turn off diffusion pump
5. Wait twenty minutes
6. Close backing line
7. Turn off rotary pump
8. Turn off coolant water supply
9. Vent rotary pump

A.3. Hollow Cathode Operation

The section details the procedures for operating the hollow cathode. Several procedures are given, including evacuation of the vacuum chamber, discharge initiation at high and low flow rates and the procedure for turning off the system.

Vacuum System Evacuation Procedure:

1. Use new copper gaskets on opened flanges
2. Close all flanges tightening 2-3 times
3. Close all gas feed valves
4. Check continuity of electrical feeds to cathode
5. Turn on water to turbo pump
6. Turn on diaphragm pump
7. Turn on Pirani gauge
8. Wait till pressure drops below 1mbar
9. Turn on turbopump
10. Turn on penning gauge
11. Check after 30 mins that rotations are steady at 720 Hz

12. Open all valves on cathode line downstream of flow controller
13. Leave for 24 hrs to evacuate and deoxygenate

Cathode On Procedure at high flow rates (>$5x10^{-7}$ kgs^{-1})

1. Check chamber pressure is sufficiently low (<$1x10^{-6}$ mbar)
2. Close valves immediately surrounding flow controller
3. Open needle valve to an approximate desired level (with rough correlation between needle valve setting and flow rate already established)
4. Turn on keeper supply (0V, 13.3mA)
5. Operate heater at 4.5 to 6W for 90s (if in use)
6. Ramp up keeper voltage until discharge initiates

Cathode On Procedure at low flow rates (<$5x10^{-7}$ kgs^{-1})

1. Check chamber pressure is sufficiently low (<$1x10^{-6}$ mbar)
2. Turn on flow controller electronics, ensure gas correction factor on electronics is set to correct level, 1.39 for Argon
3. Set flow controller
4. Turn on gas feed
5. Turn on keeper supply (0V, 13.3mA)
6. Operate heater at 4.5 to 6W for 90s (if in use)
7. Ramp up keeper voltage until discharge initiates

Cathode Off Procedure

1. Turn off keeper supply
2. Turn off flow controller/close needle valve
3. Close all feed line valves
4. Open needle valve fully, ensuring feed lines are above atmospheric pressure
5. Turn off vacuum pumps
6. Let nitrogen system bring chamber up to atmospheric pressure
7. Remove feed line from rear of cathode inlet

8. Open flange

In some cases experiments will be carried out with the same setup. In others alteration of the cathode is required. In the latter case the vacuum system must be opened, then re-evacuated as before.

Appendix B

Plasma Conditions

B.1. Remarks

Measurements were made on the plasma characteristics of the discharge. An unshielded Faraday Cup was used as a Langmuir probe to determine plasma potential. This allowed the electron temperature to be established. This in turn allowed a calculation of the electron number density. Under certain assumptions, the Debye length in the cathode could then be calculated. Errors in the measured saturation currents, definition of plasma potential and the perturbations to the plasma caused by the large probe meant that this data was not felt to be reliable enough to lie in the main body of the text.

B.2. Principles

As electrons are more mobile than ions, negative charge is lost from the plasma more quickly leading to a buildup of positive charge. This will stabilise at a point where the positive charge of the plasma column is enough to retain electrons such that the electron and ion losses are equal. The discharge therefore floats at what is known as the plasma potential.

A biased surface in contact with the plasma will collect either electrons or ions from the plasma, dependent on the applied voltage. The voltage at which the ion and electron currents to the detector are equal is known as the floating potential. Measurements of the floating potential and the collected electron and ion currents at their saturation points allow a determination of the plasma potential. The unshielded Faraday Cup was used as a Langmuir probe in this manner by biasing the voltage on the cup and measuring the collected current. Fig B.1 shows measurements of detected current under three different discharge conditions.

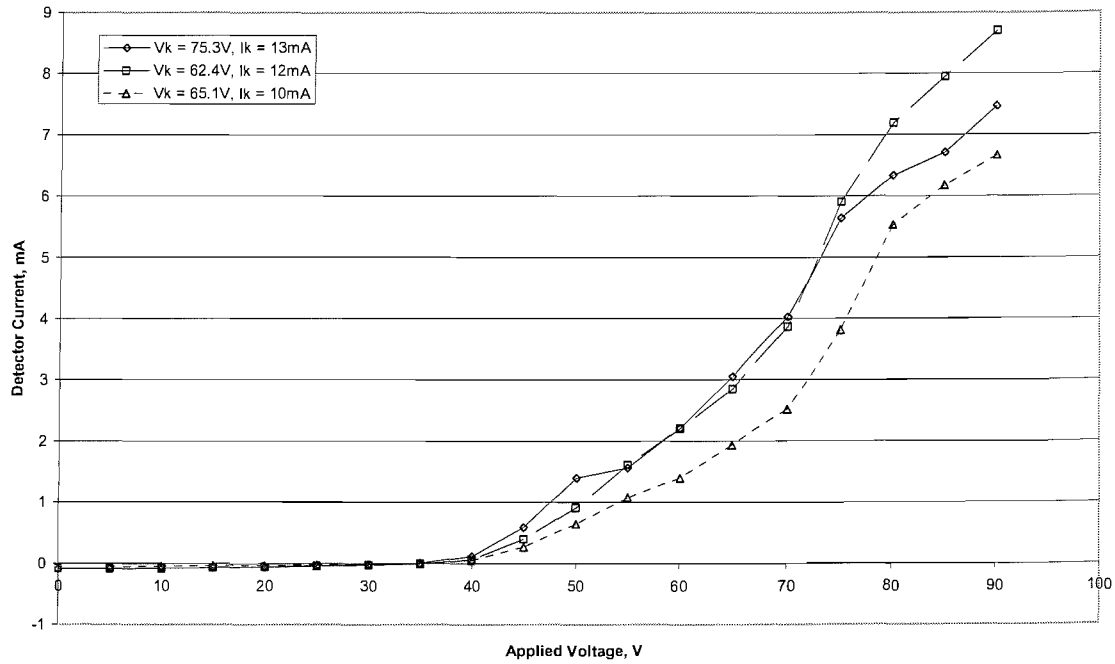

Fig B.1 Measured Current-Voltage Curve for Unshielded Faraday Cup

In each case the floating potential was around 35-36V. The plasma potential is greater than the floating potential by a factor of just over 2 at 75-80V. This is the point where the gradient of the curves decrease. A high plasma potential is expected as the plasma is very close to the keeper which is at a similar high voltage. Above the plasma potential the current reaches the maximum, or electron saturation current. It can be seen from fig 2.1 that the ion saturation current is a fraction of a mA, while the electron

saturation current at a minimum around 70% of the keeper current, and could be significantly higher, with values of 90% reported in larger cathodes [116].

For a steady sheath, the electrons approximate the Maxwellian distribution. The electron number density can therefore be determined through the Boltzmann relation:

$$\frac{n_e}{n_i} = \exp\left(\frac{eV}{kT_e}\right) \qquad \text{B.1}$$

Therefore, in a logarithmic plot of collected current against applied voltage, the gradient allows a calculation of the electron temperature, seen in fig B.2

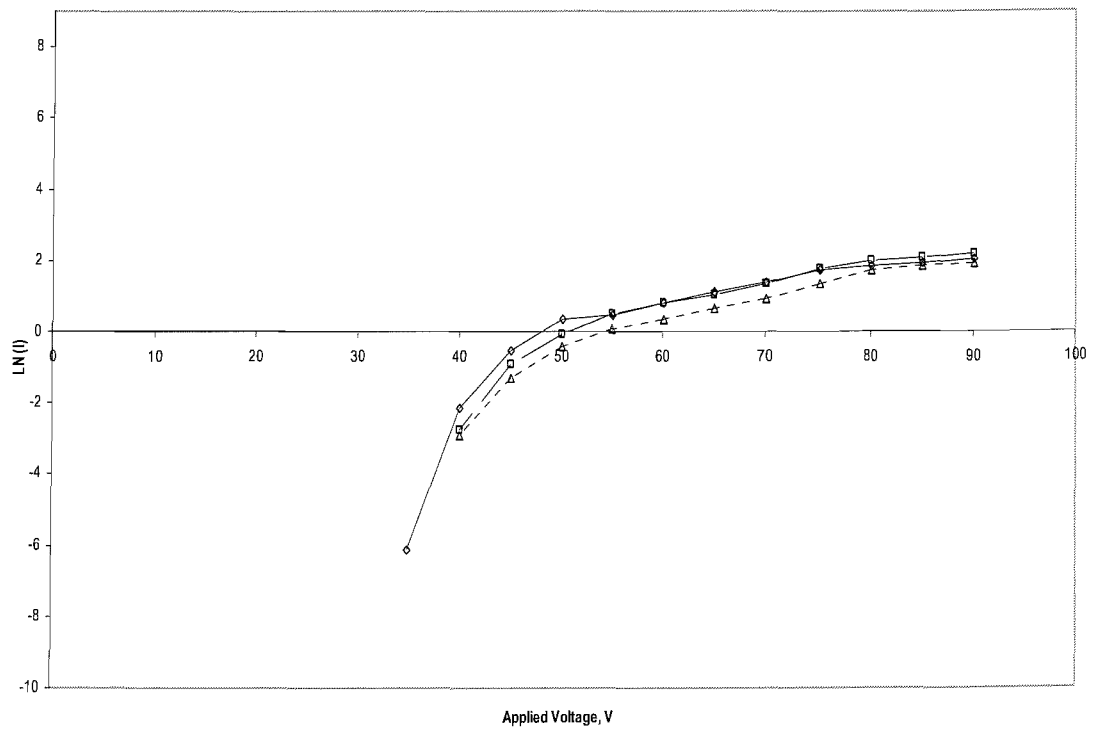

Fig B.2 Plot of applied detector voltage against $\log_e$ current

Above 50V where the plot flattens out, the gradient for each trace is around 0.125. This equates to an electron temperature of approximately 90,000K or 7.76eV.

This is substantially higher than existing thrusters (typically several thousand K), but the current is much lower so an increased electron temperature is expected. If the electron current, I_e, which transits the cathode orifice is 90% of the keeper current and is given by:

$$I_e = en_e\left(\frac{kT_e}{2\pi m_e}\right)^{1/2} A_{or} \qquad \text{B.2}$$

e is the electronic charge, n_e is the electron number density, the middle term comes from the Boltzmann equation and describes electron velocity and A_{or} is the orifice area. The electron number density is therefore around $5x10^{18}$ m^{-3} for an electron current of 12mA, an orifice area of $3.14x10^{-8}m^2$ and an electron temperature of 90000K. Number densities of the order 10^{17} to 10^{18} m^{-3}, have been observed in working hollow cathodes used for ion propulsion [64,114].

Under the assumption that in the spot mode, the electron temperature is invariant throughout the plume [91] and that the calculated values of electron number density in the cathode are correct, an estimation of the Debye length in the cathode can be performed using the measured values of electron temperature and number density.

$$\lambda_D = \sqrt{\frac{\varepsilon_0 kT_e}{e^2 n_e}} \qquad \text{B.3}$$

This gives a Debye length of 9 microns. As current was decreased this would rise due to the decrease in electron number density. This could be the reason that the plume is observed to extinguish at low currents, where the Debye length gets too big as the interior diameter must be several times this value for a plasma column to form.

Appendix C

Images of Micro Hollow Cathode in Operation

C.1 Spot mode operation

Photographs of the discharge operating in the spot mode were made at keeper cathode separations of 0.5mm to 0.7mm and flow rates of $1x10^{-6}$ kg/s. All images are of the impregnated insert cathode.

Fig C.1 13.3mA Spot mode, lateral

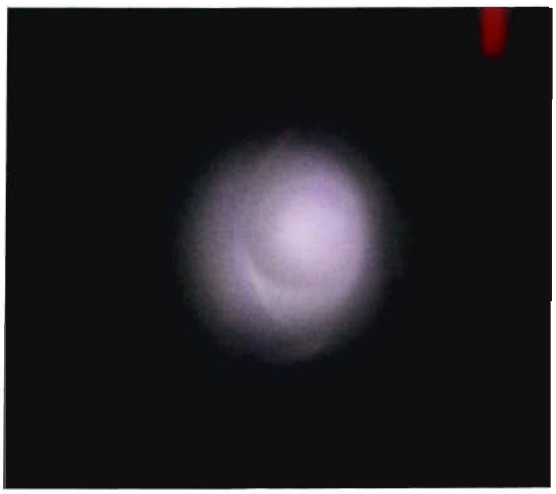

Fig C.2 13.3mA Spot Mode, Axial

Figures C.1 and C.2 show axial and lateral views of the impregnated insert cathode discharge operating in the spot mode at the highest operating current of 13.3mA, a low discharge voltage around 60V. The plasma is optically dense, 2.5cm in diameter, bounded by the floating anode and approximately 3 cm long. The characteristic glow of the plasma results from the interactions between electrons, atoms and ions in the discharge. The wavelengths of radiation emitted from the discharge would indicate the ion species present if a spectrometer was used. A schematic of the cathode setup can be seen in fig C.3

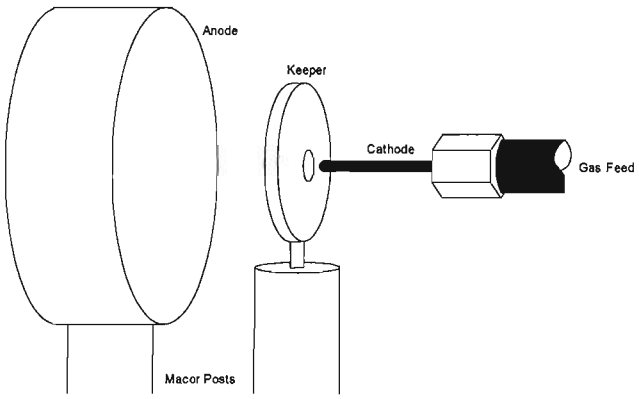

Fig C.3 Cathode Setup

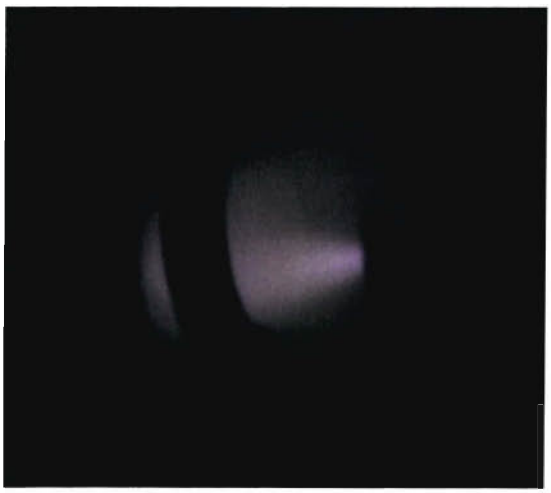

Fig C.4 10mA Spot mode, lateral

Fig C.5 10mA Spot mode, axial

Figs C.4 and C.5 show the same discharge conditions as those in C.1 and C.2, but at a lower limiting current of 10mA.

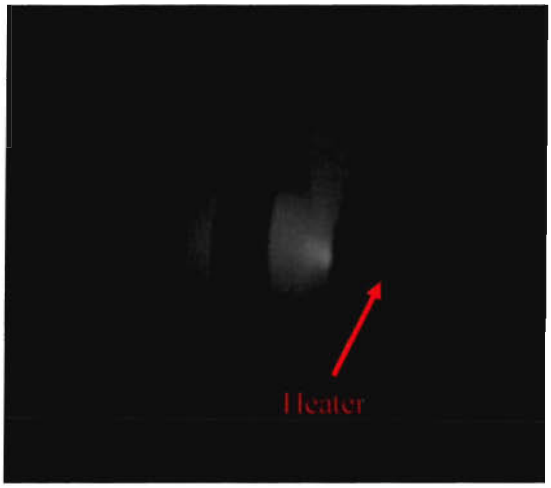

Fig C.6 7mA Spot mode, lateral inc. heater and cup

Fig C.7 7mA Spot mode, axial

Fig C.8 2mA Spot mode, lateral

Figs C.6 and C.7 show the discharge in the spot mode but at a lower current of 7mA. The heater can be seen in fig C.6 as a cylinder around the cathode body, visibly backlit by the plasma at the upstream end of the chamber. In fig C.8 the plasma can be seen at a low keeper current of 2mA. Note that as the current has been decreased the plasma

has become significantly fainter though the integrated emission spectrum appears similar with its characteristic violet glow.

B.2 Plume mode operation

Photographs taken of the discharge operating in the plume mode were made at keeper cathode separations of 0.5 to 0.7mm and flow rates of 4.5×10^{-7} kg/s.

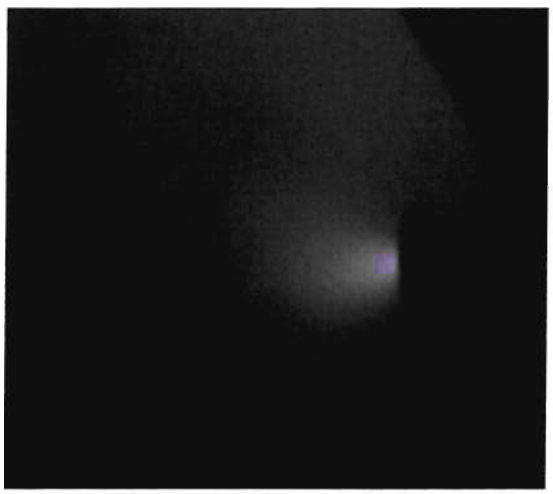

Fig C.9 13.3mA Plume mode, lateral

Fig C.10 13.3mA Plume mode, axial

Figs C.9 and C.10 show the impregnated insert cathode operating at high current in the plume mode. Luminosity is markedly down on spot mode operation at the same currents. The discharge also has a different colour, blue rather than purple, and a more diffuse boundary, with a shorter overall length and diameter of approximately 2cm in both dimensions in comparison to the spot mode.

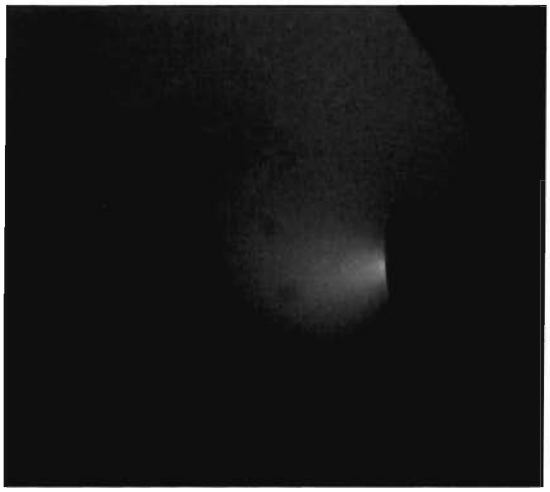

Fig C.11 10mA Plume mode, lateral

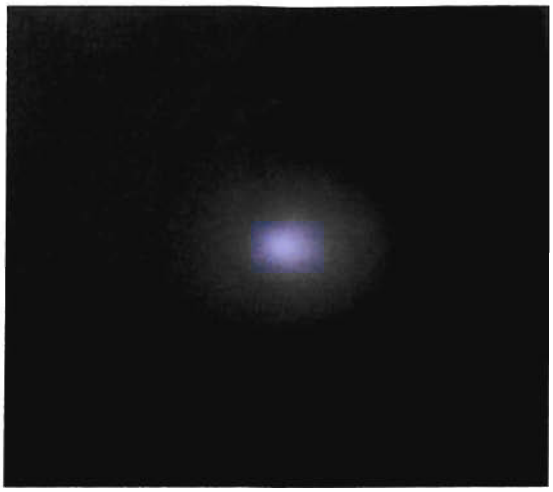

Fig C.12 10mA Plume mode, axial

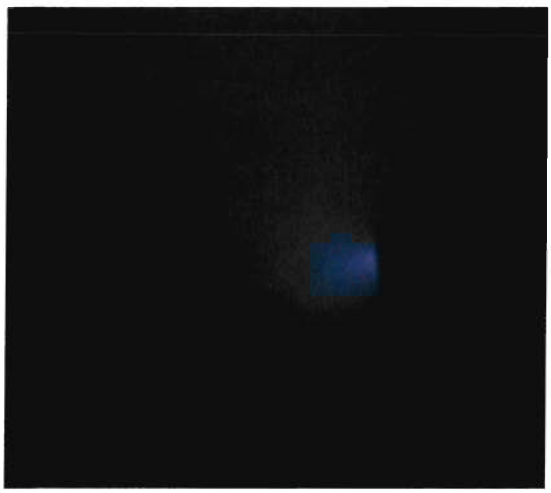

Fig C.13 7mA Plume mode, lateral

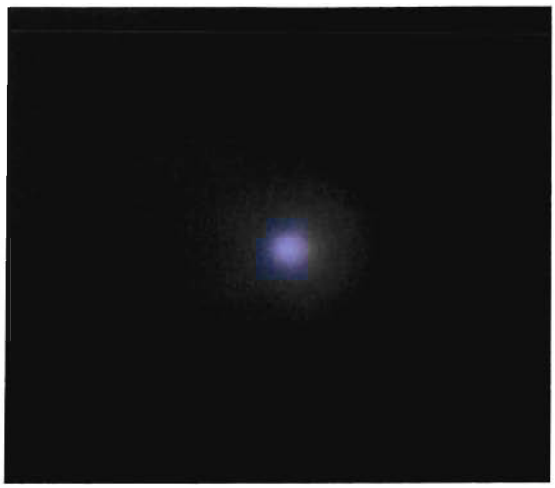

Fig C.14 7mA Plume mode, axial

Figs C.11 – C.14 show both axial and lateral views for the lower current values in plume mode operation. Plasma density appears low with a high axial variation.

References

[1] "Large Ion Beams: Fundamentals of Generation & Propagation" AT Forrester, Wiley Press (1988)
[2] "Spacecraft Systems Engineering" P Fortescue, J Stark, 2nd Edition, Wiley Press (1995)
[3] "Analysis of Hall-Effect Thrusters and Ion Engines for Orbit Transfer Missions" AIAA-96-2973, FS Gulczinski, RA Spores (1996)
[4] "Characteristics of Primary Electric Propulsion Systems" AIAA Conf. 79-2041 pp99-121 DC Byers (1979)
[5] "Spacecraft Electric Propulsion – An Overview" Jnl of Propulsion & Power Vol. 14/5 pp688-699 M Martinez-Sanchez, JE Pollard (1998)
[6] "Ablative Z-Pinch Pulsed Plasma Thruster" AIAA-2000-3257 TE Markusic, K Polzin et al (2000)
[7] "Evaluation of the United Kingdom Ion Thruster" Jnl Spacecraft & Rockets Vol. 33/5 pp739-747, MW Crofton (1996)
[8] "One Millinewton FEEP Thruster Tests" IEPC-99-069 pp443-463 S Marcuccio, M Saviozzi et al (1999)
[9] Two-Dimensional Micro-Fabricated Colloid Thruster Arrays, L Velasquez-Garcia, M Martinez-Sanchez, AIAA 2004-3595 (2004)
[10] "The Interaction of Electron & Positive Ion Space Charges in Cathode Sheaths" Physical Review Vol. 33 pp954-989 I Langmuir (1929)
[11] "The Feasibility of Hollow Cathode Ion Thrusters: A Preliminary Characterisation" AIAA 2000-5354 (2000)
[12] http://www.absoluteastronomy.com/reference/project_orion
[13] http://www.absoluteastronomy.com/reference/project_daedalus
[14] http://www.aboutnuclear.org/view.cgi?fC=Space,History
[15] "Design & Performance Analysis of the Electric Power Sub-System for a Multi-Mission Microsatellite" Acta Astro. Vol. 44/1 pp31-40 M Pastena, M Grassi (1999)
[16] "Chemical Microthrusters: Effects of Scaling on Combustion" AIAA 2001-3711 C Bruno (2001)
[17] "Design Considerations for Ion Microthrusters" IEPC-97-072 GJ Yashko, GB Giffin, DE Hastings (1997)
[18] "Very Low Power DC Plasma Jet Microthrusters" AIAA 2001-3791 H Horisawa, I Kimura (2001)
[19] "Performance Improvement of Pulsed Plasma Thruster for Micro Satellite" IEPC-01-152 M Igarishi, N Kumagai et al (2001)
[20] "Performance and Heat Loss of a Coaxial Teflon Pulsed Plasma Thruster" IEPC-01-151 F Rysanek, RL Burton (2001)
[21] "FEEP-5 Thrust Validation in the 10-100μN Range with a Simple Nulled Pendulum Thrust Stand: Integration Procedures" IEPC-01-288 D Nicolini, E Chesta et al (2001)
[22] "State of the art Radio Frequency Ion Sources for Space Propulsion" Rev Sci Instrum Vol. 65/5 pp1741-1744, KH Groh, HW Loeb (1994)

[23] "Magnetic Confinement Studies for Performance Enhancement of a 5-cm Ion Thruster" G Sandonato et al IEEE Trans. Plasma Science Vol. 24/6 pp 1319-1329 (1996)
[24] "Scaling of Ion Thrusters to Low Power" IEPC-97-098 SP Grisnik, MJ Patterson (1997)
[25] "Hollow Cathode Microthruster Performance" IEPC-01-226 M Patterson, J Foster (2001)
[26] "Origin of the Electron-Bombardment Ion Thruster" Jnl Spacecraft Vol. 18/4 pp289-292 HR Kaufman (1981)
[27] "The Compatibility of Hollow Cathode Characteristics with a Variety of Ion Thruster Designs" IEPC-99-133 pp732-739 DG Fearn, SW Patterson (1999)
[28] "Recent Development Activities in Hollow Cathode Technology" IEPC 01-270 MJ Patterson, MT Domonkos (2001)
[29] "Discharge Initiation in the T6 Thruster Hollow Cathode" AIAA 2000-3532 SW Patterson, M Jugroot, DG Fearn (2000)
[30] "An Investigation of Ion Engine Erosion by Low Energy Sputtering" PhD thesis, Olivier B. Duchemin, California Institute of Technology
[31] "A First-Principles Model for Orificed Hollow Cathode Operation" AIAA 92-3742 A Salhi, PJ Turchi (1992)
[32] "Electron Emission from a Hollow-Cathode Based Plasma Contactor" Jnl Spacecraft & Rockets Vol. 29/6 pp820-829 JD Williams, PJ Wilbur (1992)
[33] "Low-Current, Xenon Orificed Hollow Cathode Performance for In-Space Applications"; Domonkos, Patterson & Gallimore, NASA/TM—2002-211574 (2002)
[34] "The Results of Researching of Low-Current Self-Heated Hollow Cathodes on Electric Current Range from 0.3 up to 0.5A" IEPC 2001 A Loyan, N Koshelev (2001)
[35] "An Evaluation of Hollow Cathode Scaling to Very Low Power and Flow Rate" ERPS 1997 MT Domonkos, AD Gallimore, MJ Patterson (1997)
[36] "Theoretical Modeling of Orificed Hollow Cathode Discharges" IEPC-93-024 A Salhi, PJ Turchi (1993)
[37] "Improved Ion Containment Using a Ring-Cusp Ion Thruster" Jnl Spacecraft Vol. 21/5 pp488-495 JS Sovey (1984)
[38] "Magnetic Confinement Studies for Performance Enhancement of a 5-cm Ion Thruster" IEEE Trans Plasma Sci Vol. 24/6 pp1319-1329 (1996)
[39] "Plasma Confinement by Localised Cusps" Physics of Fluids Vol. 19/7 pp1045-1053 KN Leung, N Hershkowitz, KR MacKenzie (1976)
[40] "Unique Hollow Cathode as a Code Validation Experiment & Candidate Non-Magnetic Ion Micro-Thruster" AIAA Paper 99-2854 M Young, E Muntz et al (1999)
[41] "New Ion source design for Ion Propulsion Application" Rev Sci Instrum 69/2 pp788-790 M Capacci, G Noci (1998)
[42] "Development & Testing of a 3cm Electron Bombardment Ion Thruster" IEPC-01-343 R Wirz, J Escobedo et al (2001)
[43] "Nasa Breakthrough Propulsion Physics Program" Acta Astra 44/2-4 pp175-182 MG Millis (1999)
[44] "Ion Propulsion Development Projects in U.S.: Space Electric Rocket Test I to Deep Space 1" Jnl of Propulsion & Power Vol. 17/3 pp517-526 JS Sovey, VK ()

[45] "Improvement of 20mN Xenon Ion Thruster" IEPC-99-153 T Ozaki, Y Kasai, E Nishida (1999)
[46] www.esa.int/gsp/completed/neo/simone.html
[47] "Recent Development Activities in Hollow Cathode Technology" IEPC 01-270 MJ Patterson, MT Domonkos (2001)
[48] "The Compatibility of Hollow Cathode Characteristics with a Variety of Ion Thruster Designs" IEPC-99-133 pp732-739 DG Fearn, SW Patterson (1999)
[49] "Development Steps of the RF-Ion Thruster RIT" IEPC-01-105 H Bassner, R Killinger, et al (2001)
[50] "A Microwave Plasma Cathode Elecrton Gun for Ion Beam Neutralisation" Rev Sci Instrum 69/2 pp1153-1155 C Fusellier, L Wartski et al (1998)
[51]"Development of Microwave Discharge Ion Thruster for Asteroid Sample Return Mission" Kuninaka H, Satori S AIAA96-2979 (1996)
[52] "Ionised Gases" A Von Engel (1955)
[53] "Proof and Analysis of the Pendulum Motion of Beam Electrons in a Hollow Cathode Discharge" Jnl Phys D: Appl Phys 34 pp1683-1689 G Stockhausen, M Kock (2001)
[54] "Thermionic Emission, Field Emission and the Transition Region" Physical Review 102/6 pp1464-1473 EL Murphy, RH Good (1956)
[55] "A First Principles Model for Orificed Hollow Cathode Operation" AIAA 92-3742 A Salhi, PJ Turchi (1992)
[56] "Electron Emission in Intense Electric Fields" Proc Roy Soc pp173-181 RH Fowler, L Nordheim (1928)
[57] "Field-emitter arrays for vacuum microelectronics" Spindt et al IEEE Transactions on Electron Devices 38/10 pp2355- 2363 (1991)
[58] "Simplified Analysis of Point-Cathode Electron Sources" Jnl of Applied Physics 38/13 pp4944-4957 TE Everhart (1967)
[59] "Direct Current High-Pressure Glow Discharges" Jnl Appl Phys 85/4 pp2075-2080 RH Stark, KH Schoenbach (1999)
[60] "Studies of the Properties of the Hollow Cathode Glow Discharge in Helium and Neon" Jnl Appl Phys 35/10 pp2887-2894 DJ Sturges, HJ Oskam (1964)
[61] "Next-Generation 5/10 KW Ion Propulsion Development Status" IEPC-01-089 MJ Patterson, JE Foster et al (2001)
[62] "High Current Hollow Cathode Development" IEPC-01-274 CB Carpenter, MJ Patterson (2001)
[63] "Recent Development Activities in Hollow Cathode Technology" IEPC 01-270 MJ Patterson, MT Domonkos (2001)
[64] "The Study of the Physics of Hollow Cathode Discharges" IEPC-93-026 AK Malik, DG Fearn (1993)
[65] "Phenomenological model describing orificed hollow cathode operation" DE Siegried, PJ Wilbur, AIAA Jnl 21/1 pp5-6 (1983)
[66] "Plasma diagnostics"; Weizmann (2001)
[67] http://en.wikipedia.org/wiki/Debye_length
[68] "Scaling Relations for Design & Operation of Orificed Hollow Cathodes" AIAA 94-3133 A Salhi, PJ Turchi (1994)

[69] "Low-Pressure Hollow Cathode Glow Discharge Plasma for Broad Beam Gaseous Ion Source" Rev Sci Instrum 69/2 pp853-855 EM Oks, AV Vizir, GY Yushkov (1998)
[70] "Particle Simulation of the Main Chamber of a Kaufman-Type Ion Thruster" 3rd Intl Conf on Spacecraft Propulsion ESA SP-465 pp1-4 M Jugroot, JK Harvey (2000)
[71] "DSMC Neutral and Charged Particle Simulation of a Kaufman-Type Ion Thruster" 10th Intl Congress on Plasma Physics M Jugroot, JK Harvey (2000)
[72] "Numerical Modelling of Ion Thruster Hollow Cathode Interior Flow" AIAA 97-0793 DM Murray, OR Tutty, SB Gabriel (1997)
[73] "Microhollow cathode discharge stability with flow and reaction" D Hsu et al J. Phys. D: Appl. Phys. 36 2898-2907 (2003)
[74] "Computation of Neutral Gas Flow From a Hall Thruster Into a Vacuum Chamber" AIP Conference Proceedings Iain D. Boyd, Chunpei Cai, Mitchell L. R. Walker and Alec D. Gallimore (2003)
[75] "Theoretical model of a hollow cathode plasma for the assessment of Insert and Keeper lifetimes" IG Mikellides, I Katz et al, AIAA2005-4234 (2005)
[76] "The Effect of Discharge Wall Temperature on Ion Thruster Performance" AIAA Jnl Vol. 24/2 pp278-283, PJ Wilbur, JR Brophy (1984)
[77] "Xenon and Kypton Availability for Electric Propuslion - An Updated Assessment" RP Welle AIAA-93-2401 (1993)
[78] "Total Cross Sections for Electron Scattering by Ne, Ar, Kr and Xe" Jnl Phys B: Atom Molec Phys 12/6 pp979-1002 FJ de Heer, RH Jansen, W van der Kaay (1979)
[79] CRC Handbook of Chemistry & Physics, 79th Edition (1998)
[80] "Theory of the Sputtering Process" Physical Review 102/6 DE Harrison (1956)
[81] "A Review of Low Energy Sputtering Theory and Experiments" IEPC 97-068 OB Duchemin, JR Brophy, CE Garner et al (1997)
[82] "A Doubly Charged Ion Model for Ion Thrusters" Jnl Spacecraft Vol. 14/8 pp461-468 RR Peters, PJ Wilbur, RP Vahrenkamp (1977)
[83] "Measurement of Doubly Charged Ions in Ion Thruster Plumes" IEPC-01- 310 GJ Williams, MT Domonkos, JM Chavez (2001)
[84] "Resolving Carbon Sputter Issues" MKS Data Sheet, J Sellers
[85] "Low Energy Xenon Ion Sputtering Yield Measurements" IEPC-01-309 MA Mantenieks, JE Foster et al (2001)
[86] "An Experimental Investigation of the Hollow Cathodes For Low-Power Ion Thruster" IEPC-99-124 OA Gorshkov, VA Muravlev (1999)
[87] "Characterisation of the FMT-2 Discharge Cathode Plume" IEPC-99-104 GJ Williams, TB Smith, TA Patrick, AD Gallimore (1999)
[88] "Improved Impregnated Cathode" R. Levi, J. Appl. Phys. 26, 639 (1955)
[89] "Life Model of Hollow Cathodes Using a Barium Calcium Aluminate Impregnated Tungsten Emitter" IEPC 01-276 SD Kovaleski (2001)
[90] "Thermographic Investigation of 3.2mm Diameter Orificed Hollow Cathodes" AIAA 98 MT Domonkos, AD Gallimore, MJ Patterson (1998)
[91] "Low-Current Hollow Cathode Evaluation" AIAA-99-2575 MT Domonkos, AD Gallimore, GJ Williams, MJ Patterson (1999)
[92] "High Current Hollow Cathode Phenomena" Jnl of Propulsion & Power 8/3 pp635-643 VJ Friedly, PJ Wilbur (1992)

[93] "Researching of Running–in, Starting, Transition Thermal Processes of Self-Heated Hollow Cathode in Electric Current Range from 5 up to 25A" IEPC-99-131 SA Lobov, AV Loyan (1999)
[94] "Experimental Investigation of a Hollow Cathode Discharge" IEPC-93-025 A Salhi, RM Myers, PJ Turchi (1993)
[95] "Characterisation of the high current hollow cathode for the T6 ion thruster" DG Fearn, SW Patterson AIAA-98-3346 (1998)
[96] "Mars Missions Using Solar Electric Propulsion" Jnl Spacecraft & Rockets Vol. 37/1 pp71-77 SN Williams, V Coverstone-Carroll (2000)
[97] "Time-Critical Low-Thrust Orbit Transfer Optimisation" Jnl Spacecraft & Rockets Vol. 29/2 pp286-288 RL Burton, C Wassgren (1992)
[98] "Evaluation of the Mini-Hollow Cathode Emission Source for the Analysis of Microsamples" Applied Spectroscopy Vol. 42/8 pp1379-1387 JY Ryu, RL Davis et al (1988)
[99] "Microhollow Cathode Discharge Excimer Lamps" Physics of Plasmas Vol. 7/5 pp2186-2191 KH Schoenbach, A El-Habachi, MM Moselhy, W Shi (2000)
[100] "Review of the EP Activities of US Academia" AIAA 2001-3227 AD Gallimore et al (2001)
[101] "The Compatibility of Hollow Cathode Characteristics with a Variety of Ion Thruster Designs" IEPC-99-133 pp732-739 DG Fearn, SW Patterson (1999)
[102] "Microhollow cathode discharges" Applied Physics Letters 68/1, pp 13-15 KH Schoenbach et al (1996)
[103] "Dispenser cathodes for CRTs", LR Falce (Unknown)
[104] "An investigation of physical processes in a hollow cathode discharge" DG Fearn, CM Philip AIAA 72-416 (1972)
[105] http://www.slac.stanford.edu/grp/kly/muri/murib.htm
[106] "InO_x thin films, candidates for novel chemical and optoelectronic applications" G. Kiriakidis, N. Katsarakis, M. Bender, E. Gagaoudakis and V. Cimalla Institute of Electronic Structure and Laser (2000)
[107] "Investigation of the Discharge Characteristics of the T6 Hollow Cathode Operating on Several Inert Gases and a Kr/Xe Mixtures" IA Rudwan, SB Gabriel 34th COSPAR Scientific Assembly (2002)
[108] http://en.wikipedia.org/Knudsen_number
[109] http://en.wikipedia.org/wiki/Reynolds_number
[110] "The isentropic relation in plasmas" KT Burm J. Phys. A (Math Gen) 37 pp4141-4146 (2004)
[111] http://www.spots.ca/~belfroy/thermoManualA/thermodynamicsI.html
[112] http://www.answers.com/topic/speed-of-sound
[113] "A Users Guide to Vacuum Technology" JF O'Hanlon, Wiley Press (2004)
[113a] http://www.tau.ac.il/~phchlab/experiments/vacuum/sime_vacuum.html
[114] "A Study of Hollow Cathode Discharge Characteristics" AIAA 9/11 pp2191-2196 CM Philip (1971)
[115] "Breakdown in vacuum and gases" S Fink, SCENET Workshop for Low Temperature High Voltage Problems in Electric Power Engineering (2004)
[116] "A Particle and Energy Balance Model of the Orificed Hollow Cathode" MT Domonkos, AIAA–2002–4240 (2002)

[117] "Thermal runaway phenomenon of a neutralizer hollow cathode" Kudo I, Toda Y et al AIAA-82-1891 (1982)
[118] "Non-Equilibrium Air Plasmas at Atmospheric Pressure: Chapter 6 - DC and Low Frequency Air Plasma Sources" U Kogelschatz, YS Akishev et al (2004)
[119] "Performance Evaluation of a 50 kW Hall Thruster" DT Jacobson, RS Jankovsky AIAA–99–0457 (1999)
[120] "Parametric Investigation of Orifice Aspect-Ratio Effects on Low-Current Hollow Cathode Power Consumption" Domonkos, Gallimore, and Patterson, AIAA98-3345 (1998)
[121] http://www.slac.stanford.edu/grp/kly/muri/murib.htm
[122] "Inert Gas Thruster Technology" Jnl Spacecraft & Rockets Vol. 20/1 pp77-83, HR Kaufman, RS Robinson, DC Trock (1983)
[123] "Development & Testing of a 3cm Electron Bombardment Ion Thruster" IEPC-01-343 R Wirz, J Escobedo et al (2001)